KINETICS AND DYNAMICS STUDY ON THE ALLOSTERIC PATHWAY OF PHOSPHOFRUCTOKINASE FROM *ESCHERICHIA COLI*

A Dissertation

by

CUIJUAN TIE

Submitted to the Office of Graduate Studies of
Texas A&M University
in partial fulfillment of the requirements for the degree of

DOCTOR OF PHILOSOPHY

May 2008

Major Subject: Biochemistry

KINETICS AND DYNAMICS STUDY ON THE ALLOSTERIC PATHWAY OF PHOSPHOFRUCTOKINASE FROM *ESCHERICHIA COLI*

A Dissertation

by

CUIJUAN TIE

Submitted to the Office of Graduate Studies of
Texas A&M University
in partial fulfillment of the requirements for the degree of

DOCTOR OF PHILOSOPHY

Approved by:

Chair of Committee,	Gregory D. Reinhart
Committee Member,	Mary Bryk
	Nick Pace
	Deborah Siegele
Head of Department,	Gregory D. Reinhart

May 2008

Major Subject: Biochemistry

ABSTRACT

Kinetics and Dynamics Study on the Allosteric Pathway of Phosphofructokinase from *Escherichia coli.*

(May 2008)

Cuijuan Tie, B.S., Nanjing University, China;

M.S., China Academy of Science

Chair of Advisory Committee: Dr. Gregory D. Reinhart

Phosphofructokinase from *Escherichia coli* (EcPFK) is allosterically regulated by MgADP and phosphoenolpyruvate (PEP), which act to activate or inhibit, respectively, by changing the substrate (Fru-6-P) affinity of the enzyme. Both ligands bind to the same allosteric site in EcPFK. Therefore, the questions we want to address are how these two molecules regulate EcPFK and how the allosteric signal is propagated throughout the enzyme.

EcPFK has 28 potential site-site interactions. These interactions in turn derive from multiple copies of 6 potentially unique homotropic interactions and 4 potentially unique heterotropic interactions. Making hybrid tetramer of EcPFK is used to isolate a single heterotropic interaction. To improve the yield of the 1:3 hybrid, the *in vivo* hybrid formation method was developed. Four heterotropic interactions were isolated by this manner and re-evaluated. The same kinetics characteristics were obtained for each 1:3 hybrid from both the *in vivo* and *in vitro* method.

To address the question of how the allosteric signal is transmitted throughout EcPFK, we identified residues (G184, Asp59 and S157) that are important for the allosteric regulation for both PEP inhibition and MgADP activation. The impact of each mutation on individual interaction is unique and also suggests that the structural basis for PEP inhibition is different from that for MgADP activation. Most importantly, since the sum of each heterotropic interaction with a modification in only one subunit is equal to the total heterotropic interaction with a modification in all four subunits, this result indicates that the heterotropic allosteric signal transmission is realized in a single subunit. The 23Å heterotropic interaction, which contributes the most to the PEP inhibition, was chosen to study the dynamic properties. Fluorescence was used to study the dynamic perturbations of the 23Å interaction upon ligand binding. Taking advantage of the hybrid formation strategy and the tryptophan-shift mutagenesis method, a tryptophan residue can be placed at different individual locations throughout the native subunit containing the 23Å heterotropic interaction. The steady-state anisotropy and lifetime measurement at each tryptophan position indicate that the 23Å allosteric interaction involves the perturbation of side-chain dynamics both near and quite far away from the respective ligand binding sites.

DEDICATION

To my parents, my husband and my son

To my sister and my brother

To all the people who have helped or encouraged me

ACKNOWLEDGEMENTS

I sincerely give my thanks and appreciations to my boss, Dr. Greg Reinhart. With your guidance and encouragement, I had a great experience in my Ph.D. career. You have not only expanded my vocabulary in English, but also my way of thinking of science. I think I am very lucky to have you as my advisor since you care not only about research, but also about the person doing the research. Boss, it is not easy for me to express my "big thank you" in English, but the "thank you" is from my heart.

I also thank my committee members, Dr. Nick Pace, Dr. Mary Bryk and Dr. Deborah Siegele, for their patience, understanding and guidance through my career.

A very special thanks goes to all the Reinhart lab "family" members. Although my hometown is Beijing, China, the Reinhart lab is my hometown in the United States. Thanks go to Dr. Michelle Lovingshimer, she was always the first editor of my thesis or paper; Dr. Mauricio Lasagna, the fluorescence expert with a lot of patience to show me the fluorescence technique. I would like to thank Dr. Aron Fenton, Dr. Jason Quinlan, Dr. Monique Parichartanakul, Scarlett Blair, Andrew Bigley, Rockann Mosser, Stephanie Perez, Maria Mcgresham, Amanda Lambert, Bobby Laird and Lin Fan for sharing good and bad stories every day. I will remember the scientific and non-scientific stories shared during lunchtime. Thanks go to my dear classmates for helping each other as being an international student: Chonghua Li, Lichun Li, Lin Fan, Lei Wang and Hongjun Jin.

Finally, I would like to take this opportunity to thank all the people who have been instrumental to my education.

NOMENCLATURE

Abbreviations

°	Degrees or denotes standard state
A	Generally denotes substrate or single letter code for Alanine
Å	Angstroms
ADP	Adenosine 5'-diphosphate
Ala	Alanine
AMP	Adenosine 5'-monophosphate
Arg	Argnine
Asp	Aspartate
ATP	Adenosine 5'-triphosphate
BCA	Bicinchoninic Acid
BsPFK	Phosphofructokinase from *Bacillus stearothermophilus*
C	Single letter code for the nucleotide cytosine
D	Single letter code for Aspartate
DTT	Dithiothreitol
E	Generally denotes enzyme or single letter code for glutamate
EcCPS	Carbamoyl-phosphate synthetase from *Escherichia coli*
EcPFK	Phosphofructokinase from *Escherichia coli*
EDTA	Ethylenediamine tetraacetic acid
EPPS	N- [2-Hydroxyethyl] piperazine-N'-3-propanesulfonic acid
F	Single letter for phenylalanine

FBP	Fructose-1, 6-bisphosphate
FBPase	Fructose-1, 6-bisphosphatase
Fru-6-P	Fructose-6-phosphate
G	Single letter code for the nucleotide guanine
GDP	Guanosine 5'-diphosphate
Glu	Glutamate
Gly	Glycine
H	Single letter code for histidine
Hb	Hemoglobin
I	Generally denotes inhibitor
IMP	Inosine monophosphate
K	Single letter code for lysine
KSCN	Potassium thiocyanate
L	Single letter code for leucine
LB	Luria Bertani broth
LbPFK	Phosphofructokinase from *Lactobacillus delbrueckii*
Lys	Lysine
M	Methionine
Mg	Magnesium
MES	2-[N-Morpholino] ethanesulfonic acid
MOPS	3-[N-Morpholino]propanesulfonic acid
mPFK	Phosphofructokinase from mouse

MW	Molecular Weight
N	Single letter code for asparagine
NADH	Nicotinamide adenine dinucleotide, reduced form
NAD^+	Nicotinamide adenine dinucleotide, oxidized form
NATA	N-acetyl-tryptophanamide
P	Generally denotes product
PAGE	Polyacrylamide gel electrophoresis
PEP	Phosphoenolpyruvate
PFK	Phosphofructokinase
PGA	Phospoglycolate
Q	Single letter code for glutamine
R	Single letter code for arginine
RmPFK	Phosphofructokinase from rabbit muscle
S	Generally denotes substrate or the single letter code for serine
SDS	Sodium dodecyl sulfate
Tris	Tris [hyroxymethyl] aminomethane
V	Single letter code foe valine
W	Single letter code for tryptophan
X	Generally denotes an allosteric ligand or an activator ADP
Y	Denotes an inhibitor specifically PEP or the single letter code for tyrosine

Mathematical Terms

AC	The signal amplitude at frequency ω
DC	The average signal at frequency ω
K_{ia}°	Thermodynamic dissociation constant for A in the absence of effector
K_{ia}^{∞}	Thermodynamic dissociation constant for A in the saturating presence of effector
K_{ix}°	Thermodynamic dissociation constant for X in the absence of substrate
K_{ix}^{∞}	Thermodynamic dissociation constant for X in the saturating presence of substrate
ε	Extinction coefficient
[A]	Concentration of ligand/substrate
[E]	Concentration of enzyme
[ES]	Concentration of enzyme substrate complex
ΔG	Coupling free energy
ΔG_a	Coupling free energy for A
ΔG_{aa}	Coupling free energy for the interaction between A and A
$\Delta G_{a/y}$	Coupling free energy for A in the saturating presence of Y
ΔG_{ay}	Coupling free energy for the interaction between A and Y
ΔG_y	Coupling free energy for Y
ΔG_{yy}	Coupling free energy for the interaction between Y and Y
$\Delta G_{y/a}$	Coupling free energy for Y in the saturating presence of A
μM	Micromolar

μg	Microgram
I	Intensity
K	Dissociation constant
Ka	The association constant or the Michaelis constant for A
$K_{1/2}$	The concentration of ligand that produces half-maximal change
k_{ca}	The catalytic rate constant at saturating substrate concentrations
K_d	Dissociation constant
KDa	Kilodalton
Km	Michaelis constant
M	Molar or demodulation
Max	Maximal change in activity or Hill number
mg	Milligram
mL	Milliliter
mM	Millimolar
n	Binding stoichiometry
n_H	Hill number
nm	Nanometer
ns	Nanosecond
p	Polarization
Q	Coupling constant for an allosteric interaction which alters binding affinity
Q_{aa}	Coupling constant for the interaction between A and A
Q_{ay}	Coupling constant for the interaction between A and Y

R	Gas constant
r	Anisotropy
r_0	The anisotropy without rotational diffusion (limiting anisotropy)
r_∞	The anisotropy approached as a result of the depolarization effect of the hindered rotation
[S]	Concentration of substrate
T	Temperature
τ	Fluorescence life time
U	Units
v	Initial velocity
V_{max}	Maximal velocity
V_o	Initial rate of turnover
W_{ax}	Coupling constant for an allosteric interaction which alters the maximal velocity
[X]	Concentration of effector
θ	Rotational correlation time
η	viscosity of the solution
κ	Boltzman constant
m°	Modulation
δ	Phase angle
σ	The phase shift
Φ1	The rotational correctional time for the fast local motion
Φ2	The rotational correctional time for the slow global motion

TABLE OF CONTENTS

CHAPTER Page

LIST OF TABLES

LIST OF FIGURES

FIGURE Page

FIGURE Page

FIGURE Page

FIGURE Page

CHAPTER I

INTRODUCTION

Regulation is very important in all kinds of activities. At the macroscopic level in general, a regulation is a legal restriction promulgated by government administrative agencies through rulemaking. At a microscopic level in life science, regulation occurs at different levels, including DNA replication, RNA transcription, protein synthesis and post-translational modification. Different levels of regulation in life science gives the cell control over its structure and function and is the basis for cellular differentiation, morphogenesis and the versatility and adaptability of any organism.

Here, we are going to focus on allosteric enzyme regulation, which is a level of protein regulation. In living cells, there are hundreds of different enzymes working together. Living cells neither synthesize nor breakdown more material than is required for normal metabolism and growth. All of this necessitates precise control mechanisms for turning metabolic reactions on and off. Enzymes play major roles in the regulation process. Enzymes catalyze specific biochemical reactions without being consumed in the process and accelerate the reaction tremendously. They are frequently regulated, in contrast to inorganic catalysts, which generally cannot be regulated. Enzymes that are regulated usually stand at cross points of metabolic pathways. There are two basic means

---

This dissertation follows the style and format of *Biophysical Journal*.

to regulate an enzyme: 1) regulate the synthesis of the enzyme or 2) regulate the activity of the enzyme. Enzyme synthesis regulation refers to controlling both transcription of the mRNA needed for enzyme synthesis and translation of the mRNA to protein. In prokaryotic cells, the transcriptional level of enzyme synthesis involves the activation or inhibition of transcription by regulatory proteins that can bind to DNA and either block or enhance the function of RNA polymerase. At the translational level of enzyme synthesis, the bacteria may produce antisense RNA that is complementary to the mRNA coding for the enzyme. When the antisense RNA binds to the mRNA by complementary base pairing, the mRNA cannot be translated into protein and the enzyme is not synthesized. A right balance exists between the enzyme synthesized and consumed in the cell. Enzyme activity regulation is controlled mainly by covalent modification, such as phosphorylation and ubiquitination, and allosteric effects. In addition, some enzymes are stimulated or inhibited when they are bound by regulatory proteins. Others are activated by proteolytic cleavage, which is an irreversible process. The advantage of allosteric regulation is that it may allow fine-tuning of a metabolic pathway since enzyme activity is modulated at a different level. In addition, the allosteric regulation process is reversible. Therefore, enzyme allosteric regulation is particularly important in major metabolic pathways (glycolysis, Krebs cycle, urea cycle, gluconeogenesis, *etc*.), which impact other important and energetically expensive pathways.

Allosteric Regulation

The term allostery comes from the Greek allos, "other," and stereos, "space," referring to the regulatory site of an allosteric protein being separate from its active site. Feedback control is a natural example of allosteric regulation, which means the end product of a pathway can modulate the upstream enzyme activity**.** The allosteric regulation of an enzyme or protein refers to the situation when an effector molecule binds at the protein's allosteric site (that is, a site different from the protein's active site) and either enhances the protein's function (allosteric activators), or diminishes the protein's function (allosteric inhibitors). This regulation can occur in two ways: (1) by altering substrate affinity (K-type system) or (2) by altering the catalytic rate (V-type system). Since a greater percentage of allosteric enzymes are regulated via changes in substrate affinity (K-type system), including glycogen phosphorylase, phosphofructokinase, pyruvate kinase, we are going to focus on K-type regulation and the models used to account for these types of allosteric effects.

Allosteric communication occurs between ligand binding sites. When the ligands are different from each other, it is a heterotropic effect. When the ligands are the same as each other, a homotropic effect is observed. The allosteric effect between different ligand binding sites may have cooperativity. Cooperativity is a characteristic of most oligomeric allosteric proteins and is defined as a nonhyperbolic substrate or ligand saturation profile (Reinhart, 1988). The changes in ligand binding affinity are observed with changing of the ligand concentrations. With increasing ligand concentration, positive cooperativity is observed as an increase in ligand binding affinity, while

negative cooperativity is shown as a decrease in ligand binding affinity. Non-cooperative binding is observed when the ligand binding affinity does not change.

For the heterotropic effect, the binding of an allosteric ligand can increase or decrease the binding affinity of substrate, and vice versa. Heterotropic cooperativity may be observed due to the ligand binding and can be found in two classes: (1) heterotropically induced homotropic cooperativity and (2) subsaturating heterotropic cooperativity. The first class describes that the binding of the effector changes the coupling between substrate binding sites. The homotropic cooperativity between the substrate binding sites can be negative or positive. The second class arises when the effector is at intermediate concentrations and is positive regardless of the nature of the heterotropic interaction (Reinhart, 1988).

For the homotropic effect, positive cooperativity is shown by sigmoidal binding profiles and occurs when the binding of the first ligand enhances the binding affinity of the second one. When there is no cooperativity, the binding of the first ligand does not affect the binding of the subsequent ligand, which is a hyperbolic binding profile. Negative cooperativity is observed when the subsequent binding affinity decreases and can be seen by a shallow slope in the binding profiles (Reinhart, 2004).

Allostery is a direct, rapid and efficient regulatory mechanism to respond to the changes in the concentration of small molecules in the cell. Thus, the allosteric effect and how it is transmitted through the enzyme has been extensively studied in the past decades. Different methods were applied to address this question. For example, site-directed mutagenesis is a method used to establish the importance of a specific amino

acid residue (Lau et al., 1987; Lau and Fersht, 1987 and 1989; Wang and Kemp, 1999; Kimmel and Reinhart, 2000; Pham et al., 2001). Another way to investigate allosteric regulation has been the use of hybrid enzymes to isolate and characterize specific allosteric interactions and study their function (Ackers et al. 1992; Kimmel and Reinhart, 2001; Fenton et al., 2004). In addition, by taking advantage of the known crystal structures of homologous enzymes in different ligation states, the structural stability constants were determined for each residue in an enzyme by Freire and colleagues (based upon the comparison to other crystal structures and using the COREX algorithm). The stability constants for each residue were mapped onto the structure of the protein to understand what role protein stability plays in ligand binding and the transmission of the allosteric information (Hilser et al., 1998; Freire, 1999; Luque and Freire, 2000). Recently, researchers have focused on finding an allosteric site in a protein since it provides promising alternatives for drug discovery (Hardy et al., 2004; Lindsley and Rutter, 2006). Hardy and colleagues apply a tethering method for trapping inhibitory small molecules at the sites away from the active site by reversible disulfide bond formation in Caspase. The tethering method is based on the reversible formation of a disulfide bond between a native or engineered cysteine residue in the protein and a member of a library of thiol-containing fragments. Eventually, a previously unreported and conserved allosteric site in a deep cavity at the dimer interface 14 Å from the active site was found. This site contains a natural cysteine that, when disulfide-bonded with a specific compounds, prevents peptide binding at the active site. In short, many methods

have been developed and used to identify specific residues and important regions of proteins involved in the transmission of an allosteric signal.

To improve on understanding how allosteric enzymes function, phosphofructokinase from *E. coli* (EcPFK) is used as a model system in this thesis.

Classic Models for Allosteric Regulation

Traditionally, researchers used two-state theories, such as the concerted model Monod-Wyman-Changeux (MWC) and the sequential model (KNF), to explain allosteric regulation in oligomeric proteins, including positive cooperativity, allosteric activation and allosteric inhibition. The two states are the T-state or "tense state" and the R-state or "relaxed state". The T-state is the state when the inhibitor can bind to the protein. The R-state is the state of the protein when the substrate and the activator can bind.

The MWC model predicts that the total allosteric effect would be realized in a single interaction in an oligomeric protein (Monod et al., 1965). When substrate binds to the free enzyme, it shifts the equilibrium to the "R" state in a concerted transition (Figure 1-1A). Positive cooperativity is observed when the first substrate binding event facilitates the binding of the following substrates. Activators also bind to the "R-state", and shift the equilibrium towards the "R-state". In the presence of an activator, the enzyme is already in the "R-state", so the substrate saturation profile lacks cooperativity. On the other hand, when an inhibitor binds to the enzyme, the equilibrium is shifted towards the "T-state" in a concerted transition reducing the number of "R" sites

available to bind substrate. Thus, when performing a substrate saturation profile at any given inhibitor concentration, positive cooperativity will be observed since the number of the competent substrate binding sites are increased. The equilibrium is shifted back towards the "R-state" with increasing the number of accessible "R" sites. A major shortcoming to the concerted model is its inability to explain negative cooperativity, part of which was the motivation for the development of the sequential model.

The KNF model predicts that there are equal contributions from each binding event (Koshland et al., 1966). It assumes an induced-fit situation in which a conformational change occurs when a ligand binds to one subunit of the enzyme (Figure 1-1 B). This conformational change can affect the conformational change of the other neighboring subunits, either positively or negatively depending on the character of the ligand. The subsequent subunits change conformation sequentially with the binding of each ligand equivalent. As a result, the complete conversion from one state to another is observed only when all sites are bound with ligand.

The MWC and KNF models are not accurate for all allosteric enzymes. They only recognize the existence of binary complexes for either enzyme and substrate or enzyme and effector, but not the ternary complex with both substrate and effector bound, particularly when the effector is an inhibitor. Moreover, the R state and T state are only two potential conformations observed during the ligand binding process. A more complete analysis of allosterism was developed, in which changes in ligand binding are described by free energy, rather than structural changes. This linkage analysis will be the

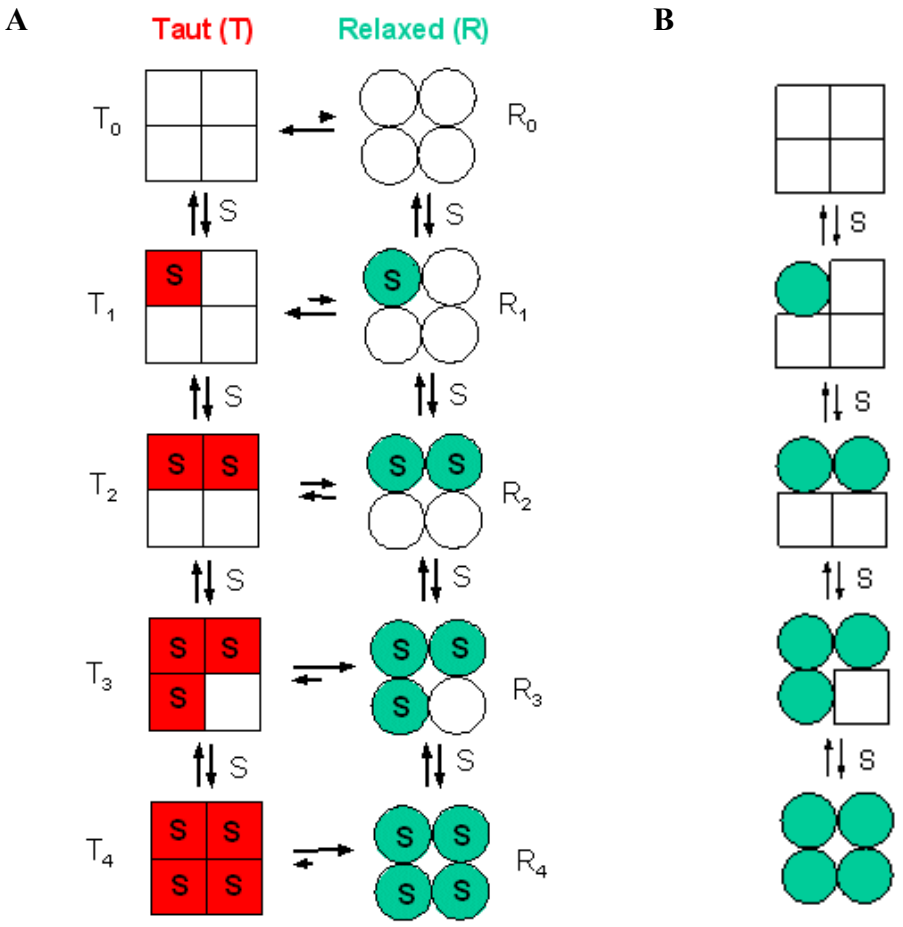

Figure 1-1 Diagrams of the MWC model and the KNF model for allosteric regulation of a tetrameric protein. S is the substrate. □ represents T state, ○ represents R state. Figure (A) represents the concerted model, when substrate bound; all of the subunits change conformation at the same time. Figure (B) describes the sequential model. Each subunit is able to change conformation individually. The complete conformational change for the tetramer needs substrates bound to all subunits. While these two models are elegant in their simplicity, they do not accurately describe the allosteric effect.

focus of the following paragraphs (Wyman, 1964; Weber, 1972 and 1975; Reinhart, 1983, 1985,1988 and 2004).

Linkage Analysis

Thermodynamic linkage is used as a framework to investigate the allosteric interactions (Figure 1-2). The idea of linkage was first proposed by Wyman (1964 and 1967). Later Weber (1972 and 1975) applied this analysis to describe an allosteric effect between two ligands binding to two separate sites on a protein. Moreover, the thermodynamic basis was established when the binding effect was considered in free energy terms (Weber, 1972 and 1975; Reinhart, 1983, 1985,1988 and 2004).

The linkage analysis approach describes ligand binding in free energy terms without assuming the nature of structural changes caused by ligand binding. The basic principle of thermodynamic linkage is reciprocity. That is to say that the effect that substrate (A) has on the binding of effector (X) to the enzyme (E) must equal that of (X) on the binding of (A) to (E). E, A, X and P represent enzyme, substrate, effector and product, respectively. The dissociation constants for each equilibrium in the thermodynamic box are described as follows:

$$K_{ia}^{\circ} = \frac{[E][A]}{[EA]} \qquad (1\text{-}1)$$

$$K_{ia}^{\infty} = \frac{[EX][A]}{[XEA]} \qquad (1\text{-}2)$$

$$K_{ix}^{\circ} = \frac{[E][X]}{[EX]} \qquad (1\text{-}3)$$

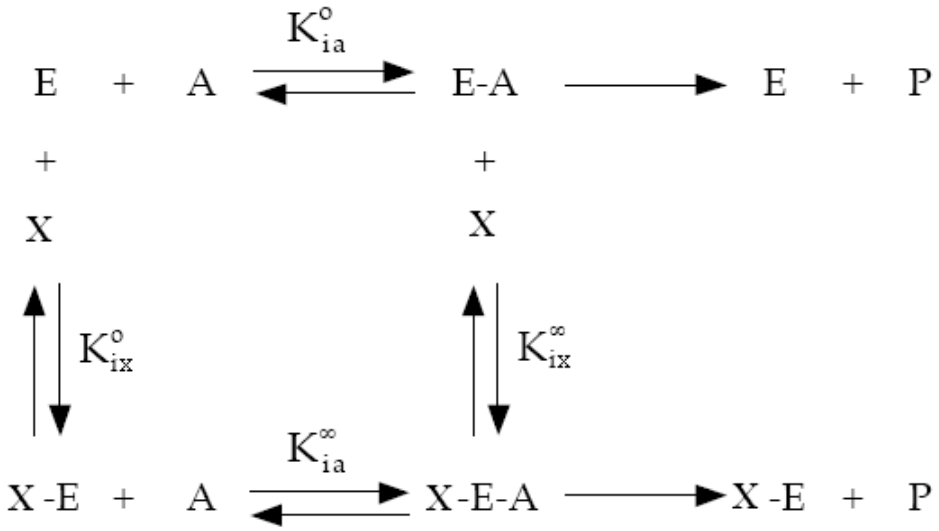

Figure 1-2 Thermodynamic box for a single substrate (A) and a single allosteric effector (X). There are four different ligation states that the enzyme can adopt: E, EA or XE or XEA. Each ligation state is unique and can have different functional properties. This is in contrast to the two-state models, which only allow for the existence of the T-state or the R-state, without the ternary complex because the enzyme can bind only one type of ligand, either A or X, but not both.

$$K_{ix}^{\infty} = \frac{[EA][X]}{[XEA]} \qquad (1\text{-}4)$$

where K_{ia}° and K_{ia}^{∞} represent the dissociation constants of A in the absence of X and in the saturation concentration of X, respectively. K_{ix}° and K_{ix}^{∞} represent the dissociation constants of X in the absence of A and in the saturation concentration of A, respectively. The influence between A and X can be described by the coupling constant Q_{ax}, which gives the nature and magnitude of the coupling between A and X.

$$Q_{ax} = \frac{K_{ia}^{\circ}}{K_{ia}^{\infty}} = \frac{K_{ix}^{\circ}}{K_{ix}^{\infty}} \qquad (1\text{-}5)$$

Q_{ax} also represents the thermodynamic disproportionate equilibrium constant for the following reaction:

$$XE + EA \leftrightarrows XEA + E$$

$$Q_{ax} = \frac{[XEA][E]}{[XE][EA]} \qquad (1\text{-}6)$$

The value of Q_{ax} describes the nature of the effect caused by X. When $Q_{ax} > 1$, X is an activator and when $Q_{ax} < 1$, X is an inhibitor. When $Q_{ax} = 1$, X has no effect on the binding of A to E. Since Q_{ax} is a thermodynamic parameter, the equilibrium constant is related to the coupling free energy by the following equation:

$$\Delta G_{ax} = -RT \ln Q_{ax} \qquad (1\text{-}7)$$

Correspondingly, inhibition has a positive coupling free energy; activation has a negative coupling free energy; zero coupling free energy means there is no allosteric

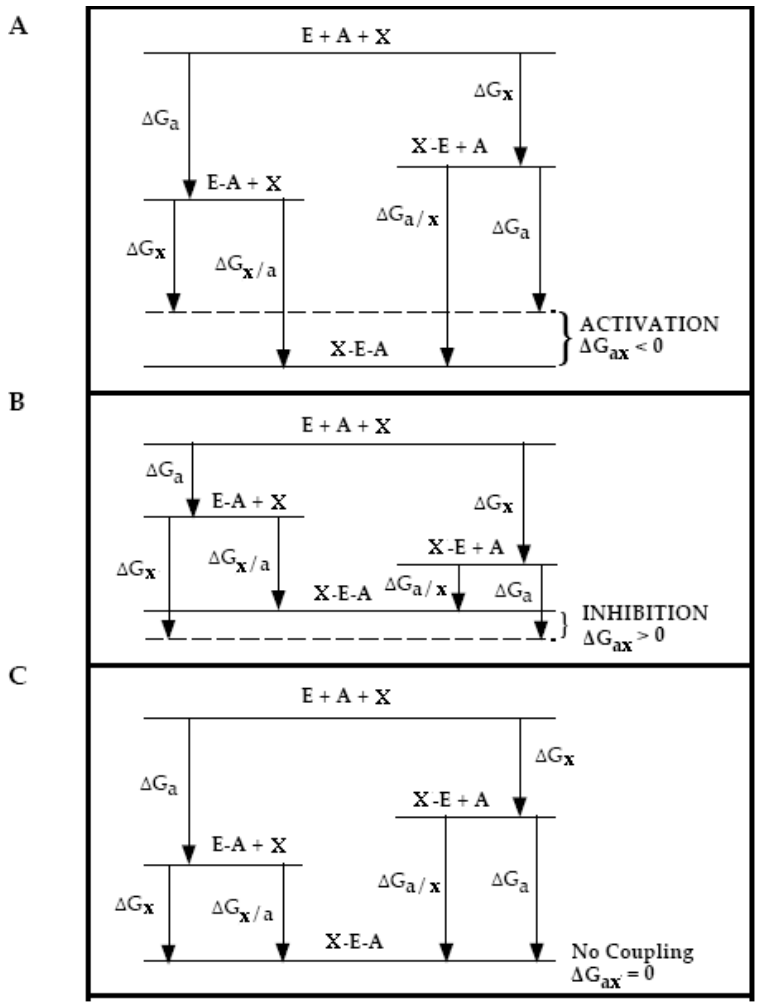

Figure 1-3 Three coupling free energy diagrams representing either (A) activation, (B) inhibition or (C) no allosteric effect at all for the binding of two individual ligands (A or X) to an enzyme E in which ΔG_{ax} is the coupling free energy associated with binding A and X. (*A*) When $\Delta G_{ax} < 0$, activation occurs. (*B*) When $\Delta G_{ax} > 0$, inhibition occurs. (C) When $\Delta G_{ax} = 0$, no allosteric effect is measured. Diagrams adapted from Weber (1972 and 1975).

effect (Figure 1-3).

The rate equation for the mechanism shown in Figure 1-2 can be written if the substrate is assumed to achieve rapid equilibrium during steady-state (Reinhart, 1983; Symcox and Reinhart, 1992):

$$\frac{v}{[E]_t} = \frac{V^\circ K_{ix}^\circ [A] + QW_{ax}[A][X]}{K_{ia}^\circ [X] + K_{ix}^\circ [A] + K_{ix}^\circ [X] + Q_{ax}[A][X]} \qquad (1\text{-}8)$$

where v is the initial velocity, V° is the maximal activity in the absence of X. K_{ia}° is the dissociation constant for substrate A in the absence of effector X and K_{ix}° is the dissociation constant for effector X in the absence of substrate A, respectively and W_{ax} is the ratio of V^∞/V°. V^∞ is the maximal activity in the saturation concentration of effector X. When the maximal activity is affected by the allosteric ligand, W_{ax} will not be equal to 1.

Experimentally the coupling constant, Q_{ax}, can be obtained by determining the apparent dissociation constants for the substrate A as a function of effector concentration and can be graphically depicted for X being an inhibitor or an activator (Figure 1-4). The dependence of the apparent dissociation constant of substrate, $K_{0.5,}$ on the effector concentration can be determined by the following equation:

$$K_{0.5} = K_{ia}^\circ \left[\frac{K_{ix}^\circ [X]}{K_{ix}^\circ + Q_{ax}[X]} \right] \qquad (1\text{-}9)$$

Although no cooperativity is predicted by Equation 1-8 and Figure 1-2, Equation 1-9 can still be applied to an oligomeric protein, like EcPFK (Reinhart, 1983). The apparent

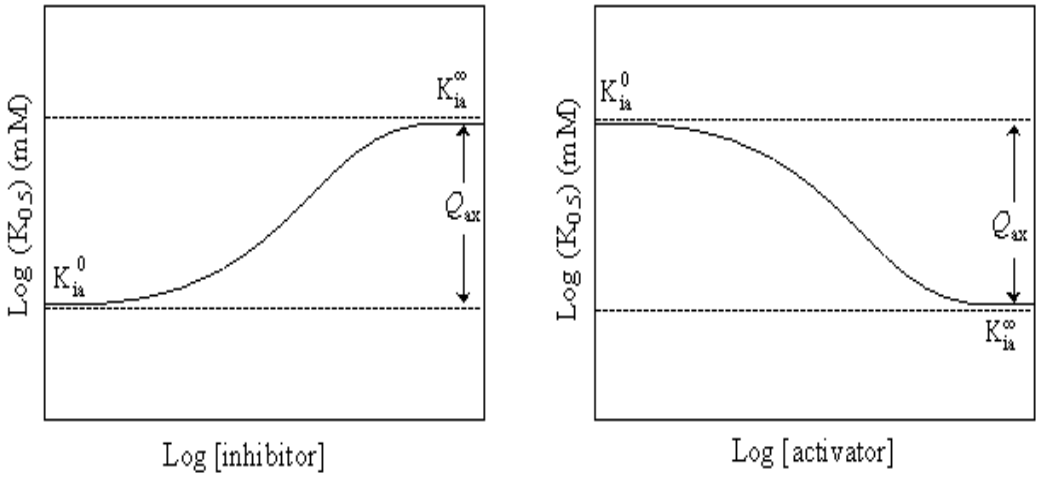

Figure 1-4 Graphical representation of the coupling constant Q_{ax}, which is the difference between the two plateaus. The apparent dissociation constant for substrate $K_{0.5}$ increases as a function of inhibitor concentration and decreases as a function of activator concentration.

dissociation constant for substrate, $K_{0.5}$ is the concentration at which the velocity is at half maximum and is described by the Hill equation (Hill, 1910):

$$\frac{v}{[E]_t} = \frac{k_{cat}[A]^{n_H}}{K_{0.5}^{n_H} + [A]^{n_H}} \qquad (1\text{-}10)$$

where v is the rate of the reaction, E_T is total enzyme active sites, k_{cat} is the turnover number and n_H is the Hill number that depicts cooperativity in substrate binding. When $n_H > 1$, positive cooperativity is observed; when $n_H < 1$, negative cooperativity is obtained; and when $n_H = 1$, there is no cooperativity.

Phosphofructokinase

Phosphofructokinase (PFK, EC 2.7.1.11) may be classified in three groups differing in molecular mass: from mammals, yeast and bacteria. This enzyme from mammalian cells has been most studied (Li et al., 1999; Kemp and Gunasekera, 2002), has a subunit molecular weight from 75000 to 95000 Da, and forms a tetramer that aggregates to oligomers (Reinhart and Lardy, 1980). PFK from yeast is a $\alpha_4\beta_4$ octamer with subunit molecular masses of 112000 to 118000 Da. All the PFKs from eukaryotes have complex allosteric regulation (Clifton and Fraenkel, 1982; Poorman et al., 1984). Bacterial PFKs form a tetramer with a molecular weight of 34000 Da for each subunit. In general, PFKs from all different sources are inhibited by ATP and citrate, and activated by ADP, AMP, fructose-2, 6-bisphosphate and cyclic AMP.

Phosphofructokinase from *E. coli* (EcPFK) catalyzes the first committed step in glycolysis, which is the transfer of a phosphoryl group from MgATP to fructose-6-

phosphate (Fru-6-P) to produce MgADP and fructose-1, 6-bisphosphate (FBP) (Figure 1-5). EcPFK has a molecular weight 34000 Da for each subunit. MgADP activates EcPFK by increasing the affinity for Fru-6-P, which is a response to the low energy in the cell. Phosphoenolpyruvate (PEP) is a downstream product of glycolysis, and it inhibits EcPFK by decreasing the affinity of EcPFK for Fru-6-P. Thus, EcPFK is subject to "K-type" regulation (Uyeda, 1979; Evans et al., 1981). Other molecules that have been shown to regulate EcPFK activity include MgGDP (activator), MgATP (inhibitor) and 2-phosphoglycolate (inhibitor) (Blangy et al., 1968; Kolartz and Buc, 1982; Johnson and Reinhart, 1992, 1994 and 1997; Tlapak-Simmons and Reinhart, 1994 and 1998). The other substrate for EcPFK is MgATP. Although the allosteric interaction between MgATP and the effectors is relatively small (Johnson and Reinhart, 1992), it still contributes to the allosteric regulation of EcPFK and makes the allosterism complex. Both MgADP and PEP bind to the same allosteric site in EcPFK. Therefore, we are interested in investigating how these two molecules regulate EcPFK from the same site with different effects. Most importantly, how allosteric information is transmitted between active sites and allosteric sites is the key question to be addressed.

So far, PFKs from different bacterial sources have been studied. In our lab, the other extensively studied PFK is from *Bacillus stearothermophilus* (BsPFK). EcPFK and BsPFK have many similar characteristics. They show 73% similarity and 54% identity in amino acid sequence (Figure 1-6). The crystal structures of both enzymes have been solved and the α-carbon traces are nearly superimposable (Evans and Hudson, 1979;

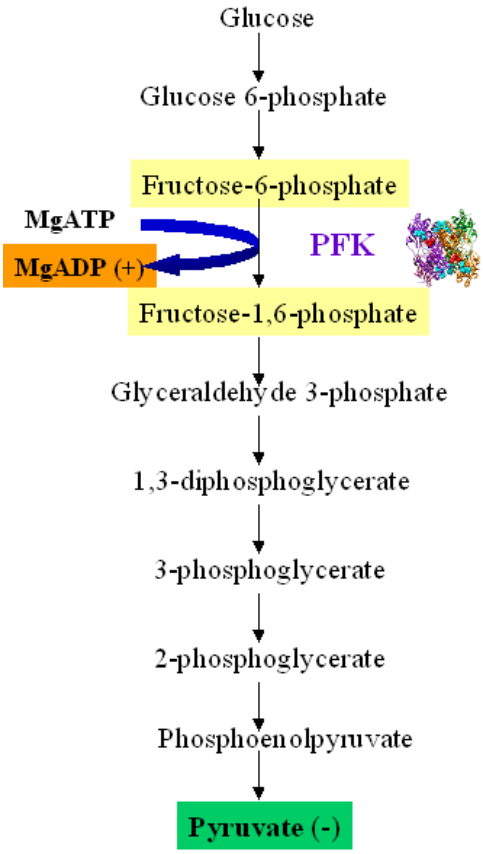

Figure 1-5 The reaction catalyzed by Phosphofructokinase (PFK) within the glycolytic pathway. MgADP activates and PEP inhibits PFK.

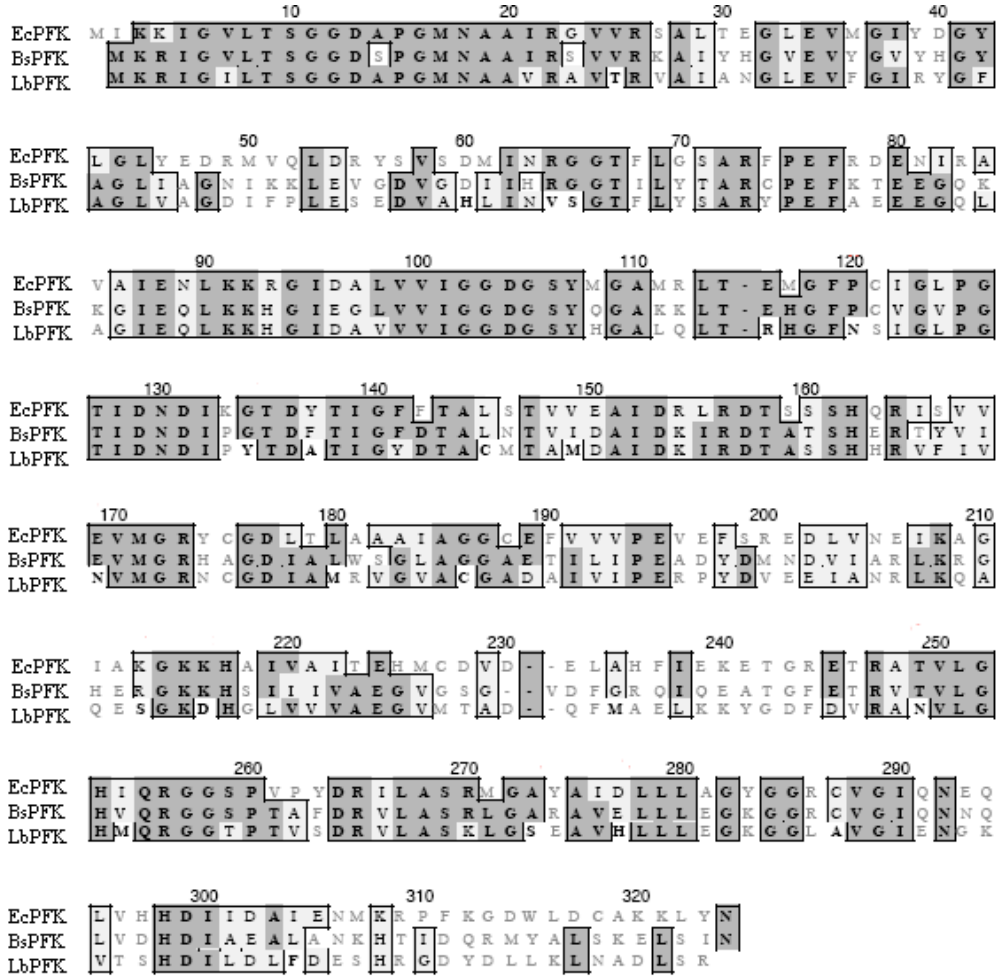

Figure 1-6 Sequence alignments of PFKs from different bacterial sources. EcPFK is PFK from *E. coli*. BsPFK is PFK from *Bacillus stearothermophilus.* LbPFK is PFK *Lactobacillus delbrueckii*.

Evans et al., 1981; Shirakihara and Evans, 1988). The crystal structures of EcPFK and BsPFK show the binding site residues to be almost identical (Shirakihara and Evans, 1988; Schirmer and Evans, 1990; Evans et al., 1986). Both enzymes are homotetramers (with subunit molecular weight ~34 KDa) arranged as a dimer of dimers. Each subunit is composed of a large domain and a small domain, and each domain contains a central β-sheet sandwiched between several α-helices. Both the Fru-6-P and the allosteric effector binding sites are located at the two different dimer-dimer interfaces of the protein. Thus, residues from both sides of the interface are involved in binding. Each subunit contributes two half Fru-6-P (active) sites and two half allosteric sites, resulting in an average of each subunit containing one full active site and one full allosteric site (Figure 1-7). In detail, the Fru-6-P site is at the cleft between the large domain and the small domain. The MgATP binding site, located close to the Fru-6-P binding site, is located entirely in the large domain.

The two PFKs have a lot of similarity in general characteristics. However, the kinetic and allosteric characteristics are quantitively different. Without any effectors and in the presence of saturating concentration MgATP, EcPFK displays positive cooperativity for Fru-6-P binding with a Hill number of 3.8 (Blangy et al., 1968; Johnson and Reinhart, 1992), but there is no such cooperativity observed for BsPFK (Valdez et al., 1989). However, subsaturating heterotropically induced homotropic cooperativity is observed for BsPFK in which positive cooperativity between Fru-6-P binding sites is observed only at intermediate PEP concentrations (Reinhart et al., 1989; Kimmel, 2001; Kimmel and Reinhart, 2001). The other effector, MgADP, has strong

allosteric activation with respect to EcPFK, but has a minimal effect on BsPFK. Below 16°C, no activation is observed in BsPFK. Very little activation is observed at 25°C. With increasing temperature, the activation is increased. This temperature-induced crossover of allosteric response by MgADP is not observed in EcPFK (Braxton et al., 1994). In summary, the extent of PEP inhibition is greater and MgADP activation is smaller for BsPFK than EcPFK. The allosteric properties of BsPFK are also dependent on pH (Deville-Bonne et al., 1991), unlike those of EcPFK.

Phosphofructokinase from *Lactobacillus delbrueckii* subspecies *bulgaricus* (LbPFK) is another enzyme studied in our laboratory. LbPFK was reported to be non-responsive to MgGDP or MgADP. Inhibition of activity by PEP was observed at pH 6 but not at pH 8.2 (Le Bras et al., 1991). The amino acid sequence of this relatively non-allosteric PFK is 47% identical and 66% similar to that of EcPFK, and 56% identical and 74% similar to BsPFK (Figure 1-6). The structure of LbPFK is similar to EcPFK and BsPFK (Paricharttanakul et al., 2005). On one hand, this enzyme can be used as a blank template to study allosteric regulation since it displays weak allosteric responses. On the other hand, sequence alignment between EcPFK and LbPFK may suggest some important residues for EcPFK allosteric communication.

Focusing on phosphofructokinase from *E. coli*, it is a homotetramer with each subunit having a molecular mass of 34 KDa. The crystal structure is shown in Figure 1-7. A single EcPFK subunit has on average one active site and one allosteric site. Therefore, a tetramer has four identical active sites and four identical allosteric sites. All these sites

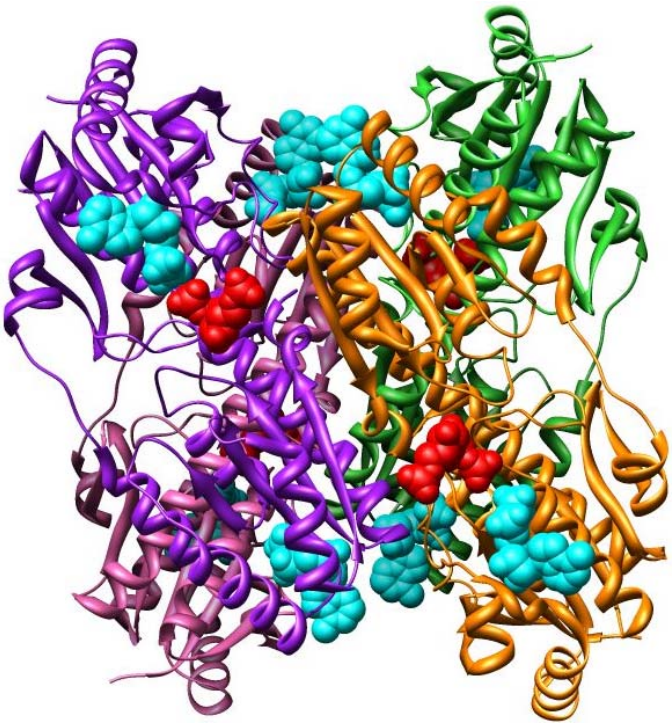

Figure 1-7 Crystal structure of EcPFK with the products, fructose-1, 6-bisphosphate (FBP) and MgADP bound, in the active site; and MgADP, in the allosteric site. Subunits are colored in purple, green, pink and orange. FBP and MgADP are shown in red and cyan, respectively.

can potentially interact with each other, giving a total of 28 possible pair-wise allosteric interactions between the eight binding sites. Of the 28 pair-wise allosteric interactions, 16 are heterotropic interactions and 12 are homotropic interactions (Figure 1-8). There are potentially 10 unique interactions total, four heterotropic interaction between the active site and the allosteric site, three homotropic interactions between the active sites, three homotropic interactions between the allosteric sites (Figure 1-9). The investigation of these different kinds of interactions can provide us with an energetic blueprint that ultimately must result from the molecular basis for allosteric behavior in EcPFK. However, the complicated communications in the tetramer make the investigation difficult.

In an attempt to simplify the complicated allosteric communications, a functional hybrid tetramer of EcPFK has been constructed in which only a single active site and a single allosteric site are capable of binding their respective ligands with high affinity. Also, surface charge mutations have been added to the mutant PFK that allow the separation of the different hybrid species. Both the hybrid BsPFK and EcPFK tetramers have been made successfully *in vitro* (Ortigosa et al., 2004; Fenton et al., 2004). The four unique heterotropic interactions have been named as the 23Å, 30Å, 33Å, and 45Å interactions based on the distances in the EcPFK crystal structure (Figure 1-10). These distances were measured within the crystal structure from the phosphorus atom of one of the bound Fru-6-P molecules to the β-phosphorus atom on the bound ADP molecules in each of the four allosteric sites.

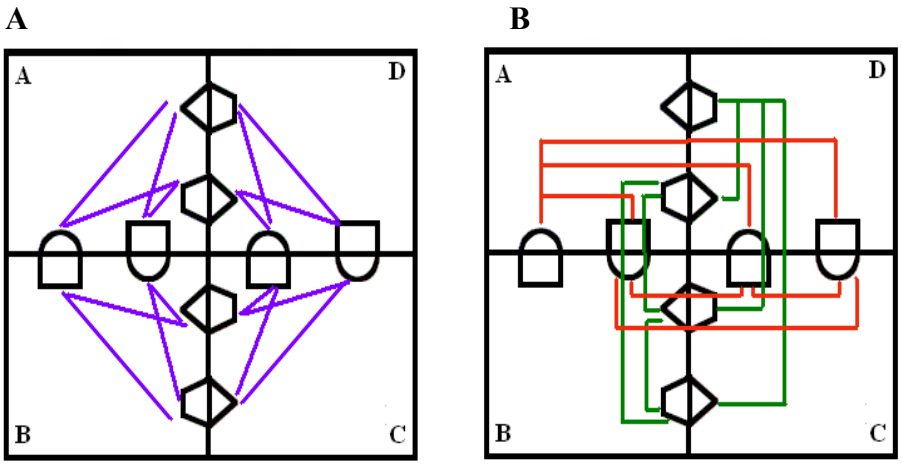

Figure 1-8 Two-dimensional representation of the PFK tetramer. The active site interface lies vertically and the allosteric site lies horizontally at each individual interface. (A) shows the 16 heterotropic interactions (shown in purple). (B) shows the 6 homotropic interactions between the active sites (shown in green) or allosteric sites (shown in red).

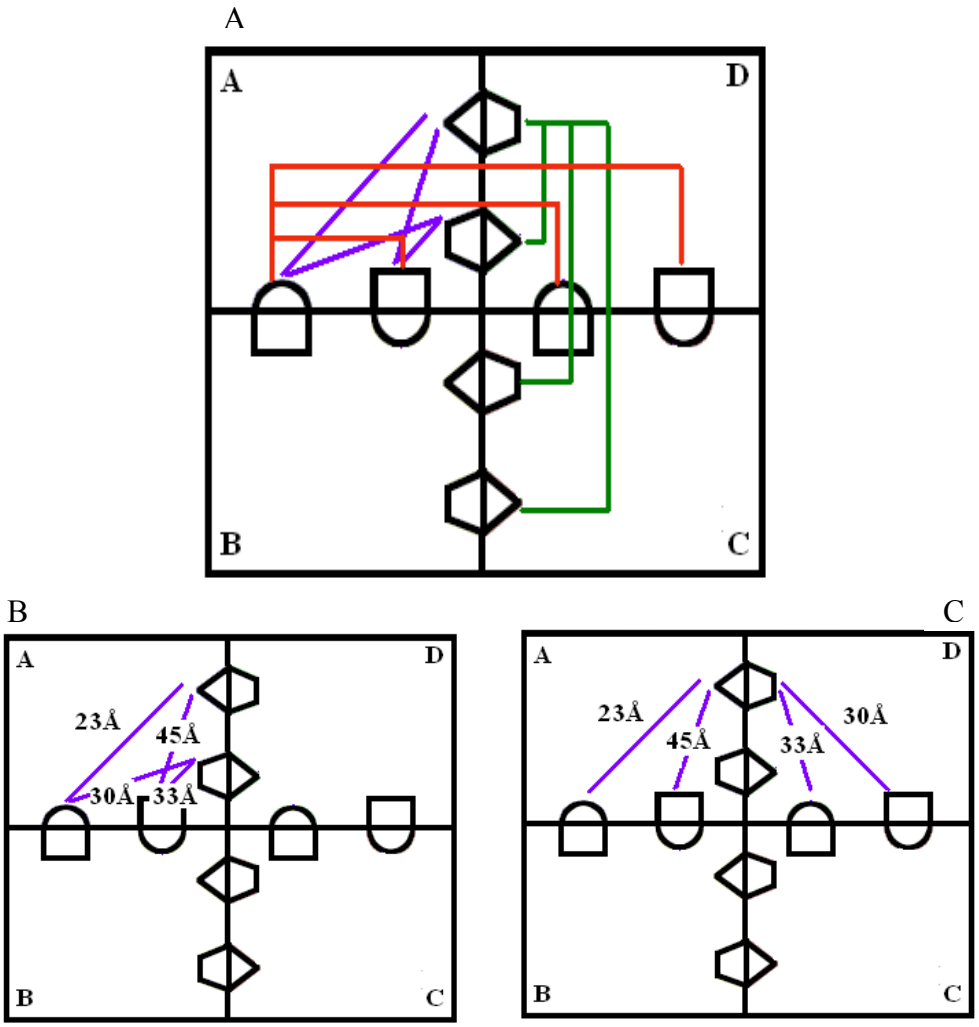

Figure 1-9 (A) The 10 unique interactions are shown: the three homotropic interactions between active sites are in green, the three homotropic interactions between allosteric sites are in red; and the four heterotropic interactions are in purple. The four unique heterotropic interactions are shown in either (B) one subunit or (C) two subunits.

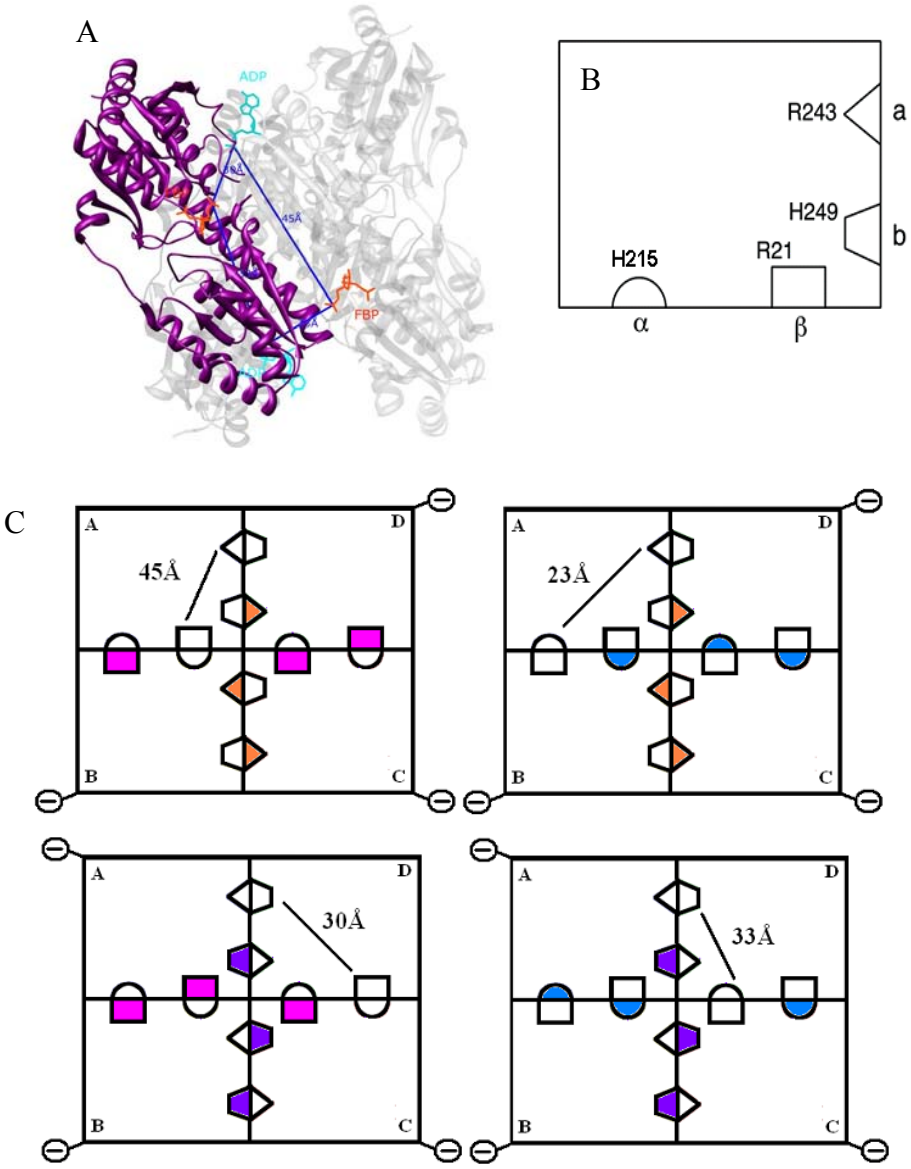

Figure 1-10 Representation of the four heterotropic interactions in EcPFK. (A) is the crystal structure of EcPFK showing the four heterotropic interaction in one subunit. (B) is the two dimensional representation of the active site residues and the allosteric site residues used to represent the four heterotropic interactions. (C) shows the four heterotropic interactions individually. There is only one native subunit in each EcPFK tetramer.

In this study, the coupling free energy between active site and allosteric site for the four unique heterotropic interactions were quantified, and residues that are important for the allosteric signal transmission in each heterotropic interaction have been pinpointed. In addition, EcPFK has one native tryptophan at position 311, which is a fluorescence probe that can be used to measure the dynamic properties of EcPFK. Moreover, by substituting conserved phenylalanine or tyrosine residue with tryptophan and mutating the native tryptophan to phenylalanine, tryptophan was placed in various positions in the 1:3 hybrid EcPFK containing the 23Å heterotropic interaction. By measuring steady-state anisotropy and fluorescence lifetime, each tryptophan was used to monitor the local motion within the native subunit that containing the 23Å heterotropic interaction in different ligation states. Eventually, tryptophan will be placed at all possible positions to map the dynamic region in EcPFK.

Related Studies on Allosteric Regulation

Allosteric regulation has been recognized for half a century, but questions have lingered concerning the mechanics of allosteric regulation, and the structural coupling between allosteric and active sites.

Hemoglobin has been extensively studied as a prototype for understanding mechanisms of allosteric regulation. Hemoglobin is a tetramer consisting of two αβ dimers and functions as oxygen transporter in blood. Positive cooperativity is observed when oxygen binds. By making hybrid forms of hemoglobin that contain different numbers of oxygen bound subunits (resulting in the 10 possible hybrids), Ackers and

coworkers identified how cooperativity is transmitted through the protein (Holt and Ackers, 1995). The model is called the Symmetry Rule and is based on the cooperative free energies measured for each of the 10 species, where the cooperative free energy is the difference in the binding free energy measured for the hybrid tetramer and the two dimers that comprise that hybrid tetramer (Ackers et al., 1992 and 2002). Recent studies demonstrate that the symmetric tetramer responds in a synchronous fashion to asymmetric ligation and mutation (Figure 1-11). Thus, communication among the four heme binding sites is not uniform, and tetrameric symmetry is not maintained over the process of O_2 binding (Ackers and Holt, 2006).

The lactose repressor (LacI), another well-studied allosteric system, is a DNA-binding protein which inhibits the expression of genes coding for proteins involved in the metabolism of lactose in bacteria. When lactose is absent, the *lac* repressor is active and binds with high affinity to its operator. When lactose is present, *lac* repressor binding to its operator is inhibited. Kathleen Matthew's group studies the allosteric regulation of the LacI system. Although the crystal structures for the repressed and induced states of LacI are available, the structures do not provide direct information regarding the dynamic allosteric mechanism during the transition between these states. However, recent advances provide the opportunity to decipher contributions to allosteric communication between DNA and the inducer binding sites in the protein. The relevant motions can be interpolated *in silico* using targeted molecular dynamics simulation (TMD) to predict the most probable atomic-level allosteric routes in LacI. The advantage of TMD is that it uses two experimentally determined structures to constrain the

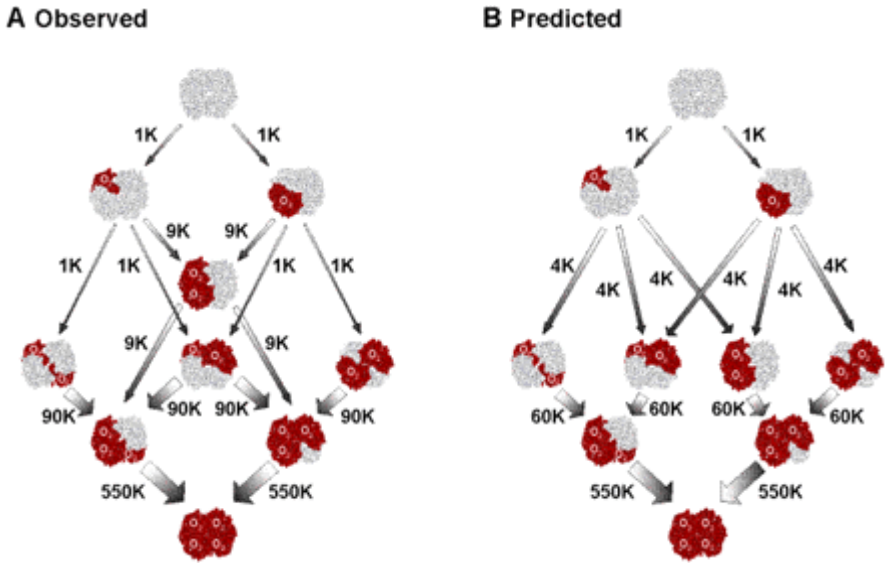

Figure 1-11 Hemoglobin binding cascade, experimental and predicted (adapted from Ackers and Holt, 2006). The stepwise changes in binding constants for each ligation step are shown. Each stepwise K is referenced to the first binding constant, to either the α-subunit heme or to the β-subunit heme. (A) The microstate constants were measured using thermodynamic linkage analysis. Placing one ligand on each dimer is essentially noncooperative under the experimental conditions, whereas placing two ligands on a single dimer occurs with positive cooperativity. (B) The microstate constants predicted by a simple two-state model in which both dimers within the tetramer respond equivalently to ligation.

simulation, dramatically reducing the number of requisite calculations but still retaining the spatial and temporal resolution necessary to reveal relevant motions. The key results predicted by the simulation indicate that movements originate asymmetrically in the inducer-binding site near D149 of one monomer and propagate to the adjacent monomer via a network of noncovalent interactions of three interconnected routes (Zhan, et al., 2006; Wilson et al. 2007).

The Ranganathan group applies a sequence–based statistical method for quantitatively mapping the global network of amino acid interactions in proteins (Lockless and Ranganathan, 1999). The idea of this method is to try to estimate the thermodynamic coupling between residues in a protein. In a protein, the coupling of two sites, whether for structural or functional reasons, should cause the two positions to co-evolve. Three structurally and functionally different protein families were analyzed by doing multiple sequence alignment. They found a small subset of residues forming a network that links distant functional sites in the tertiary structure. In addition, mutagenesis results were consistent with their analysis data.

General Principles of Fluorescence

The phenomenon of luminescence occurs when photons are emitted from an excited state, and includes fluorescence and phosphorescence. The Jablonski diagram shown in Figure 1-12 describes potential energy levels for an excited electron and shows the difference between these two phenomena. S_0, S_1 and S_2 are the ground, first and second state, respectively. Vibration energy levels, described as 0, 1, 2, exist within each

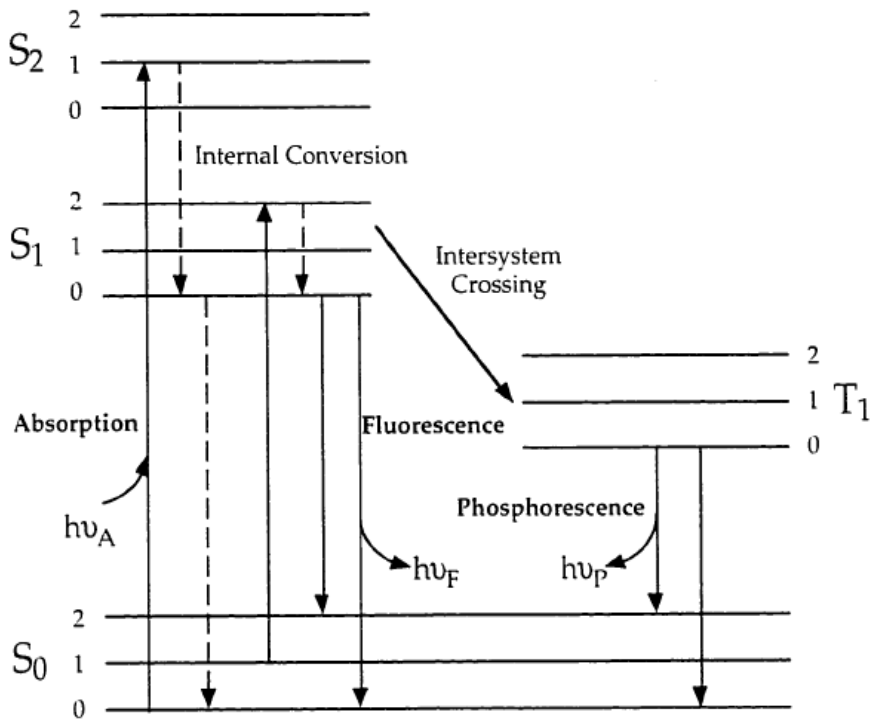

Figure 1-12 Jablonski diagram. An electron is excited to the S_1 or S_2 state by absorption of light. The electron loses energy as it relaxes to the lowest vibrational level of the s_1 singlet state. Most of the time the electrons return to the ground state and in the process emits light, fluorescence. Less often the electron goes through intersystem crossing to the triplet state before relaxing to the ground state, phosphorescence (Lakowicz, 1999 as described originally by Jablonski).

of these electronic energy states. At room temperature, the majority of electrons exist in the lowest energy level, S_0. When light is absorbed, electrons obtain energy and jump to high energy levels of either S_1 or S_2. Through internal conversion, electrons relax to the lowest vibrational energy level of the S_1 state. This process takes on the order of 10^{-12} seconds and is complete before light emission. Fluorescence occurs when the electrons fall from S_1 to the ground state S_0 and release energy in the form of light. The time for this process is on the order of 10^{-8} seconds, or 10 nanoseconds (Lakowicz, 1999). During this time scale many biological events can occur, including local conformational change, rotational motion of large molecules, and protonation and deprotonation (Munro et al., 1979). Phosphorescence occurs when the system undergoes intersystem crossing. That is to say the electrons relax to the T_1 or triplet state before returning to the ground state. In the triplet state T_1, the electrons are unpaired, which means their spins are of the same orientation. However, $S_1$and S_2 states are named as singlet energy states and electrons are paired with spinning different orientation. Return of electrons from S_1 or S_2 to the ground state S_0 do not require the electrons to change their spin orientation, while such a change is needed for the electrons return from T_1 to S_0. The emission from T_1 is called phosphorescence. Since electrons generally decay to ground state, which is the lowest energy level, relatively, the energy of light emitted is less than the energy of light absorbed. The net result is a "Stoke's shift", a shift to higher wavelength for fluorescence light relative to the absorption wavelength. Since emission occurs in the lower energy level, the emission spectrum, a plot of fluorescence intensity vs. wavelength, is not influenced by the excitation wavelength.

Fluorescence lifetime

Fluorescence is emitted in an exponential manner as an electron transitions to the ground state. This decay is described as equation 1-11:

$$I = I^o e^{-k_f t} \qquad (1\text{-}11)$$

where I is the intensity at any time t, I^o is the initial fluorescence intensity at time zero, k_f is the rate constant for the radiative decay process (Figure 1-13). However, other non-radiative decay processes occur during the same time frame. Non-radiative decay processes include intersystem crossing (k_{is}), internal conversion (k_{ic}), and collision quenching ($k_q[Q]$). Thus, the rate of experimental decay is usually much faster than k_f and can be described as equation 1-12:

$$I = I^o e^{-k_{total} t} \qquad (1\text{-}12)$$

where $k_{total} = k_f + k_{is} + k_{ic} + k_q [Q]$ (Cantor and Schimmel, 1980)

The fluorescence lifetime (τ) is given by the reciprocal of all the rate constants in the decay, as shown in equation 1-13:

$$\tau = \frac{1}{(k_f + k_{is} + k_{ic} + k_q[Q])} \qquad (1\text{-}13)$$

The lifetime of the radiative process is defined as (τ_0), shown in equation 1-14:

$$\tau_0 = \frac{1}{k_f} \qquad (1\text{-}14)$$

It should be noted that lifetime does not mean all the excited electrons decay in time τ. τ describes the relaxation time for the excited state.

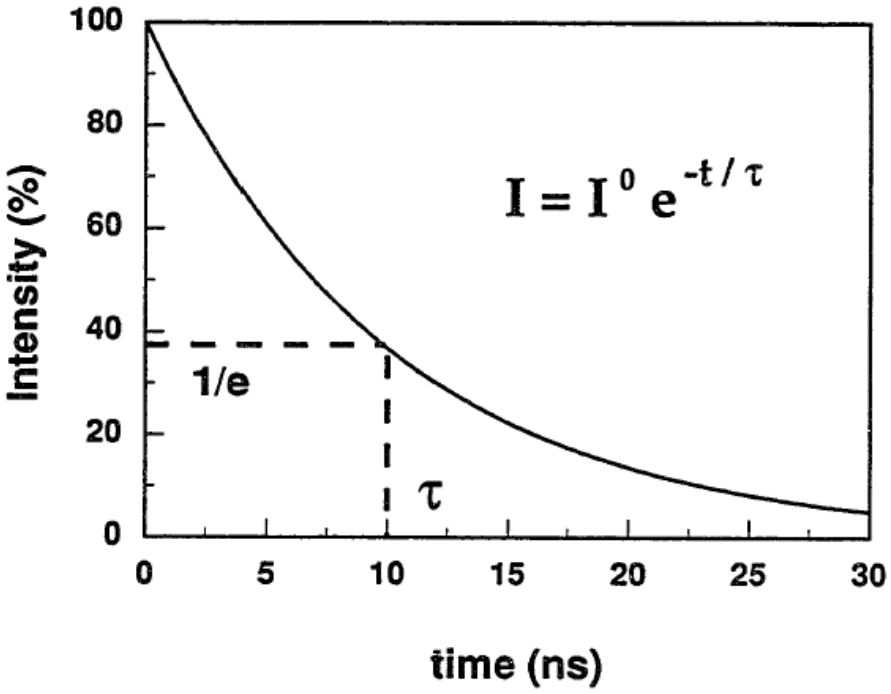

Figure 1-13 Exponential decay of fluorescence intensity. The graph shows the percentage intensity as a function of time for a hypothetical fluorophore, which has a single lifetime at 10 nanoseconds. The fluorescence lifetime is equal to the time where 1/e (63%) molecules have relaxed to the ground state.

Steady-state anisotropy

Anisotropy or polarization is a measurement that describes the rotation of macromolecules in solution. Either intrinsic fluorescence, tryptophan, or extrinsic fluorescence, an attached fluorescence probe, can be used to monitor anisotropy. In the measurement, a sample is excited by vertically polarized light and the subsequent emission is measured through a polarizer either oriented vertically, parallel to the direction of the excitation direction, or horizontally, perpendicular to the excitation direction (Figure 1-14). The anisotropy (r) or polarization (p) is defined in the following equations.

$$r = (I_{\parallel} - I_{\perp})/ (I_{\parallel} + 2I_{\perp}) \qquad (1\text{-}15)$$

$$p = (I_{\parallel} - I_{\perp})/ (I_{\parallel} + I_{\perp}) \qquad (1\text{-}16)$$

Anisotropy is generally used instead of polarization because of its additive nature when a mixture of fluorophores is present. The relationship between anisotropy and polarization is expressed in equation 1-17 and 1-18:

$$p = \frac{3r}{2 + r} \qquad (1\text{-}17)$$

$$r = \frac{2p}{3 - p} \qquad (1\text{-}18)$$

Steady-state anisotropy is measured by exciting the sample with vertically polarized light and detecting the amount of depolarization of the sample by measuring emission light vertically and horizontally. However, the emission detector may not have the same sensitivity to the vertically and horizontally polarized light. This is corrected by measuring a G-factor, which is a ratio of $I_{\parallel}$ and $I_{\perp}$ when the exciting light is

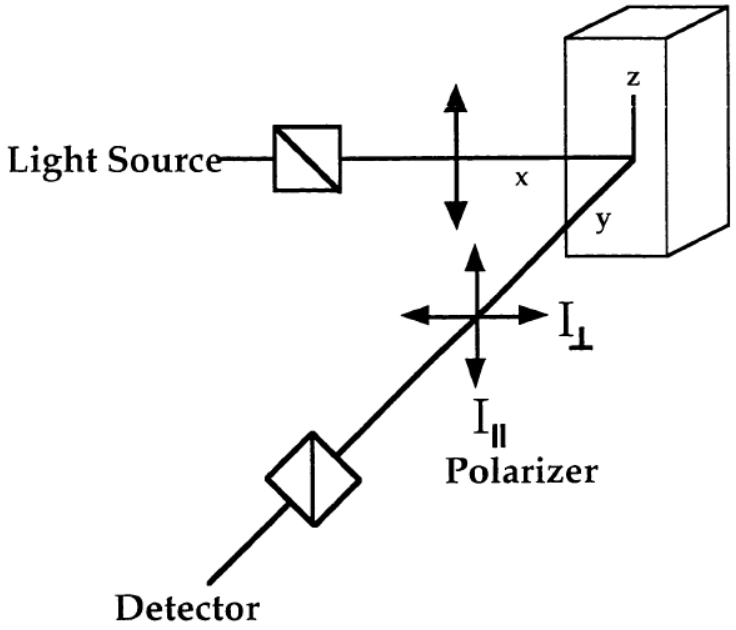

Figure 1-14 Schematic representation of measurement of fluorescence anisotropy. A fluorescent molecule that is oriented near the Z-axis is photoselected for excitation. The total intensity of emitted light is equal to $I_{\parallel} + I_{\perp}$.

horizontally polarized. In a homogeneous solution, the ground state is randomly oriented. When excited by a polarized light, the fluorophore that has absorption transition dipole oriented along the z-axis is excited. This phenomenon is called photoselection. Generally, the absorption along the z-axis is related to $\cos^2\theta$, where θ is the angle between the absorption dipole and z-axis. Under this condition of photoselection, the maximal anisotropy is 0.4 or for polarization is 0.5. Additionally, the excitation wavelength will determine the position of the absorption dipole, and also with the internal conversion leading to the excited ground state, therefore the θ angle can change. For this reason, r_0, which is the anisotropy in the absence of rotational diffusion and energy transfer, is wavelength dependent. Thus, when exciting at longer wavelengths, or at lower energy levels, r_0 has larger values; when exciting at lower wavelengths, or at higher energy levels, r^0 has a smaller values.

Finally, rotation of the fluorophore, either from the local movement of the point of attachment or from the macromolecule's global rotation, may also induce depolarization after absorption. The simplest case for spherical rotors is explained by the Perrin equation (1-19) (Perrin, 1926). The rearranged form is given by equation (1-20), which was used to analyze the data.

$$\frac{1}{r} = \frac{1}{r_0}\left(1 + \frac{\tau}{\theta}\right) \qquad (1\text{-}19)$$

$$\theta = \frac{r\tau}{(r_0 - r)} \qquad (1\text{-}20)$$

where r_0 is the anisotropy without rotational diffusion, θ is the rotational correlation time for the diffusion process, which is the average of global and local rotation in the steady

state, and τ is lifetime of the fluorophore. The anisotropy decays in an exponential manner are similar to intensity decay. θ represents the reciprocal of decay rate constant:

$$r = r_0 e^{-t/\theta} \qquad (1\text{-}21)$$

rotational diffusion is able to be measured using fluorescence only if the rotation rate is similar to the lifetime of fluorescence decay. Rotation correlation time of the macromolecule is related to its physical properties by the following equation:

$$\theta = \frac{\eta v}{\kappa t} \qquad (1\text{-}22)$$

where η is the viscosity of the solution, v is the volume of the macromolecule, κ is Boltzman constant, and t is the absolute temperature. Using Perrin equation, the expected anisotropy for a fluorophore in solvents or for a labeled macromolecule can be calculated. In addition, the rotational correlation time, which represents the motion of the fluorophore, can be calculated with steady-state anisotropy and lifetime values.

Frequency-domain measurement

In order to determine the fluorescence decay rate explicitly, time-resolve techniques must be used. Generally, two methods are applied in time-resolve area: the time-domain method (pulse or impulse response approach) and the frequency-domain method (phase/modulation approach). The time-domain technique excites a sample with a quick, short burst of light and measures the following fluorescence decay (Demas, 1983). The frequency-domain method was used in the experiments and will be discussed in detail.

The frequency-domain method involves exciting a sample with light that is sinusoidally modulated at an angular (ω) frequency. The angular frequency represents

the product of 2π and the frequency of the modulated light of excitation, and is given in units of Hertz (1/sec). The modulation inherent to the excitation beam, m°, which is defined as in equation 1-23:

$$m° = \frac{AC}{DC} \qquad (1\text{-}23)$$

where AC is the signal amplitude at frequency ω and DC is the average signal (Figure 1-15). The intensity of the excitation is:

$$I = DC + AC \sin\delta \qquad (1\text{-}24)$$

where I is the intensity, δ is phase angle between 0 to 90 degree.

The sample will differ from the excitation light, which means it will emit light modulated at the same frequency but delayed in a phase by an angle (σ) and also demodulated with respect to excitation light. Although the direct measurement would be relative to the excitation beam, in reality a reference sample with known lifetime is used whose absorption and emission correspond to that of the sample. The other way is to use a scattering solution such as glycogen to divert the excitation light along the same path as that of the sample, but this may introduce error due to the non-uniform response of the phototube to different wavelengths, termed as the "color effect" (Lakowicz and Gryczynski, 1991). At multiple frequencies, the extent of demodulation and the phase shift angle by the sample are measured. The demodulation is shown in equation 1-25:

$$M = \frac{\frac{AC_S}{DC_S}}{\frac{AC_r}{DC_r}} \qquad (1\text{-}25)$$

where s is sample, r is reference. The phase shift is represented by equation 1-26:

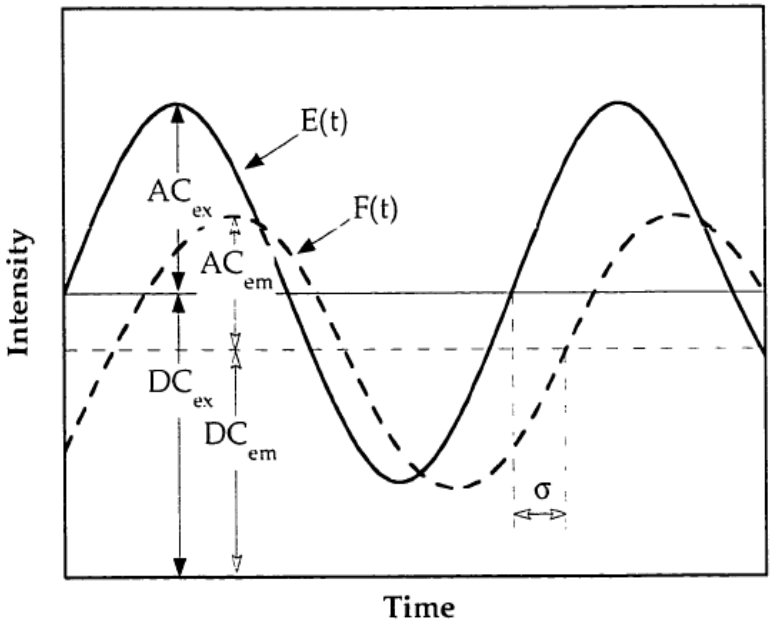

Figure 1-15 Demodulation and phase shift of the fluorescence sinusoid form relative to excitation. When the sample is excited with sinusoidally modulated light (E (t)), the relative emission (F (t)) is demodulated and delayed by phase angle σ.

$$I = DC + AC \sin(\delta+\sigma) \qquad (1\text{-}26)$$

where σ is the phase shift. The relationship at each frequency between the modulation ratio and phase shift and lifetime are described as:

$$\tan(\sigma) = \omega \tau_p \qquad (1\text{-}27)$$

$$M = [1+ (\omega \tau_m)^2]^{-1/2} \qquad (1\text{-}28)$$

τ_p is the lifetime from phase shift and τ_m is the lifetime from modulation ratio. If the sample is homogeneous with a component having a single discrete lifetime, τ_p and τ_m are equal to each other and are the same at all the frequencies (Spencer and Weber, 1969; Weber, 1981). If more than one component exists in solution, τ_p is smaller than τ_m for each frequency. Moreover, if the sample is heterogeneous, τ_p and τ_m will both decrease at each frequency. Low frequencies are more sensitive to the effects of species with longer lifetime, and high frequencies reflect the effects of shorter lifetime components (Figure 1-16). Frequency domain technique is also used to determine dynamic anisotropy, which is termed as differential polarized phase/modulation fluorometry. The advantage of dynamic anisotropy over steady-state anisotropy is the ability to separate and quantify different types of rotations. Because tryptophan in a protein has both slow global motions as well as fast local motions with the side chain, the rate of fluorescence decay in this kind of model is give by equation:

$$r(t) = (r_0- r_\infty) e^{-t/\Phi 1}+ r_\infty e^{-t/\Phi 2} \qquad (1\text{-}29)$$

where r_0 is the limiting anisotropy, r_∞ is the anisotropy approached as a result of the depolarization effect of the hindered rotation, Φ2 is the rotational correctional time for the slow global motion, Φ1 is the rotational correctional time for the fast local motion.

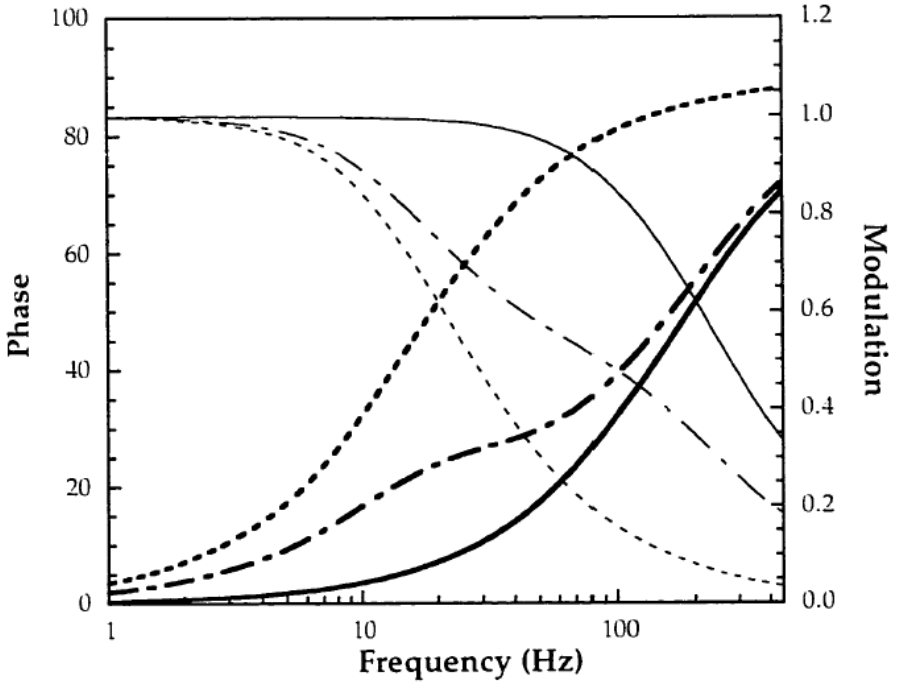

Figure 1-16 Lifetime simulations. The phase angle shift and relative modulation values decrease and increase, respectively. The relationship between phase shift or modulation and frequency depend on the lifetime of the fluorophore. In the graph, fluorophores with different lifetime are shown, 10ns (-----), 1ns (—), a 50/50 ratio mixture of 10 ns and 1 ns (·—·—·).

Dynamic anisotropy under multiple frequencies measures not only the rotational correlation time of local and global motion, but also differentiates the amplitude and rotation rate of local motion. The change of the amplitude is reflected by r_∞, and the change of the rotation rate is indicated by Φ1.

Chapter Overview

The aim of this dissertation is to try to understand the basis of allosteric signal transmission in EcPFK. In addition, we want to investigate dynamic regions of this protein and their response to different ligand binding events. This work highlights the important residues and regions for the allosteric regulation in EcPFK.

Chapter II discusses the materials, experimental procedures and data analysis used in this dissertation for the kinetic characterization of EcPFK to address how allosteric communication is transmitted within EcPFK. It also explains how the steady-state and dynamic fluorescence data were interpreted.

The focus of Chapter III is the formation of hybrid tetramers *in vivo*. The aim was to improve hybrid yield, especially for the 1:3 hybrids that contain a specific heterotropic interaction. Basically, two plasmids with different origins of replication and selection markers were used for expression of wild-type and mutant EcPFKs. After co-transformation into strain RL257 (ΔpfkB::FRT ΔpfkA::FRT), the mixtures of hybrid protein were formed in the cell. In addition, an alternative charge-tag mutation and allosteric site mutation were used to improve hybrid yields.

Based on sequence alignment between EcPFK and LbPFK and predictions that residues that lie between the active site and the allosteric site that may be important for the transmission of the allosteric signal. Chapter VI characterizes several mutant EcPFKs that have diminished allosteric response for both MgADP activation and PEP inhibition. Furthermore, the mutated residues were introduced into each of the 1:3 hybrid tetramers containing the four heterotropic interactions. The influence of each mutation on each heterotropic interaction in EcPFK was quantified with respect to PEP inhibition and MgADP activation.

Chapter V addresses the dynamic properties of the native subunit in the 1:3 hybrid containing the 23Å heterotropic interaction in EcPFK by probing different regions and evaluating the response to the binding of different ligands. Site-directed mutagenesis was used to replace phenylalanine or tyrosine residue at different locations within the protein with tryptophan. In addition, by taking advantage of the hybrid tetramer formation method, each tryptophan was placed at different position in the 1:3 hybrid tetramer containing the 23Å heterotropic interaction. From steady-state fluorescence experiments and frequency-domain measurements, anisotropy and fluorescence lifetime values were measured for each tryptophan in different ligation states. Using the Perrin equation, we interpreted the changes in dynamics at various sites in the 1:3 hybrid containing the 23Å heterotropic interaction in EcPFK.

Finally, Chapter VI summarizes the major ideas of this dissertation.

CHAPTER II

GENERAL METHODS

Materials and Methods

Materials

All chemical reagents used in buffers, protein purifications and enzymatic assays were of analytical grade, purchased from either Fisher-Scientific (Hampton, NH) or Sigma-Aldrich (St. Louis, MO). Mimetic Blue 1 agarose resin from Prometic Biosciences (Montreal, Canada) was used in protein purification. A Mono Q 10/10, anion exchange column was purchased from GE Lifescience (Charlottesville, VA) for use on their Fast Performance Liquid Chromatography (FPLC) system. DE-52 anion exchange resin was obtained from Whatman (Kent, UK). Creatine kinase and the coupling enzymes (aldolase, triosephosphate isomerase and glycerol-3-phosphate dehydrogenase in ammonium sulfate suspensions) were purchased from Roche Applied Science (Indianapolis, IN) or Sigma-Aldrich. The coupling enzymes were dialyzed against buffer containing 50 mM MOPS-KOH, 100 mM KCl, 5 mM $MgCl_2$ and 0.1 mM EDTA at pH 7.0 before use. Creatine phosphate, and the sodium salts of Fru-6-P and PEP were purchased from Sigma-Aldrich. NADH is from RPI (Natick, MA). The sodium salt of ATP and ADP were obtained from Roche Applied Sciences or Sigma-Aldrich. Site-directed mutagenesis was performed using the Altered Sites II *In Vitro* Mutagenesis System or QuickChange Site-Directed Mutagenesis System. Altered Sites II *In Vitro* Mutagenesis System was purchased from Promega (Madison, WI) and

included pALTER vector, pALTER control vector, and ampicillin repair and control oligonucleotides. QuickChange site-directed Mutagenesis System was obtained from Stratagene (La Jolla, CA). All other oligonucleotides were synthesized by Integrated DNA Technologies Inc (Coralville, IA). DNA modifying enzymes (T4 polynucleotide kinase, T4 DNA polymerase and T4 ligase) were purchased from Promega. Qiagen (Hilden, Germany**)** products were used for plasmid purifications. Glycerol stocks of BMH 71-18 muts (a mismatch repair minus strain) and XL1Blue cells were obtained from Promega and Stratagene. Deionized distilled water was used throughout.

Site-directed mutagenesis

pGDR16 and pGDR148 containing the EcPFK gene in pAlter-1 and pALter-EX2, were use to introduce mutations by following the protocol of the Altered sites II *in vitro* Mutagenesis System. Single-stranded pGDR16 and pGDR148 were made using R408 helper phage and purified (Hutchinson et al., 1978).

Firstly, each oligonucleotide was phosphorylated at 5' end using T4 polynucleotide kinase to increase the number of mutants obtained. Then, the mutated oligonucleotide(s) and the ampicillin resistance repair oligonucleotide were annealed to the single stranded DNA. A three to one ratio of mutant oligonucleotide to ampicillin repair oligonucleotide was used to increase the possibility of obtaining a plasmid that contains both the ampicillin repair oligonucleotide and the mutant oligonucleotide(s). In addition, a five to one ratio of ampicillin oligonucleotide to ssDNA was used to increase the probability of the oligonucleotide(s) annealing to the DNA.

The oligonucleotides were extended using T4 DNA polymerase and ligated with T4 DNA ligase. The mutagenesis reaction product was transformed into a mismatch repair minus *E. coli* strain (Zell and Fritz, 1987), BMH 71-18 mutS cells (*thi, sup*E, Δ(*lac-pro*AB), [*mut*S::Tn10], [F′, *pro*AB, *lac*I^qZΔM15]) (Kramer et al., 1984), using the calcium chloride method (Cohen et al., 1972), and grown on Luria-Bertani (LB) plates (10 g/L tryptone, 5 g/L yeast extract and 10 g/L sodium chloride, 15 g/L agar) with ampicillin 100 μg/mL and incubated overnight at 37°C. Meanwhile, the transformation products were inoculated into LB+Amp media and grew overnight. The plasmids from the overnight culture or from the colonies were purified using Qiagen plasmid miniprepare kit. Then the purified plasmids were transformed into competent JM109 (e14–(McrA–), *recA1, endAl, gyrA96, thi-l, hsdR17,* (*r*K– *m*K+), *supE44, relA1,* Δ(*lac-proAB*) [F′, *traD3, proAB, lacI*q*Z*Δ*M15*]) because of the instability of BMH cells. Plasmids were purified from JM109 cells and sequenced using Sanger-Didoxy method to confirm the mutated DNA sequence (Sanger et al., 1977).

QuickChange Site-directed Mutagenesis System was also used to introduce additional mutations. Two complementary oligonucleotides with the mutation of interest were annealed to the denatured parent plasmid and extended during themo-cycling by PfuTurbo DNA polymerase. After the PCR reaction, the products were digested by DpnI endonuclease that digests the nonmethylated parental DNA template. The newly synthesized DNA was methylated and transformed into XL1Blue cells, and the plasmid was purified and sequenced to verify the sequence of the mutant DNA.

Wild-type EcPFK and all of the mutant proteins were expressed from the pALTER mutagenesis vector that was transformed into competent RL257 cells (MQ Δ*pfkB* :: FRT Δ*pfkB*:: Δ*pfkA,* MQ is a lac^+ laq^{iq} derivation of MC4100), a PFK-1 and PFK-2 deficient strain (Lovingshimer et al., 2006).

Protein purification

The purification of wild-type and mutant EcPFK proteins followed the protocol of Johnson et al. (1992) with modifications. RL257 cells containing the plasmid of interest were grown to OD600 = 0.6 and then induced by 2 mM IPTG in LB broth containing either 20 μg/mL chloramphenicol, 100 μg/mL ampicillin or both at 37 °C. Cells were harvested by centrifugation at 4,000 RPM using a Beckman Model J-6B centrifuge. Pelleted cells were stored at -20°C for later use. The frozen cells were resuspended in 30-40 mL Buffer A (50 mM Tris-HCl pH 7.5, 5 mM $MgCl_2$ and 1 mM EDTA) and set on ice. Cells were lysed by sonication using a Sonic Dismembrator Model 550 (Fisher Scientific). Fifteen-second pulses were used followed by a one-minute rest period to allow the cells to cool. A total sonication time of 8 minutes was used. The crude lysate was clarified by centrifugation at 12,000 RPM for 1 hour in a Beckman J2-21 centrifuge equipped with a JA-20 rotor. The supernatant was incubated in the presence of DNase at 37 °C for 15 minutes and then centrifuged for another hour to get rid of the remaining cell debris. The supernatant containing EcPFK was diluted to 100 ml and loaded onto Mimetic Blue A column that has been equilibrated with Buffer A. The column was then washed with 100 mL of Buffer A to remove any unbound protein. Buffer A with 1.5 M NaCl present was used to elute EcPFK and fractions were

collected. Each fraction was measured for its absorbance at 280 nm and also its activity (Figure 2-1). The fractions having enzymatic activity were pooled, dialyzed against Buffer A and concentrated using Amicon Ultra-15 (100K). SDS-PAGE (Laemmli, 1970) was performed to check the protein purity (Figure 2-2). If there were multiple bands on the SDS-PAGE gel, the protein was passed through an anion-exchange column, either a DE-52 column or a Mono Q 10/10 column on Pharmacia FPLC, and eluted with 0 to 1 M NaCl gradient. Fractions were collected and assayed. The fractions have PFK activity were pooled, dialyzed against Buffer A and stored at 4 °C. A representative purification table is shown Table 2-1.

Protein concentration

Determination of protein concentration was performed using the Bicinchoninic Acid (BCA) Protein Assay from Pierce (Smith et al., 1985) or calculated using the extinction coefficient of PFK 0.6 mg^{-1} mL^{-1} at 280 nm (Kolartz and Buc, 1977, Pace et al., 1995).

Enzymatic activity assay

Activity measurements of EcPFK were conducted by coupling the reaction catalyzed by EcPFK to the oxidation of NADH and monitoring the corresponding decrease in the absorbance at 340 nm (Babul, 1978; Kolartz and Buc, 1982). The entire coupled assay system (including substrates, enzymes and products), as well as the MgATP regeneration system, is shown in Figure 2-3. Assays were carried out in 600 μL of an EPPS buffer containing 50 mM EPPS-KOH (pH 8.0 at 25℃), 10 mM NH_4Cl, 10 mM $MgCl_2$, 0.1 mM EDTA, 2 mM DTT, 0.2 mM NADH, 250 μg of aldolase, 50 μg of

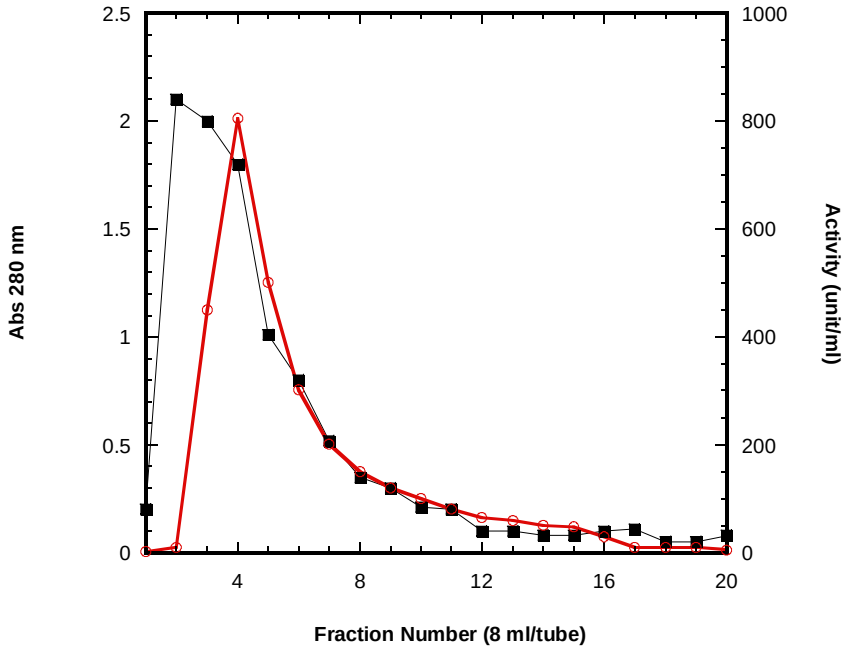

Figure 2-1 Elution profile of EcPFK from Blue A affinity column. EcPFK was eluted with 1.5M NaCl. Activity and absorbance at 280 nm are indicated by ■ and ○, respectively. Fractions 5-14 were pooled and dialyzed against with buffer.

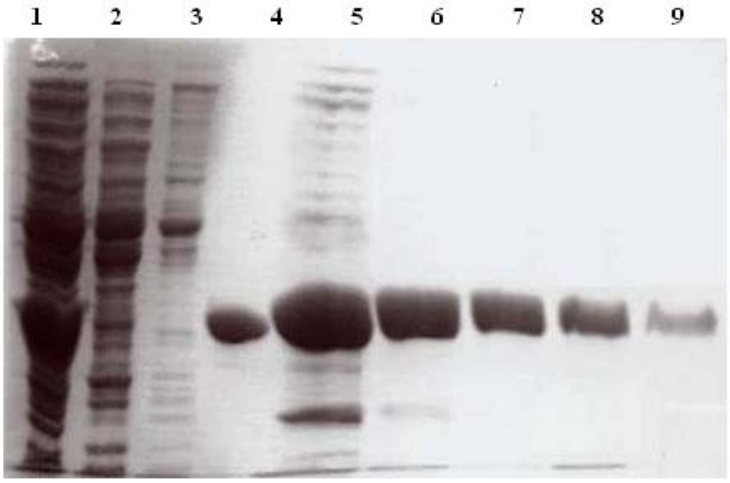

Figure 2-2 SDS-PAGE of fractions after Blue A purification. 1.Crude, 2. Flow through of load, 3. Wash, 4 Standard, 5 Fraction #4, 6 Fraction #6, 7 Fraction #8, 8 Fraction #10, 9 Fraction #12.

Table 2-1 A representative purification table for EcPFK.

Steps	Activity (unit/ml)	Protein (mg/ml)	Volume (ml)	Total Activity (Units)	Total Protein (mg)	Specific Activity (Units/mg)	Fold Purification	% Yield
Crude	420	10	51	21420	510	42	-	100
Dnase	420	10	49	20580	490	42	1	96
Blue A	1250	5	8	10000	40	250	6	47
DE-52	2000	7	4	8000	28	280	7	37

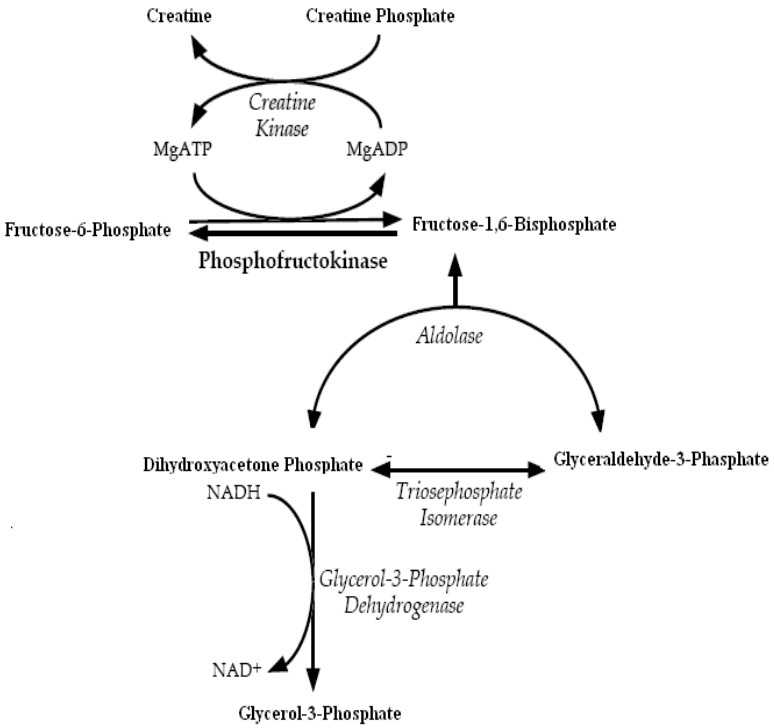

Figure 2-3 The coupling enzyme system used to assay EcPFK activity. Phosphofructokinase catalyses the phosphoryl transfer from MgATP to fructose-6-phosphate. This reaction is coupled by three enzymes (aldolase, triosephosphate isomerase and glycerol-3-phosphatedehydrogenase) to the oxidation of NADH to NAD^+, which is monitored spectroscopically at 340 nm. The enzymes involved in this process are in italics.

glycerol-3-phosphate dehydrogenase, 5 μg of triosephosphate isomerase. For maximal activity, 3 mM ATP and 5 mM Fru-6-P were added. For measuring the coupling between either Fru-6-P and PEP or Fru-6-P and MgADP, the concentration of Fru-6-P, PEP and MgADP are varied correspondingly. Assays are initiated by adding the appropriately diluted EcPFK so that the absorbance change is not greater than 0.05 absorbance units/minute. For the coupling reaction between Fru-6-P and PEP, 40 mg/mL creatine kinase and 4 mM phosphocreatine were added to regenerate MgATP from MgADP, which is one of the reaction products and is also an allosteric activator of EcPFK. When MgADP was varied, it was added as a solution of equal concentrations of MgADP and MgATP to prevent competition between MgATP and MgADP in the active site (Johnson and Reinhart, 1994). The MgADP contamination in the MgATP stock solution was measured enzymatically (Jaworek et al., 1974). All activity measurements were performed on Beckman Series 600 spectrophotometers using a linear regression calculation to convert the change in absorbance at 340 nm to enzyme activity. One unit (U) of activity is defined as the amount of enzyme needed to produce 1μmol of fructose 1,6-bisphosphate per minute.

In vitro hybrid tetramer formation

Kimmel and Reinhart (2001) devised an *in vitro* method for making hybrids of BsPFK by dissociating the enzyme tetramers into their individual subunits by modifying a method described previously (Deville-Bonne et al., 1989; Laine et al., 1992; Le Bras et al., 1995). The *in vitro* method for making hybrids has also been applied in EcPFK (Fenton and Reinhart, 2002; Fenton et al., 2004). Two parent proteins, wild type EcPFK

and mutant EcPFK, were used to form the 1:3 hybrid that presents a specific heterotropic interaction. The two parent proteins needed to for the 1:3 hybrid formation for each heterotropic interaction are shown in Table 2-2. They were purified individually as described earlier in this chapter. Seven milligram mutant protein was incubated with three milligram wild-type EcPFK for 1.5 hours at 25°C with 0.4 M KSCN. The denaturant was removed by dialysis away in Buffer A at 4°C in the presence of 2 mM Fru-6-P for three hours for re-association of the hybrid tetramers (Figure 2-4). Using sonication to obtain the crude protein mixture from the cell, the five hybrid tetramers were visualized on a 7.5% native polyacylamide gel (Figure 2-5).

Hybrid isolation and identification

The co-expressed proteins were purified from RL257 cells (Lovingshimer et al., 2006). Anionic exchange chromatography using a FPLC equipped with Mono Q column was used to separate the five hybrid tetramers based on the charge differences. Fru-6-P (2 mM) was added in the buffers during separation and additional Fru-6-P (18 mM) was added to the 1:3 hybrid after separation to stabilize the hybrid protein and prevent re-hybridization. The purity of 1:3 hybrid was confirmed on a 7.5% native polyacylamide gel (Figure 2-6).

Data analysis

Data were fit to the appropriate equation using the nonlinear least squares fitting analysis of Kaleidagraph 3.5 (Synergy) software. Initial rates obtained from kinetic assays in which the Fru-6-P concentration dependence was varied were fit to the Hill equation (Hill, 1910):

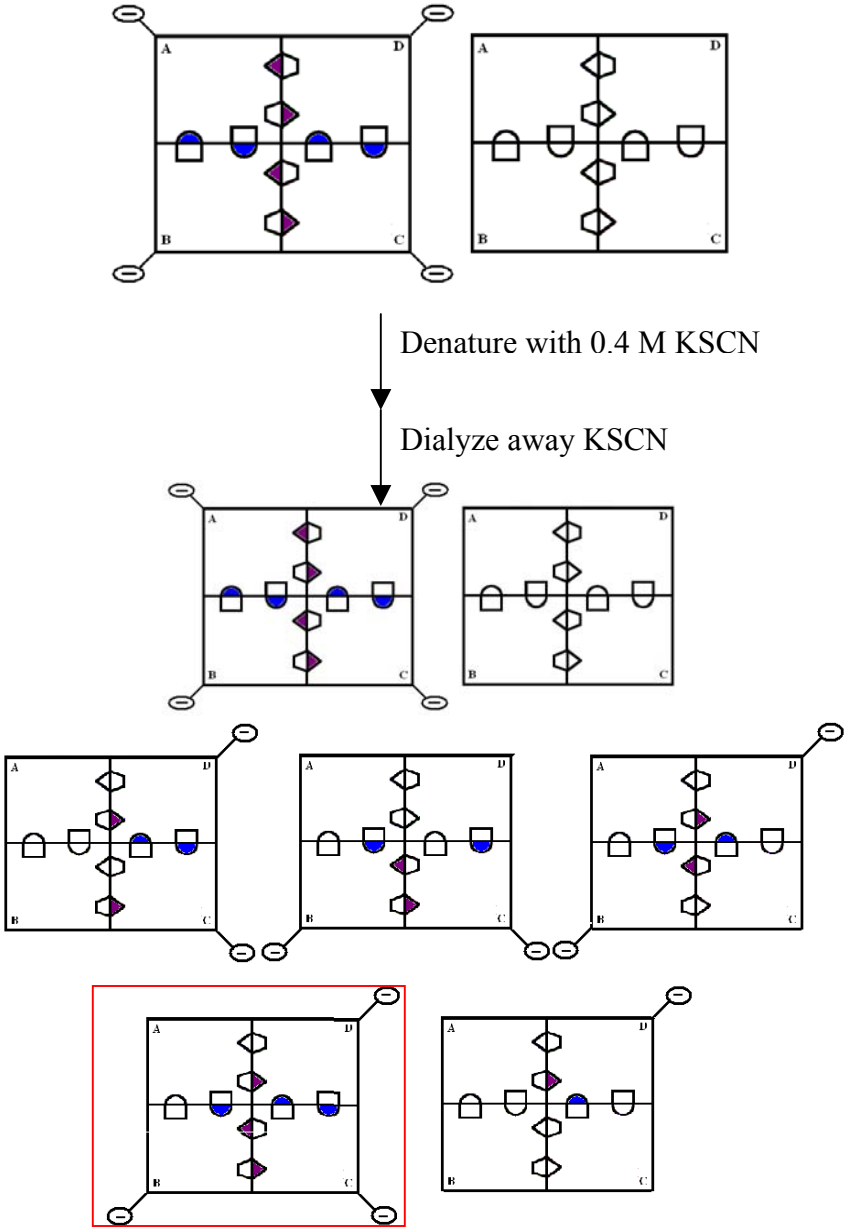

Figure 2-4 Schematic of *in vitro* hybrid formation. KSCN is used as a denaturing reagent to dissociate the EcPFK tetramer of two parent proteins. The 1:3 hybrid (in the red box) that represents a specific heterotropic interaction was isolated after removal of KSCN by dialysis against buffer A.

Table 2-2 Description of the two parental proteins used to form the 1:3 hybrids that contain each heterotropic interaction.

	Parent A	**Parent B**		
		Active site mutation	Allosteric site mutation	Charge-tag mutation
23Å	Wild-type	R243E	H215E	K90,91E
30Å	Wild-type	R243E	R21A	K90,91E
33Å	Wild-type	H249E	H215E	K90,91E
45Å	Wild-type	H249E	R21A	K90,91E

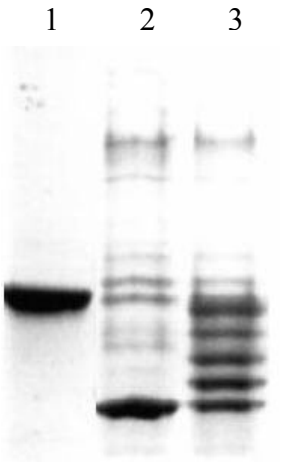

Figure 2-5 Native PAGE, Lane 1.Wild-type EcPFK, Lane 2.Charge-tag mutant protein EcPFK, Lane 3. Hybrids between wild-type and charge-tag EcPFK after cell lysis.

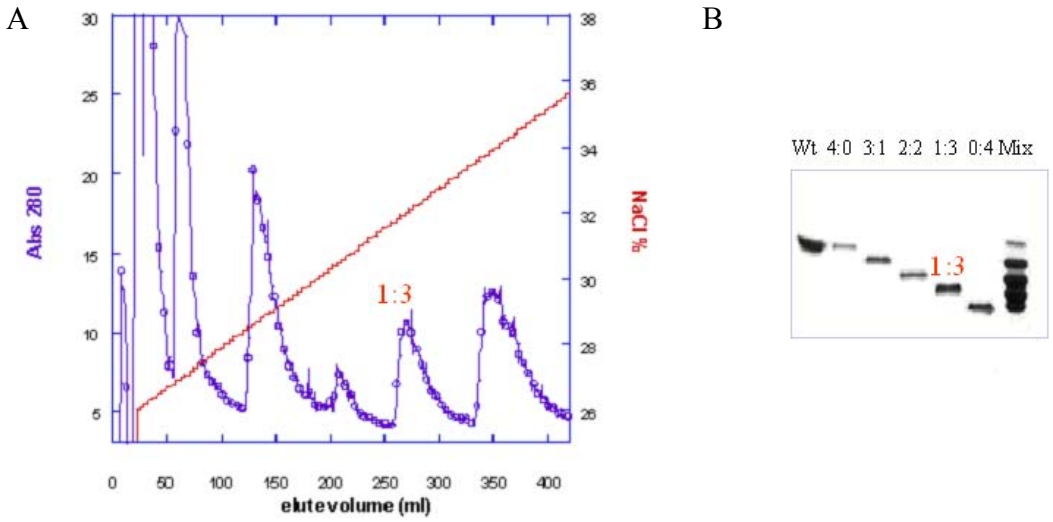

Figure 2-6 (A) Elution profile of each hybrid species by FPLC MonoQ chromatography. The absorbance at 280 nm was detected for each fraction. (B) Identification and assessment of the purity of each hybrid tetramer using 7.5% native PAGE. The 1:3 hybrid is indicated.

.

$$\frac{v}{[E]_t} = \frac{k_{cat}[A]^{n_H}}{K_{0.5}^{n_H} + [A]^{n_H}} \qquad (2\text{-}1)$$

where v = initial rate, $[E]_T$ = total enzyme active site concentration, k_{cat} = turnover number, $K_{0.5}$ = the concentration of Fru-6-P when the rate equals to one-half of the maximal activity, and n_H = the Hill coefficient. For the hybrid with a single native active site, the linear region of the Fru-6-P saturation curves at low concentration of Fru-6-P were fit to the following equation:

$$\frac{v}{E} = \left(\frac{k_{cat}}{K_m}\right)[Fru-6-P] \qquad (2\text{-}2)$$

The effect of either PEP or MgADP on the activity of mutant or wild-type EcPFK was evaluated by fitting to equation 2-3 (Figure 2-7):

$$K_{app} = K^{\circ}_{app}\left[\frac{K^{\circ}_{ix/b}[X]}{K^{\circ}_{ix/b} + Q_{ax/b}[X]}\right] \qquad (2\text{-}3)$$

where $K_{app} = K_{0.5}$ when data were fit to Hill equation, or K_{app} = the reciprocal of k_{cat}/K_m when data were fit to the linear equation, at different ligand concentration. K°_{app} is the apparent dissociation constant when [ligand] = 0, $K^{\circ}_{ix/b}$ = the dissociation constant for ligand when [Fru-6-P] = 0 and the co-substrate MgATP is saturating, and $Q_{ax/b}$ = the coupling constant between the ligand and Fru-6-P when MgATP is saturating. $Q_{ax/b}$ is related to the coupling free energy, $\Delta G_{ax/b}$ in equation 2-4, between Fru-6-P and the ligand in the saturating concentration of MgATP. The coupling constant $Q_{ax/b}$ is also defined as equation 2-5:

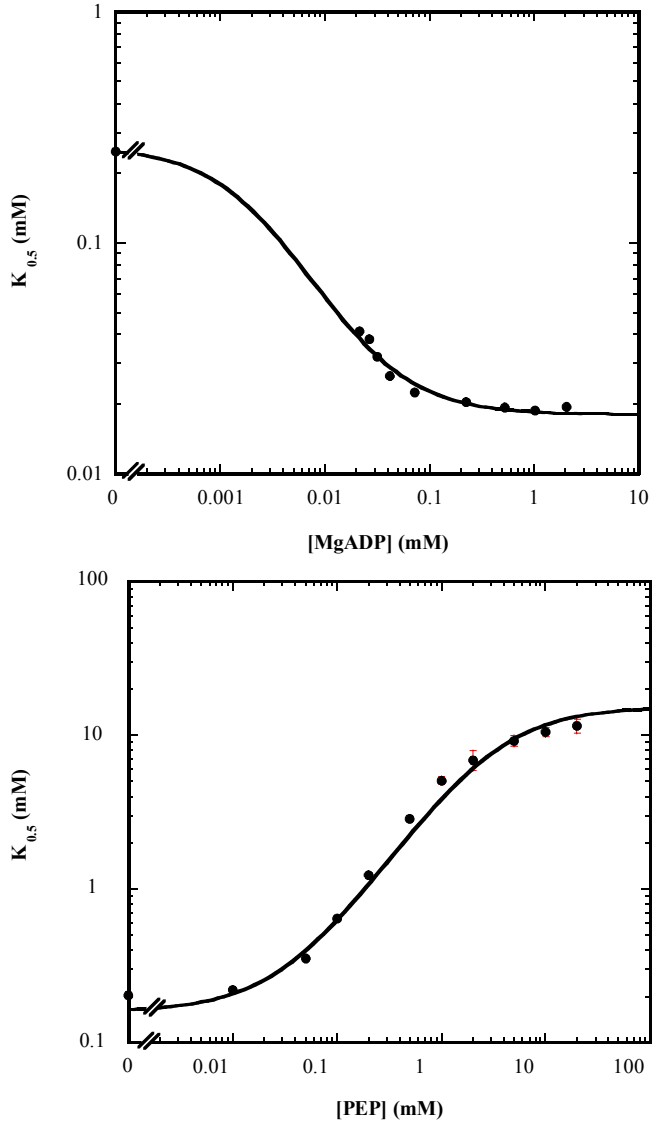

Figure 2-7 Allosteric effect of wild-type EcPFK. (A) ADP activation. (B) PEP inhibition. The $K_{0.5}$ for Fru-6-P is plotted as a function of MgADP or PEP, respectively. The line represents the best fit to equation 2-3 and was weighted to the error for each $K_{0.5}$ value. Errors are plotted, but are smaller than the data points. The concentration of MgATP was 3 mM. The enzyme reaction was performed at pH 8.0 and 8.5 °C.

$$\Delta G_{ax} = -RT \ln Q_{ax} \quad (2\text{-}4)$$

$$Qax/b = \frac{Ki^{\circ}_{ia}}{K^{\infty}_{ia}} = \frac{K^{\circ}_{ix}}{K^{\infty}_{ix}} \quad (2\text{-}5)$$

where R = the gas constant and T = absolute temperature in Kelvin.

Steady-state fluorescence measurements

Steady-state fluorescence intensity and anisotropy of a single tryptophan at different positions in the 23Å interaction were measured on an SLM-4800 updated with Phoenix hardware and software from ISS Inc. (Champaign, IL). Samples were excited using a xenon lamp (300W) and a monochromator to select light at 300 nm light. In order to measure fluorescence intensity and anisotropy, the excitation and emission polarizers were placed at appropriate positions and emission was detected through a 2 mm thick Schott WG-335 cut-on filter. All measurements were performed in 1cm × 1cm cuvettes. All fluorescence studies were performed in 50 mM Tris (pH 7.5), 5 mM $MgCl_2$, 0.2 mM EDTA. All measurements were corrected for blank contribution by measuring intensity and anisotropy of buffer with the same concentration of ligand. All the intensity changes were taken from the measurement of anisotropy. Intensity measurements were also corrected for protein dilution.

Frequency-domain fluorescence measurements

Frequency domain fluorometry was performed on the ISS K2 multi-frequency phase fluorometer. The sample was excited by the 300 nm line of a Spectra-Physics Model 2045 argon ion laser. A Pockell cell served as the light modulator. Modulation frequencies were generated by a Marconi 2022A frequency synthesizer (London). A

solution of NATA (N-acetyl-tryptophanamide, Kodak, lifetime is 2.85 ns) in phosphate buffer (pH 7/KOH) was used to avoid “color effect”. It provides a phase and modulation reference that could be measured at the same wavelength as the sample observation (Lakowicz and Gryczynski, 1991). The EcPFK subunit concentration was 10 μM for each preparation.

Emission, excitation filters and buffer conditions were identical to those used in steady-state fluorescence measurements. Fluorescence lifetime measurements were performed with excitation and emission polarizer oriented at angled 0° and 54.8° (the magic angle), respectively, to the vertical laboratory axis to avoid polarization artifacts (Spencer and Weber, 1970; Weber, 1971, 1977 and 1978). The frequency dependence of the phase and modulation of the tryptophan fluorescence for each unbound and bound enzyme form was determined at 12 modulation frequencies, which varied logarithmically from 2 to 250 MHz. Data were collected at each frequency until the standard deviations for each measurement of phase and modulation were below 0.1 and 0.002, respectively. Data acquisition was made with ISS software. Data were fit to various models, providing for a combination of discrete exponential sums or continuous distribution to describe the total lifetime component(s). Data analysis was performed with GLOBALS analysis software, obtained from the Laboratory for Fluorescence Dynamics at the University of Illinois at Urbana-Champaign.

CHAPTER III

IN VIVO FORMATION OF HYBRID TETRAMERS OF *E. COLI* PHOSPHOFRUCTOKINASE

Introduction

Phosphofructokinase (EC 2.7.1.11) from *E. coli* (EcPFK) catalyzes the first committed step in glycolysis, which is the transfer of a phosphoryl group from MgATP to fructose-6-phosphate (Fru-6-P) to produce MgADP and fructose-1, 6-bisphosphate (FBP). EcPFK is allosterically regulated by MgADP and phosphoenolpyruvate (PEP), which act to activate or inhibit, respectively, by changing the affinity of the enzyme displaying for the substrate, Fru-6-P. Both ligands bind to the same allosteric site in EcPFK. Therefore, it is very interesting to investigate how these two molecules regulate EcPFK from the same site, but in opposite directions.

EcPFK is a homotetramer with each subunit having a molecular mass of 34 KDa. The subunits are arranged as a dimer of dimers. A single EcPFK subunit has on average one active site and one allosteric site that are located at different subunit interfaces of the tetramer. Thus, each functional active site or allosteric site is composed of two half sites from each subunit. A tetramer has four identical active sites and four identical allosteric sites. All these sites can potentially interact with each other. The interactions between the binding sites are quite complex, but can essentially be reduced to ten unique interactions. There are three homotropic interactions between the active sites, three homotropic interactions between the allosteric sites, and four unique heterotropic interactions between the active sites and the allosteric sites. The investigation of these

different kinds of interactions can provide us with an energetic blueprint that ultimately must result from the molecular basis for allosteric behavior in EcPFK. However, the complicated communications within the tetramer make the investigation difficult.

To simplify the complicated communications, hybrid tetramers have been used to isolate each single heterotropic interaction. A functional tetramer of EcPFK has been constructed in which only a single active site and a single allosteric site are capable of binding their respective ligands with high affinity (Kimmel and Reinhart, 2001; Fenton and Reinhart, 2002 and 2003). Meanwhile, surface charge mutations have been added to the mutant EcPFK subunits to allow the separation of the different hybrid species. The four unique heterotropic interactions have been named as the 23Å, 30Å, 33Å, and 45Å interactions based on the distance between the different binding sites in the EcPFK crystal structure (Evans et al., 1981).

In previous studies, hybrid tetramers were generated *in vitro*, which required dissociation of a mixture of the purified parent proteins with KSCN followed by re-association of the tetramers by removing KSCN through dialysis (Chapter II). However, these experiments are time consuming and have been plagued with low hybrid yield. The current study describes a new method for producing hybrids more quickly and with a potentially higher yield by co-expressing wild-type EcPFK and the mutant EcPFK *in vivo*.

Materials and Methods

Materials

All chemical reagents used for protein purification and enzyme kinetic assay were the same as chapter II. pGDR147 and pGDR16, containing the wild-type EcPFK gene in pALTER-EX1 or pALTER-1, respectively, was used with the Altered Sites II *in vitro* Mutagenesis System (Promega) according to manufacturer's instructions to construct mutations. Mutagenesis primers are as follows:

R21A, 5'-CAG CGC AGA ACG AAC AAC CCC AGC AAT TGC GGC GTT CAT GCC TGG-3'

H215E, 5'-GGT AAT CGC CAC GAT CGC TTC TTT TTT ACC TTT CGC-3'

K211E, 5’-GAT CGC GTG TTT TTT ACC TTC CGC GAT ACC CGC-3’

K213E, 5’-GGT AAT CGC CAC GAT CGC GTG TTT TTC ACC TTT CGC GAT ACC CGC-3’

K214E, 5’-CGC CAC GAT CGC GTG TTC TTT TAC CTT TCG CGA TAC C-3’

R243E, 5'-GAT GTG GCC CAG CAC AGT TGC TTC GGT TTC ACG ACC GGT-3'

H249E, 5'-CCA CCG CGC TGG ATT TCG CCC AGC ACA GTT GCG C-3'

K2, 3E, 5'-GCT TGT CAA CAC ACC GAT TTC CTC AAT CAT GAC TAC CTC TGA AGC-3'

K90, 91E, 5'-CAG CGC ATC GAT CCC ACG TTC TTC CAG GTT TTC GAT AGC CAC-3'

The mutated DNA was sequenced across the modified site to confirm the desired mutation. Plasmids containing wild-type and mutant EcPFK genes were co-transformed into RL257 cells for protein expression.

Results and Discussions

Co-expression of wild-type and charge-tag PFK

The wild-type EcPFK gene was cloned into pALTER-Ex2 and pALTER-1 to give pGDR148 and pGDR16, respectively. The EcPFK gene in pALTER-Ex2 was kept as wild-type form. Using site-directed mutagenesis, the second and the third codons of EcPFK in pGDR16 were mutated from lysine to glutamate to change the surface charge of the protein. pALTER-Ex2 and pALTER-Ex1 have different origins of replication, p15A and ColE1, respectively. In addition, the antibiotic selection markers are different and are chloramphenicol and ampicillin, respectively. They are able to be co-transformed into competent RL257 cells (Figure 3-1).

Following an affinity purification column, anion-exchange chromatography was used to separate the five hybrid species (4:0, 3:1, 2:2, 1:3, 0:4) based on the charge differences among the hybrid tetramers. While all five hybrid species were obtained, they were not well separated. In addition, the amounts of the 1:3 and 0:4 hybrids were relatively low based on the elution profile and native gel electrophoresis (Figure 3-2).

Optimizing the yield of 1:3 hybrid

The low yield of the 1:3 hybrid was due to the low level of expression of the K2E/K3E charge-tag mutations. There are two likely reasons. First, pALTER-1 is not an

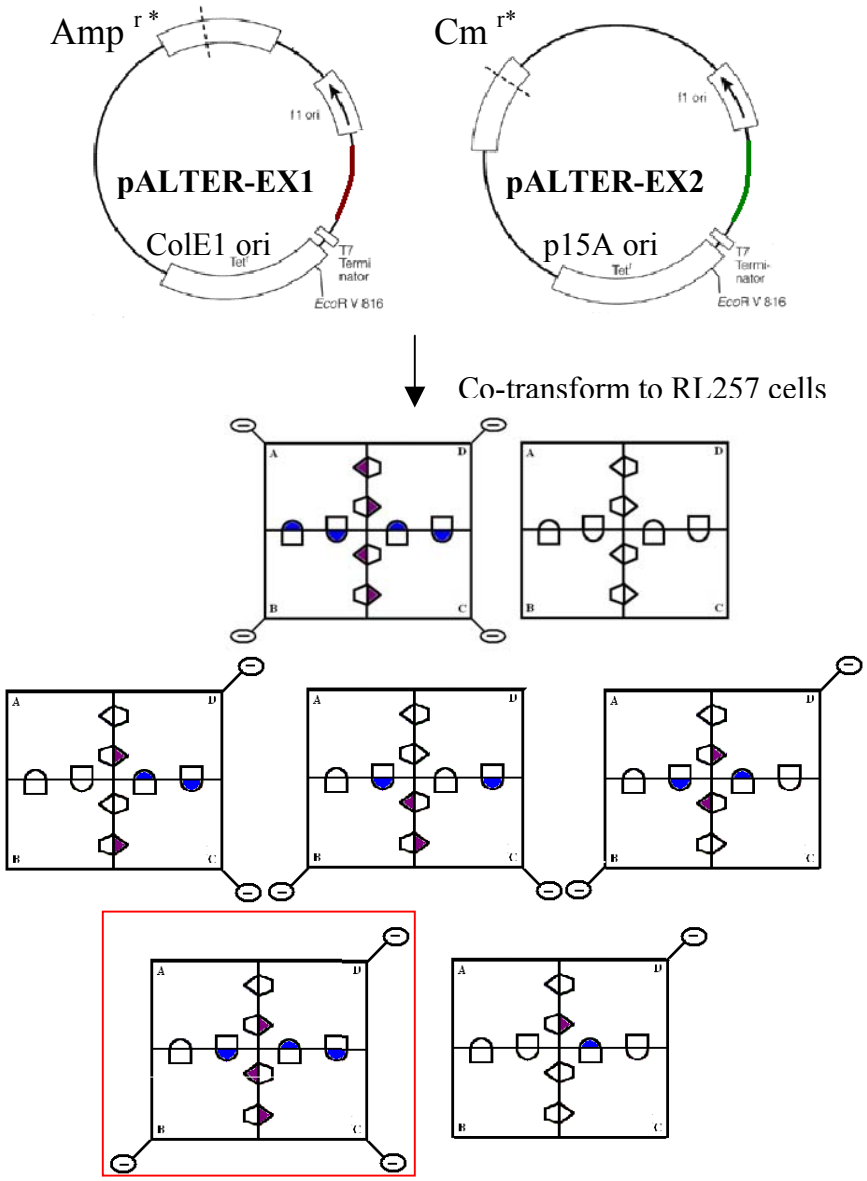

Figure 3-1 Schematic graph of *in vivo* hybrid formation. Wild-type and mutant EcPFK genes were in two plasmids with different selection markers and origins of replication. After co-expression in RL257 cells, the different hybrid tetramers were formed *in vivo*. The 1:3 hybrid that represents a specific heterotropic interaction is shown in the red box.

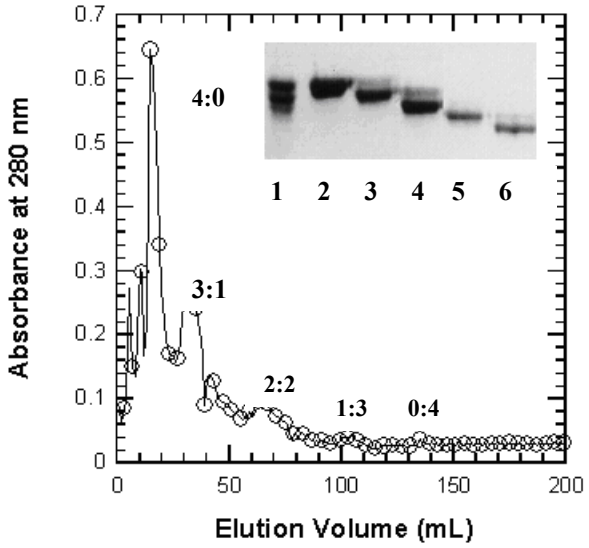

Figure 3-2 Elution profile for the hybrid species between wild-type and charge-tag (K2E/K3E) EcPFK by anion-exchange column using *in vivo* hybrid formation method. Inset: 7.5% native PAGE of separation of the different hybrid species. Lane 1. hybrid mixture, lane 2. 4:0 hybrid, lane 3. 3:1 hybrid, lane 4. 2:2 hybrid, lane 5. 1:3 hybrid, lane 6. 0:4 hybrid.

.

expression vector strictly speaking. Although other proteins express well in pALTER-1, the expression level of two proteins at the same time cannot be controlled *in vivo*. Consequently, the pALTER-1 vector was changed to pALTER-Ex1, which has the strong *tac* promoter. Second, the K2E/K3E charge-tag mutations are at the beginning of EcPFK gene and thus may influence the expression of EcPFK protein (Gold and Stormo, 1987). To address this possibility, alternative charge-tag mutations, K90E/K91E, were substituted for K2E/K3E. These charge-tag mutations have been used successfully in *Bacillus stearothermophilus*. (BsPFK). New constructs were created using the pALTER-Ex1 and the K90E/K91E charge-tag mutations. After the purification and separation, the yield of the 1:3 hybrid was about three times higher than that of the *in vitro* method (Table 3-1). In addition, the separation resolution of the five hybrid species is significantly improved compared with the K2E/K3E charge-tag (Figure 3-3). The comparison between the *in vivo* and *in vitro* method is shown in Figure 3-4. The *in vivo* method improves yield and saves time. In addition, the *in vivo* method avoids exposing the enzyme to denaturing conditions, which might produce subtle changes to the protein structure.

Alternative allosteric site mutations

In the previous study, R21A and K213E were used as the allosteric site mutations to make the hybrid tetramers. However, with K213E as the allosteric site mutation in the 23Å interaction, the expression of the 23Å mutant protein was so poor that it was very difficult to obtain the 1:3 hybrid. Other active site mutations were chosen to pair with K213E. The different combinations with K213E did not improve the expression of the

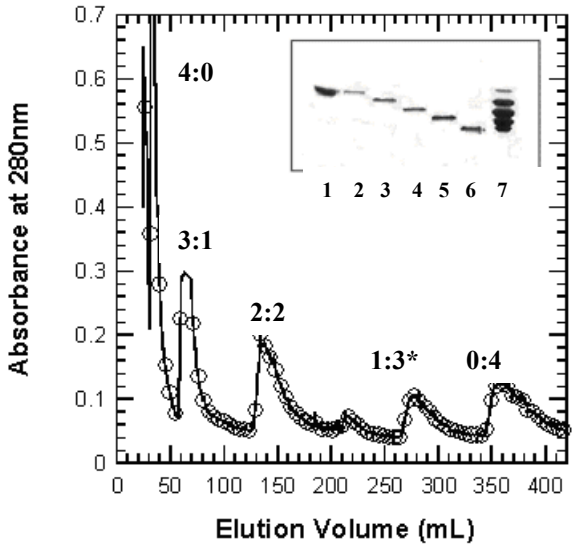

Figure 3-3 Elution profile for the hybrid species between wild-type and charge-tag (K90E/K91E) EcPFK by anion-exchange column using *in vivo* hybrid formation method. Inset: 7.5% Native PAGE of separation of the different hybrid species. Lane 1. hybrid mixture, lane 2. 4:0 hybrid, lane 3. 3:1 hybrid, lane 4. 2:2 hybrid, lane 5. 1:3 hybrid, lane 6. 0:4 hybrid.

Table 3-1 Yield comparison between *in vitro* and *in vivo* making hybrids methods.

	In vitro	*In vivo*
Load on Mono Q (mg)	10	10
Yield of all the hybrids (mg)	4.0	6.8
Yield of 1:3 hybrid (mg)	0.5	1.6
Yield of 1:3 hybrid (%)	5.0	16.0

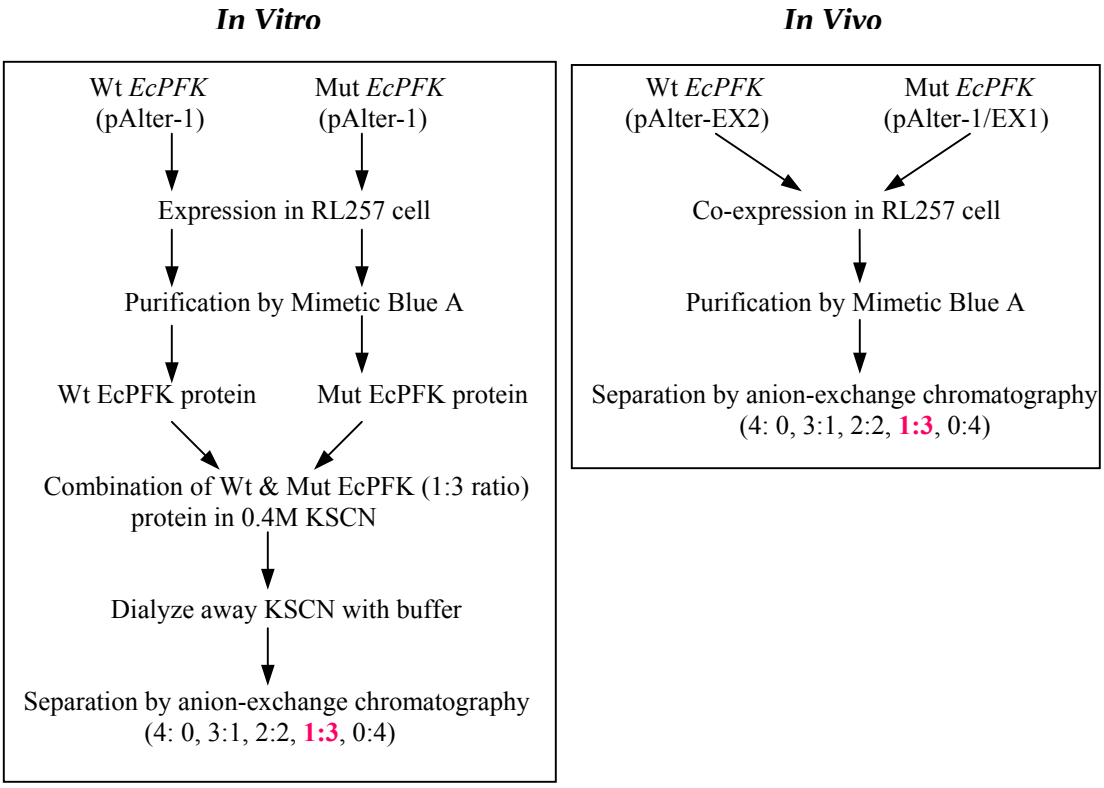

Figure 3-4 Comparison of the *in vivo* and *in vitro* methods for forming hybrid tetramers of EcPFK.

mutant protein. To improve the yield of mutant EcPFK, other allosteric site mutations were characterized, including K211E, K214E and H215E (Figures 3-5, 3-6). The kinetic data comparison is shown in Table 3-2. Among them, H215E had kinetics and properties similar to K213E and thus was used instead of K213E as the allosteric site mutation for both the 23Å and the 33Å interactions. Plotting $K_{1/2}$ for Fru-6-P affinity versus PEP or MgADP concentration over the assayable PEP or MgADP concentration range shows no PEP inhibition or MgADP activation of Fru-6-P in H215E mutation. This result is consistent with the effect of R21A and K213E mutations. However, the expression of H215E mutant EcPFK is much better than K213E mutant EcPFK. The yield of 1:3 hybrid in the 23Å heterotropic interaction with H215E as the allosteric site mutation was dramatically increased. In addition, the 23Å heterotropic interaction and the 33Å heterotropic interaction were re-characterized with H215E as allosteric site mutation. Both of them showed similar coupling free energy changes that are comparable to those with K213E as the allosteric site mutation (Table 3-3).

Co-expression of wild-type and mutant EcPFK

Based on the results we obtained from the above experiments, the *in vivo* method was applied to make the 1:3 hybrid tetramers that each contains one of the four unique heterotropic interactions. Using K90E/K91E as the charge-tag mutations, site-directed mutagenesis was performed on EcPFK gene in pALTER-Ex1 (pGDR147). The four mutant EcPFKs that will be used to make the 1:3 hybrid tetramer containing each of the four heterotropic interactions were obtained.

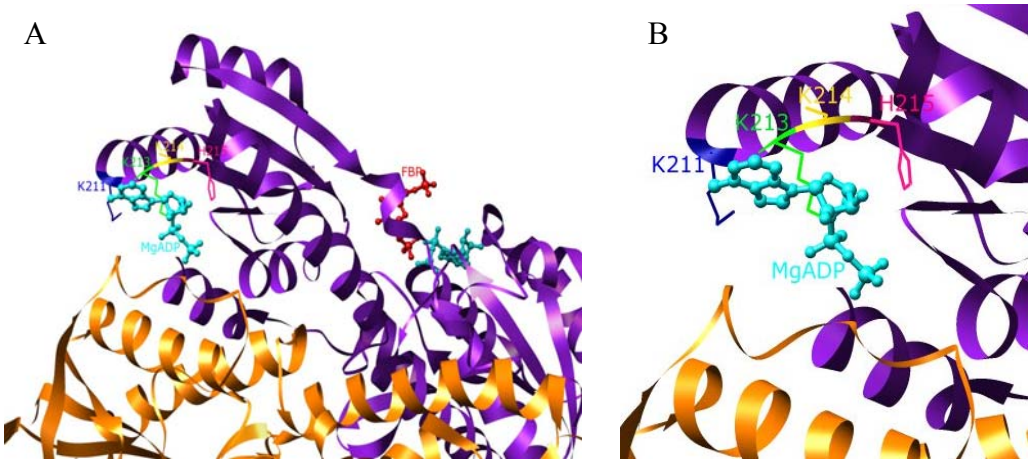

Figure 3-5 Residues around the allosteric site. (A) The active site bound with FBP in red, allosteric site bound with ADP in cyan, K213 is in green, K214 is in yellow, K211 is in blue and H215 is in pink. (B) The close view of the allosteric site interface.

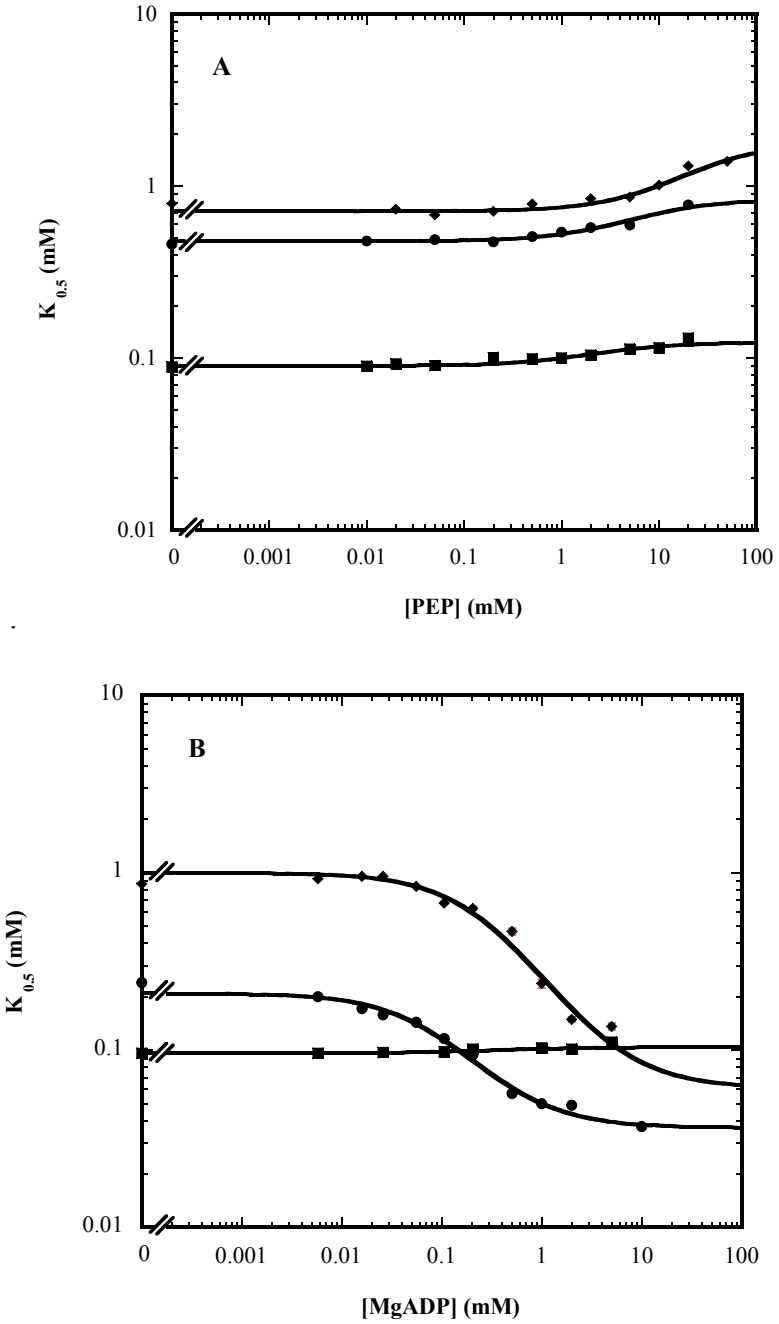

Figure 3-6 Characterizations of K211E (●), K214E (◆) and H215(■). (A) PEP inhibition. (B) MgADP activation. H215E has reduced affinity for both PEP and MgADP.

Table 3-2 Characterization of the alternative allosteric site mutations.

	K_{iy}° (mM)	K_{ix}° (mM)
WT	0.2	0.34
K213E	5.2 ± 0.3	3.4 ± 0.5
K211E	3.7 ± 0.5	0.5 ± 0.03
K214E	10.6 ± 0.6	4.4 ± 0.4
H215E	4.9 ± 0.6	14.6 ± 0.5

K_{iy}° : the dissociation constant for PEP in the absence of Fru-6-P

K_{ix}° : the dissociation constant for MgADP in the absence of Fru-6-P

Table 3-3 Coupling free energy comparisons between different allosteric site mutations in the 1:3 hybrid protein containing either the 23Å interaction or the 33Å interaction.

	ΔG_{ax}(kcal/mol)	ΔG_{ay} (kcal/mol)
23Å (K213E)	-0.73 ±0.04	0.99 ±0.08
23Å (H215E)	-0.78 ±0.05	0.96 ±0.03
33Å (K213E)	-0.99 ±0.03	-0.19 ±0.04
33Å (H215E)	-0.95 ±0.03	0.05 ±0.01

Each mutated plasmid and pGDR148, which has the wild-type EcPFK gene, were co-transformed in RL257 cells. All of four the mutated proteins are able to form the five hybrid tetramers *in vivo* (Figure 3-7). The amount of each hybrid species was different. The yield of 1:3 hybrid was relatively higher than the other hybrids except 0:4 (Figure 3-3).

Conclusions

The hybrid tetramers stratagem has been used to isolate a single heterotropic interaction. To obtain a high enough yield of the four 1:3 hybrid tetramers, each of which contains one of the four heterotropic interactions, we developed the *in vivo* hybrid formation method described in this chapter in an effort to address this issue.

The method used to generate hybrid tetramers *in vitro* has a low yield and is time consuming. Eventually, the five hybrid species were successfully made by the *in vivo* method described above. In addition, the yield of the 1:3 hybrid is increased 3-fold by changing the vector to pALTER-Ex1 and charge-tag mutations to K90E/K91E. Moreover, changing the allosteric mutation from K213E to H215E, the yield of the 1:3 hybrid in the 23Å interaction was enhanced greatly. This observation suggests that although different allosteric site mutations diminish ligand binding to the same extent, they may have different effects on the expression of EcPFK. The *in vivo* method is natural without using any denaturing reagents and it saves time relative to the *in vitro* method. Further, using the *in vivo* method, all of the different hybrid tetramers that

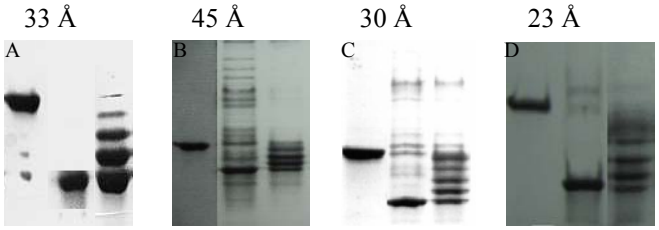

Figure 3-7 Native PAGE of the hybrids of wild-type EcPFK with mutant EcPFKs (K90, 91E charge-tag). In each panel, lane 1. wild-type EcPFK, lane 2. mutant EcPFK, lane 3. co-expressed wild-type and mutant EcPFK.

.

individually contain each of the four heterotropic interactions have been successfully made and the yield of 1:3 hybrid was increased in each case. The characteristics of the 1:3 hybrids containing each heterotropic interaction produced *in vivo* were similar to those produced *in vitro*. It can now be used for future studies of allosteric regulation in EcPFK by introducing different mutations in the specific heterotropic interactions of EcPFK.

CHAPTER IV

SELECTIVE PERTURBATION OF INDIVIDUAL ALLOSTERIC INTERACTIONS IN *E. COLI* PHOSPHOFRUCTOKINASE

Introduction

Allosteric regulation has been studied for more than 50 years in an effort to try to understand how allosteric signals are transmitted within proteins. In this chapter, EcPFK, which is an allosterically regulated enzyme, is used as a model system to study how allosteric information is transmitted within the protein. There are four unique heterotropic interactions possible in EcPFK. The allosteric contribution from each heterotropic interaction has been quantified for both activation and inhibition (Fenton et al., 2003 and 2004; Fenton unpublished data). In this study, we want to address whether a mutation that diminished the overall allosteric response in EcPFK differentially disrupts each of the four heterotropic interactions.

Two methods were used to select the residues that can diminish the allosteric response in EcPFK. The first one is based on the sequence alignment between EcPFK and phosphofructokinase from *Lactobacillus delbrueckii* subspecies *bulgaricus* (LbPFK), which shows weak allosteric regulation. LbPFK shows no MgADP activation and minimal PEP inhibition. The amino acid sequence of this relatively non-allosteric PFK is 47% identical and 66% similar to that of EcPFK. The amino acids in EcPFK were substituted with the corresponding residues in LbPFK. Twenty-two mutants were characterized previously (Paricharttanakul et al., 2005). Three of them affected the

allosteric response for both PEP inhibition and MgADP activation. Thus, by substituting the residues in EcPFK with their counterpart from LbPFK, we were able to study the role of a specific residue in the allosteric communication in EcPFK. The second method is that we propose that the residues that lie in between the active site and the allosteric site are important for the allosteric regulation. All the selected residues were substituted by alanine.

Seven residues were selected and mutated based on the above methods. The mutant EcPFKs described in this chapter were characterized by steady-state kinetics. The G184C, D59A and S157A mutant proteins have been observed to exhibit diminished allosteric response for both activation and inhibition. At 8.5°C, the G184C mutant protein showed a three-fold decrease in MgADP activation and a twelve-fold decrease in PEP inhibition. The D59A mutant protein has even stronger effect on PEP inhibition and a similar effect for MgADP activation compared to the G184C mutant protein. The S157A mutant EcPFK diminished PEP inhibition six-fold and MgADP activation seven-fold. G184 is 9Å away from the allosteric site and is in the interior of EcPFK. D59 is close to the allosteric site. The relative position of S157 is between the active site and the allosteric site in the 23Å interaction.

To study whether each of the three mutations can differentially disrupt each of the four heterotropic interactions in EcPFK, G184C, D59A and S157A were introduced into the native subunit of the 1:3 hybrid tetramers containing each heterotropic interaction using the *in vivo* hybrid formation method. The contributions of G184C, D59A and S157A on each heterotropic interaction were compared to that of each native

heterotropic interaction. Moreover, the total effect from each heterotropic interaction was compared to the total heterotropic effect in the mutant EcPFK without homotropic interactions.

Materials and Methods

Materials

All chemical reagents used for protein purification and the enzyme kinetic assay were the same as chapter II. pGDR148, containing wild-type EcPFK gene in pALTER-Ex2, was used with the Altered Sites II *in vitro* Mutagenesis System (Promega) to introduce mutations. Mutagenesis primers were synthesized by Integrated DNA Technology (IDT) as following:

G184C, 5'-CGA ATT CAC AGC CAG CGG CAA TGG CCG C-3'

G184V, 5'-CAC AAC GAA TTC ACA GCC CAC GGC AAT GGC CGC AGC-3'

G184T, 5'-CAC AAC GAA TTC ACA GCC AGT GGC AAT GGC CGC AGC-3'

D59A, 5'-ACC GCC ACG GTT GAT CAT GGC AGA AAC GCT GTA ACG-3'

D59H, 5'GCC ACG GTT GAT CAT GTG AGA AAC GCT GTA ACG G-3'

S157A, 5'- AAT ACG CTG GTG AGA AGA GGC GGT GTC ACG CAG -3'

T148A, 5'- CAG ACG GTC GAT CGC TGC TAC AAC GGT GCT CAG-3'

T145A, 5'- GTC GAT CGC TTC TAC AAC GGC GCT CAG CGC AGT GAA-3'

S164A, 5'- GCC CAT CAC TTC CAC CAC GGC AAT ACG CTG GTG -3'

Plasmid DNA was isolated using Qiagen mini preps. The DNA was sequenced across the modified site to confirm the desired mutation. Plasmids containing wild-type and mutant EcPFK genes were co-transformed into RL257 cells for protein expression. Hybrids tetramers of EcPFK were created using the *in vivo* hybrid formation method as mentioned in Chapter III.

Results and Discussions

Characterization of mutant EcPFKs

Seven EcPFKs with a single mutation were characterized. The positions of each modified residue are shown in the crystal structure of EcPFK (Figure 4-1). Positions 184 and 59 were selected based on the sequence alignment between EcPFK and LbPFK. G184 in EcPFK was mutated to cysteine that is the counterpart residue in LbPFK, D59 was mutated to histidine. The G184V and G184T mutant proteins were also made to assess the influence on coupling free energy from different amino acid substitutions at the same position. In addition, D59 was also substituted with alanine since the D59H mutation almost completely abolished the effect of PEP inhibition. The G184C mutant protein showed a three-fold decrease in MgADP activation and a twelve-fold decrease in PEP inhibition at 8.5 °C as compared with wild-type EcPFK. The G184V and G184T mutant proteins showed effects similar to the G184C mutant protein. The D59A mutant protein exhibited only a thirty-eight-fold decrease in PEP inhibition and a three-fold decrease in MgADP activation as compared to wild-type EcPFK at 8.5 °C (Table 4-1).

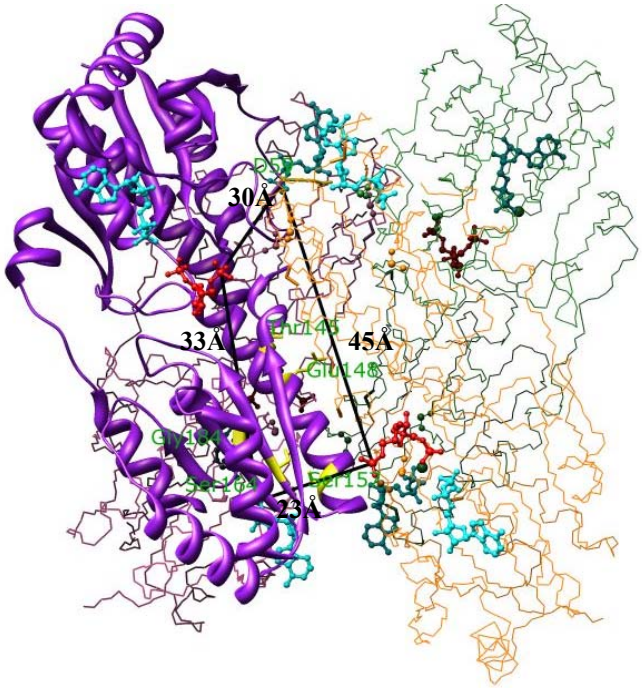

Figure 4-1 Locations of the mutated residues in the crystal structure of EcPFK. The mutated residues are colored in yellow. The four heterotropic interactions are shown in red lines. Active site with FBP bound is in red, allosteric site with MgADP bound is in cyan.

We also wished to assess whether the residues that lie between the active sites and the allosteric sites play important roles in allosteric regulation. All the proposed residues were mutated to alanine. T145 and E148 are located between the binding sites defining the 45Å heterotropic interaction. S157 and S164 are located in the 23Å heterotropic interaction. T145 and E148 are very close to the active site interface so that the mutated proteins were not very stable (Figure 4-1). Both the T145A and E148A mutant proteins have diminished allosteric response for PEP inhibition, but they do not change the coupling free energy for MgADP activation. The S164A mutant protein almost completely abolished the allosteric response for MgADP activation, but it did not influence the PEP inhibition. Only the S157A mutant EcPFK diminished both PEP inhibition six-fold and MgADP activation seven-fold. The kinetic data for each mutant EcPFK are shown in Table 4-1. In addition, the D59A mutant protein has weak binding affinity for both PEP and MgADP. This observation might be explained by the fact that D59 is located close to the allosteric site. Interestingly, the G184C mutant protein also has tight binding affinity to MgADP, but it is 9Å away from allosteric site. Both the G184C and S157A mutant proteins display tighter binding affinity towards Fru-6-P.

The G184C, D59A and S157A mutant proteins showed diminished coupling for both PEP inhibition and MgADP activation (Figure 4-2, Figure 4-3). The comparison graphs in coupling free energy term between the three mutant proteins and wild-type EcPFK are shown in Figure 4-4. The next question we wished to address is whether these reductions in allosteric response are differentially manifested in each heterotropic interaction in EcPFK.

Table 4-1 Kinetic parameters for EcPFK mutants at 8.5 °C.

	Q_{ax}	Q_{ay}	K°_{ia} (mM)	K°_{ix} (mM)	K°_{iy} (mM)
WT	14.4±0.3	0.0084±0.0001	0.3±0.003	0.03±0.002	0.08±0.002
T145A	18.2±0.7	0.05±0.001	1.3±0.02	0.08±0.006	0.69±0.02
E148A	15.0±0.8	0.08±0.004	0.57±0.03	0.12±0.01	0.05±0.005
S157A	1.8±0.1	0.05±0.002	0.05±0.0006	0.03±0.01	0.89±0.04
S164A	~1	0.064±0.0003	0.06±0.001	ND	0.083±0.003
D59H	1.7±0.05	0.15±0.002	1.5±0.07	3.1±0.6	1.9±0.03
D59A	3.3±0.07	0.33±0.02	0.44±0.005	1.67±0.12	16.2±1.5
G184C	3.4±0.1	0.022±0.001	0.042±0.001	0.007±0.003	3.81±0.12
G184T	5.9±0.35	0.02±0.004	0.12±0.007	0.02±0.0003	16.0±0.6
G184V	3.2±0.14	0.03±0.003	0.073±0.003	0.0093±0.002	4.05±0.13

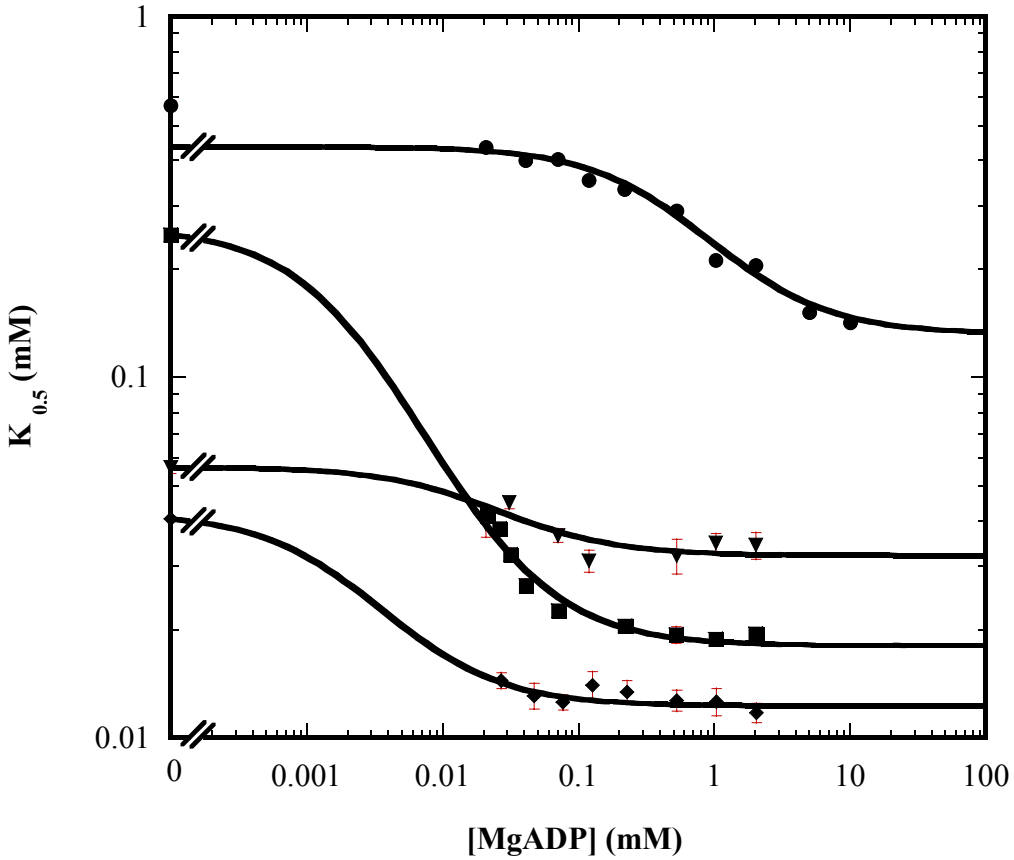

Figure 4-2 The effect of MgADP on the binding of Fru-6-P to wild-type (■), G184C (◆), D59A (●) and S157A (▼) EcPFK.

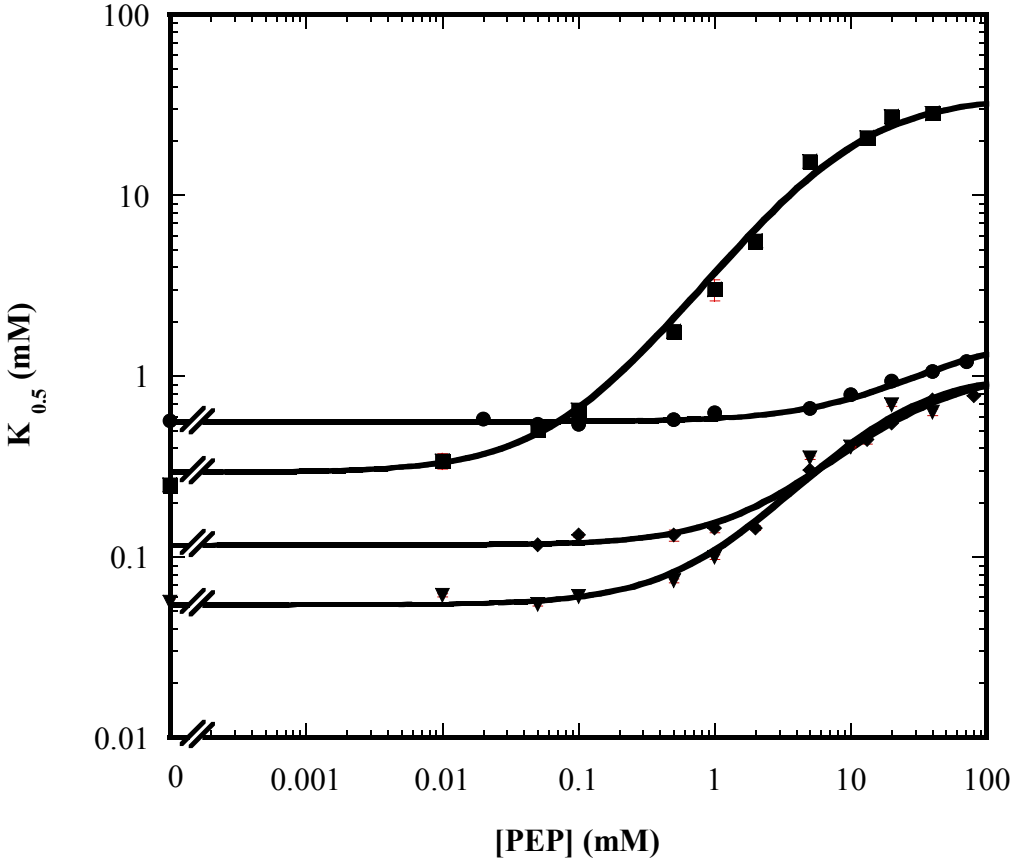

Figure 4-3 The effect of PEP on the binding of Fru-6-P to wild-type (■), G184C (◆), D59A (●) and S157A (▼) EcPFK.

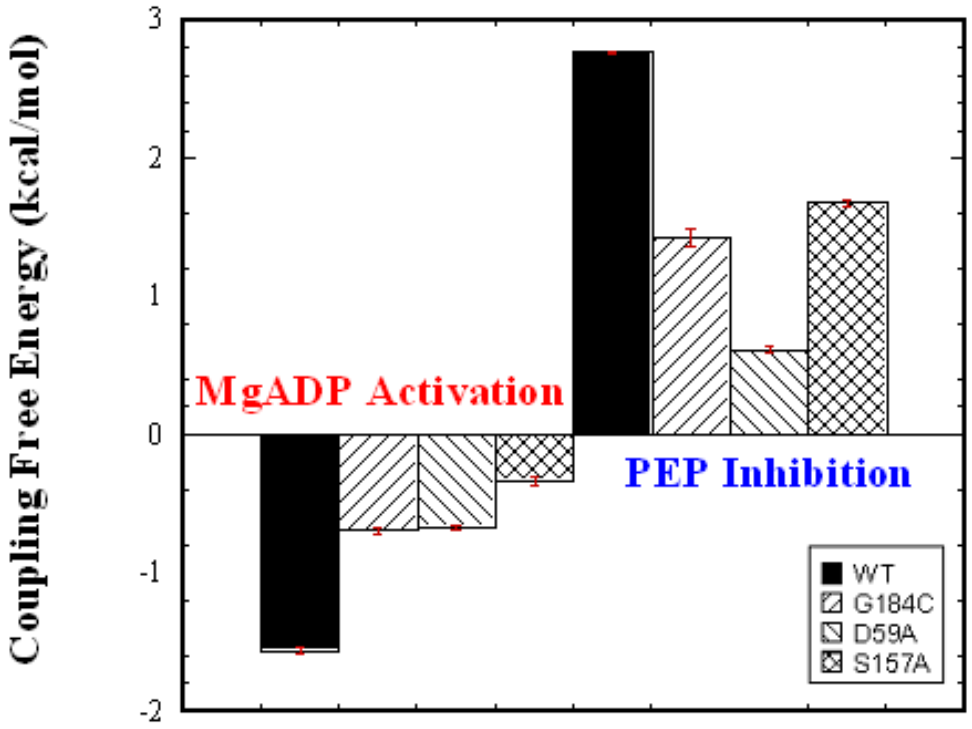

Figure 4-4 Coupling free energy comparisons between wild-type, G184C, D59A and S157A EcPFK for MgADP activation and PEP inhibition. The bar on the left for each heterotropic interaction corresponds to wild-type EcPFK (black). The second bar corresponds to G184C mutant (left striped), the third bar corresponds to D59A mutant (right striped), the bar on the right corresponds to S157A mutant (cross striped).

Introducing G184C, D59A and S157A into each heterotropic interaction

The purpose of current study is to quantify the allosteric effect of each of the three mutations in every heterotropic interaction. Co-expressing each mutant EcPFK with the parent B protein (Chapter II, Table 2-2) for each heterotropic interaction individually, all the hybrid species were formed *in vivo*. The 1:3 hybrid (1|1), contains a specific heterotropic interaction with G184C mutation in the native subunit (Figure 4-5A), was isolated and characterized. The effect of G184C on the allosteric response for each native heterotropic interaction is measured by steady-state kinetics. In the 23Å heterotropic interaction, a three-fold decrease in PEP inhibition and a minimal effect on MgADP activation were observed. In the 33Å heterotropic interaction, PEP inhibition was not changed, but a six-fold decrease in MgADP activation was observed. In the 30Å heterotropic interaction, there is no effect on PEP inhibition and two-fold increase in MgADP activation. In the 45Å heterotropic interaction, neither PEP inhibition nor MgADP activation was influenced as compared to wild-type EcPFK. In addition, the sum of each heterotropic interaction with G184C in it was comparable with the overall heterotropic interaction in EcPFK mutant tetramer (Figure 4-5B, Figure 4-6, Figure 4-7).

However, D59A mutation showed a different pattern of the allosteric response in each interaction. In the 23Å heterotropic interaction, five-fold decrease in PEP inhibition and two-fold decrease in MgADP activation were obtained. In the 33Å heterotropic interaction, PEP inhibition was enhanced and MgADP activation was almost the same as wild-type EcPFK. In the 30Å heterotropic interaction, PEP inhibition decreased to one-third and MgADP activation was completely abolished. In the 45Å heterotropic

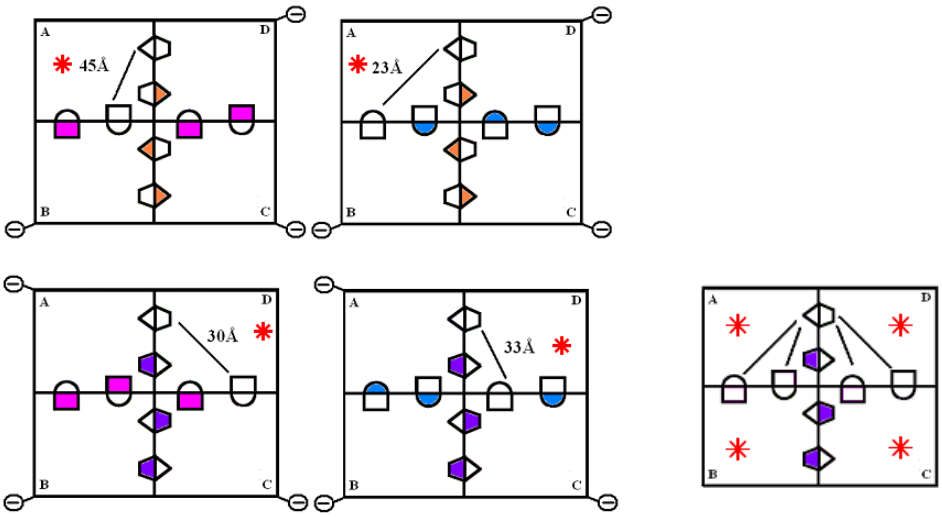

Figure 4-5 Two-dimensional representations for 1|1 and 1|4 hybrids (the first number represents the number of the active site; the second number represents the number of the allosteric site). (A) The 1:3 hybrid (1|1) contains each of the four heterotropic interaction with a specific mutation in the native subunit. (B) The control hybrid (1|4) contains all the four heterotropic interactions with a specific mutation in all the four subunits. Red ✳ represents a specific mutation.

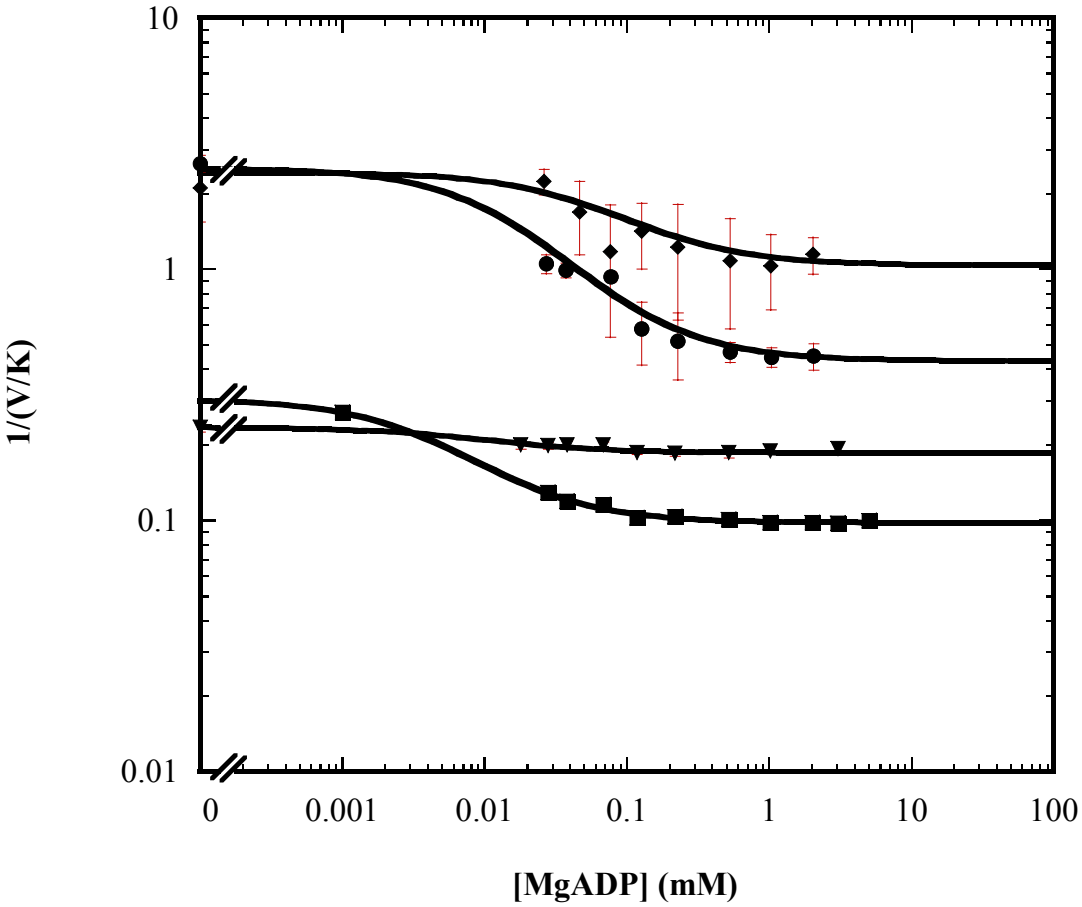

Figure 4-6 The effect of MgADP on the binding of Fru-6-P in the four heterotropic interactions with G184C mutation, 23Å (■), 30Å (●), 33Å (▼), 45Å (◆).

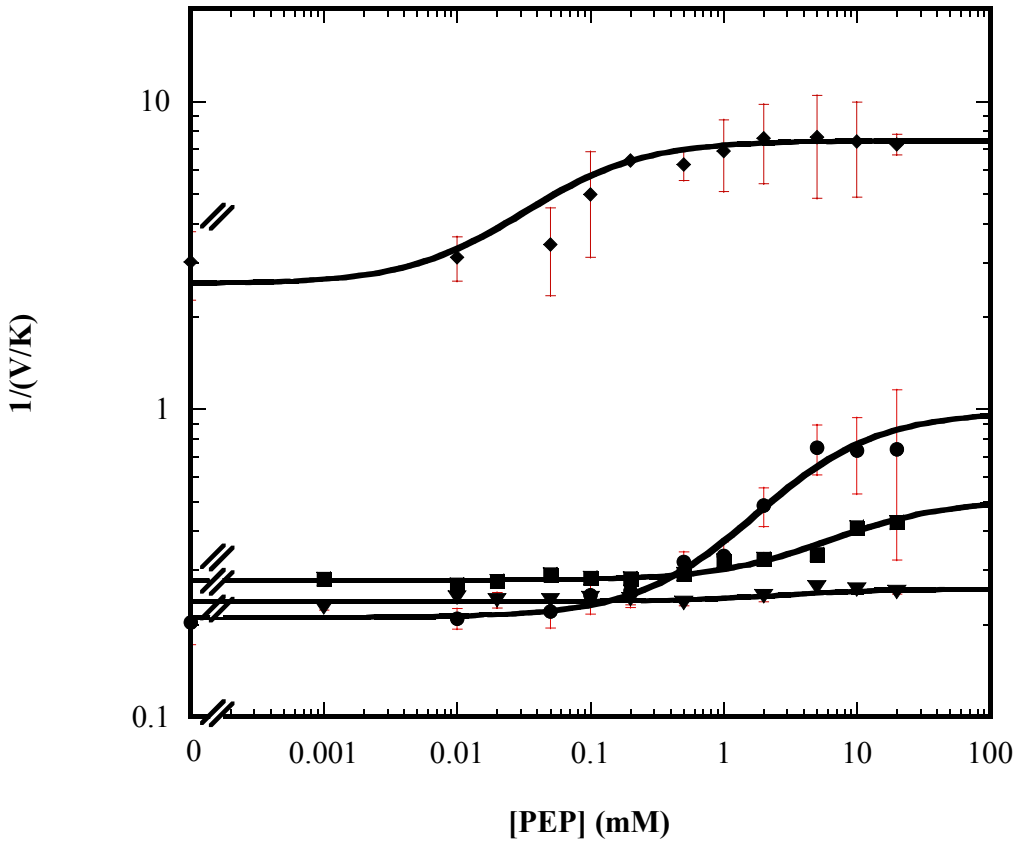

Figure 4-7 The effect of PEP on the binding of Fru-6-P in the four heterotropic interactions with G184C mutation, 23Å (■), 30Å (●), 33Å (▼), 45Å (◆).

interaction, there is no effect on PEP inhibition and two-fold increase in MgADP activation (Figure 4-8, Figure 4-9).

With the S157A mutation, in the 23Å heterotropic interaction, there is only a minor decrease in PEP inhibition and a two-fold decrease in MgADP activation. In the 33Å heterotropic interaction, PEP inhibition was increased and MgADP activation decreased three-fold. In the 30Å heterotropic interaction, both PEP inhibition and MgADP activation were not changed. In the 45Å heterotropic interaction, both PEP inhibition and MgADP activation were comparable to wild-type EcPFK (Figure 4-10, Figure 4-11). The coupling free energy comparisons between each mutant in each heterotropic interaction are shown in Figures 4-12 and 4-13.

From the above results, G184C or D59A mutations affect PEP inhibition through the 23Å interaction. D59A also has some effects on the 30Å interaction. S157A does not show any influence for PEP inhibition in each of the four heterotropic interactions. However, the influence of G184C on MgADP activation is through the 33Å interaction, D59A mainly affects the 30Å interaction greatly for MgADP activation. S157A affects both the 23Å and 33Å interactions for MgADP activation. Thus, PEP inhibition and MgADP activation are influenced differently from the same mutation. Also, the crystal structure of EcPFK (Figure 4-14) may reveal a possible explanation for why G184, D59 and S157 positions are important for MgADP activation through different heterotropic interactions. The relative positions of G184, D59 and S157 in the crystal structure are directly between the active site and the allosteric site in the 33Å interaction, the 30Å interaction and the 23Å interaction, respectively. This may indicate why G184C, D59A

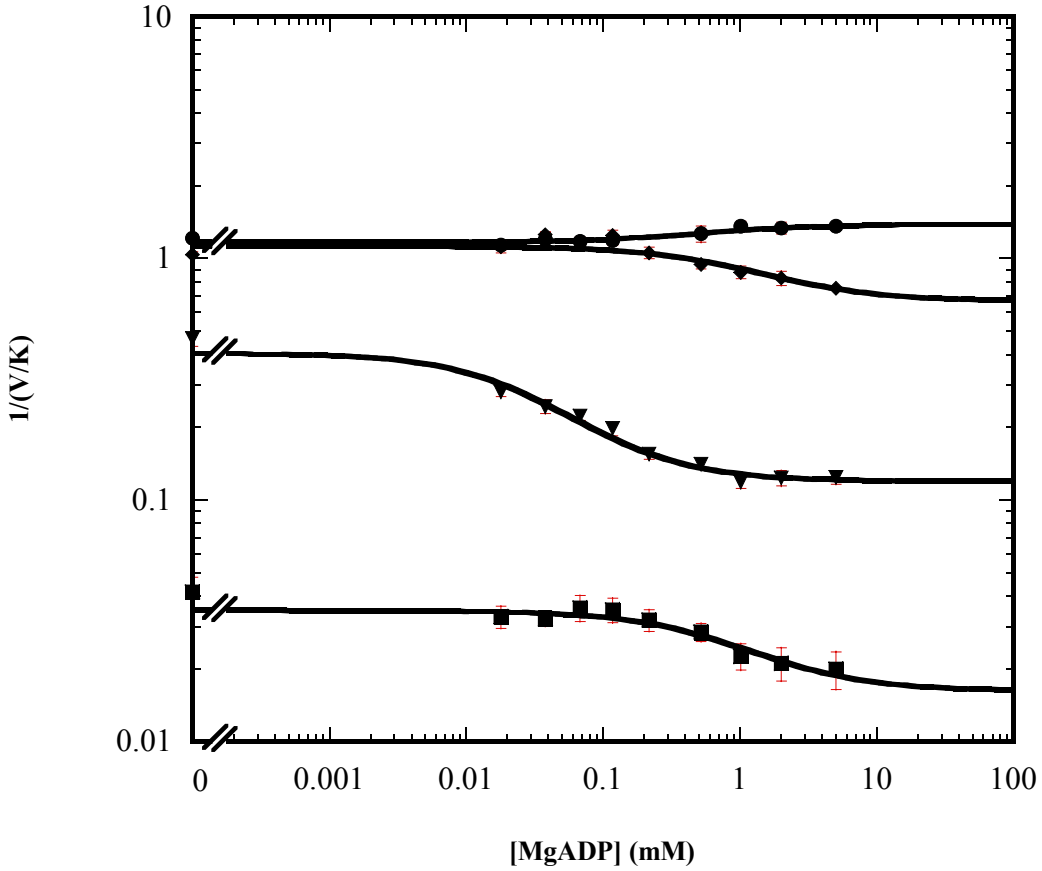

Figure 4-8 The effect of MgADP on the binding of Fru-6-P in the four heterotropic interactions with D59A mutation, 23Å (■), 30Å (●), 33Å (▼), 45Å (◆).

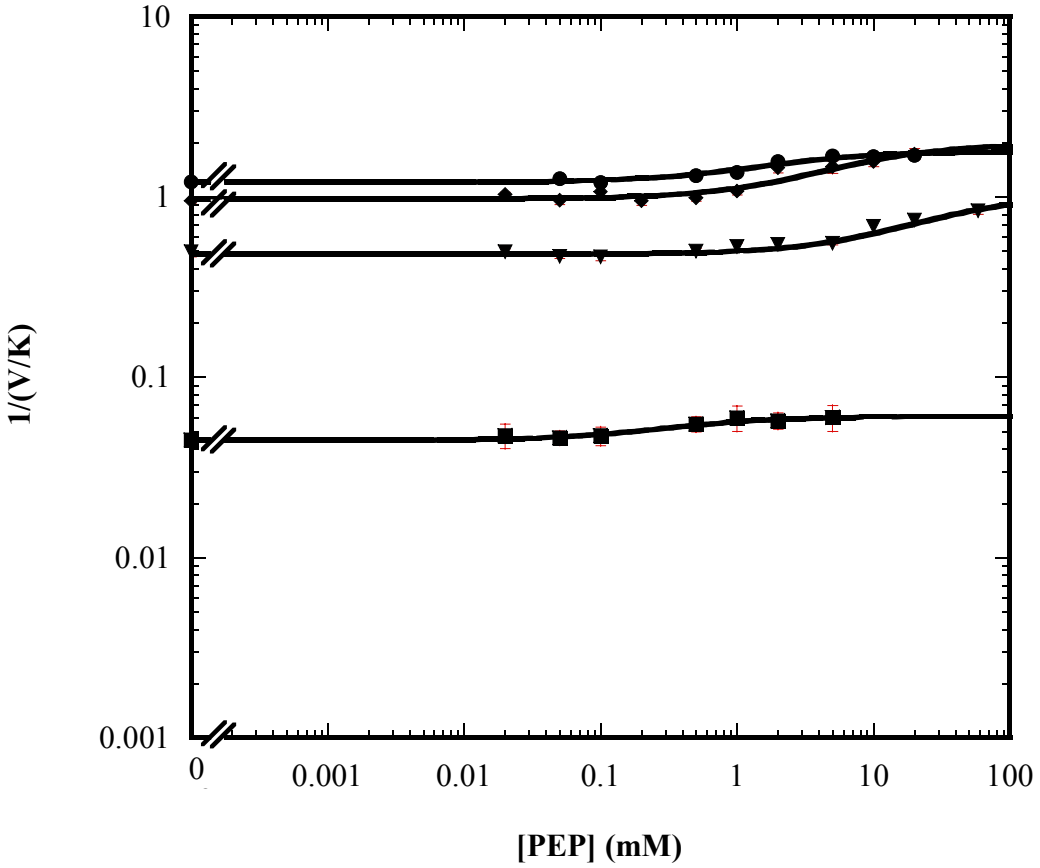

Figure 4-9 The effect of PEP on the binding of Fru-6-P in the four heterotropic interactions with D59A mutation, 23Å (■), 30Å (●), 33Å (▼), 45Å (◆).

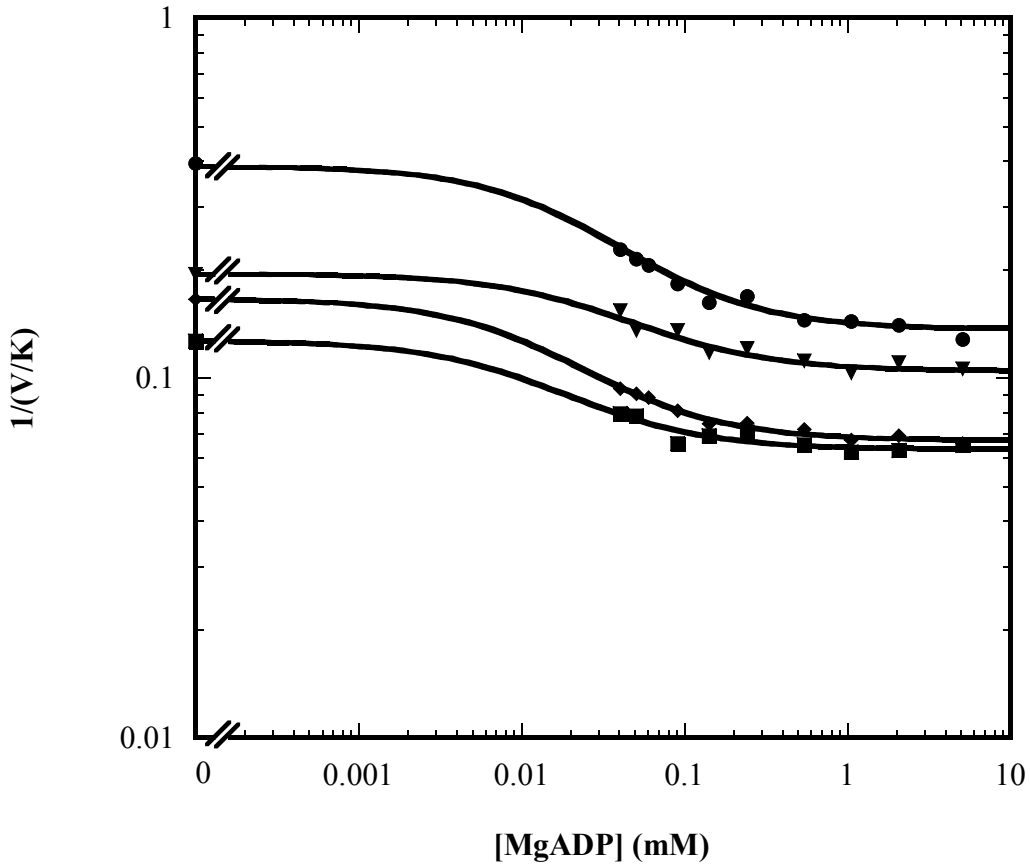

Figure 4-10 The effect of MgADP on the binding of Fru-6-P in the four heterotropic interactions with S157A mutation, 23Å (■), 30Å (●), 33Å (▼), 45Å (◆).

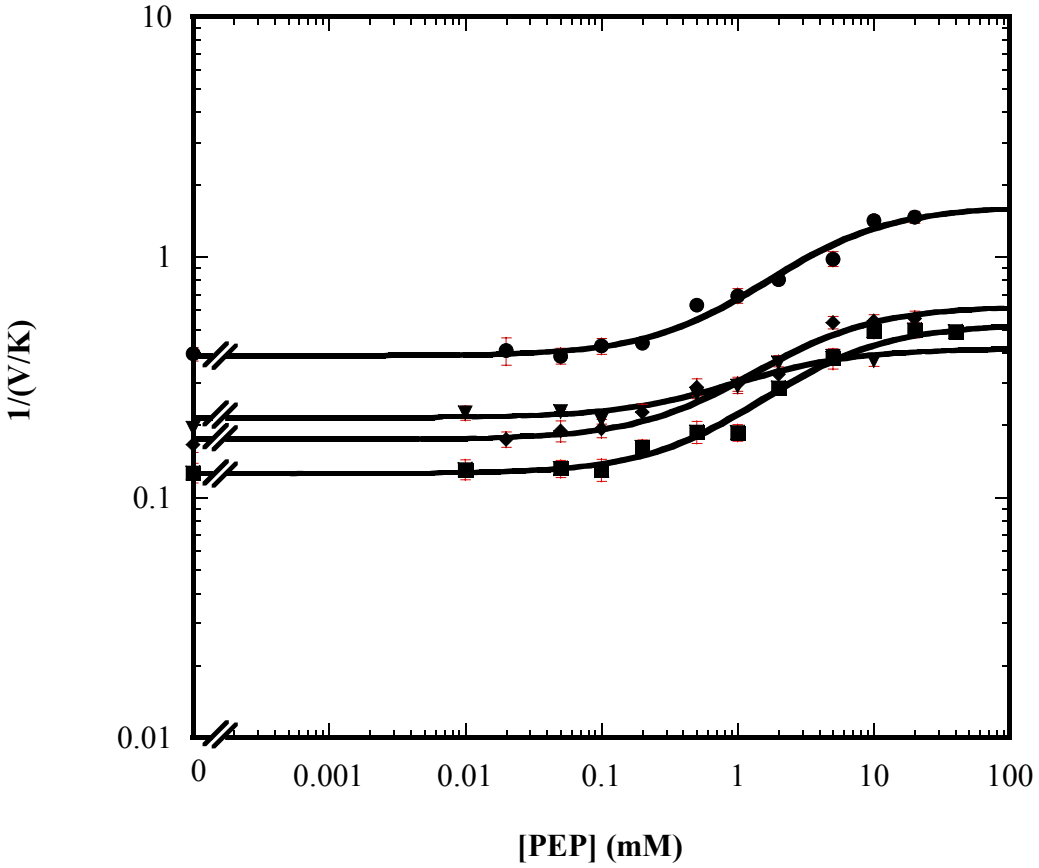

Figure 4-11 The effect of PEP on the binding of Fru-6-P in the four heterotropic interactions with S157A mutation, 23Å (■), 30Å (●), 33Å (▼), 45Å (◆).

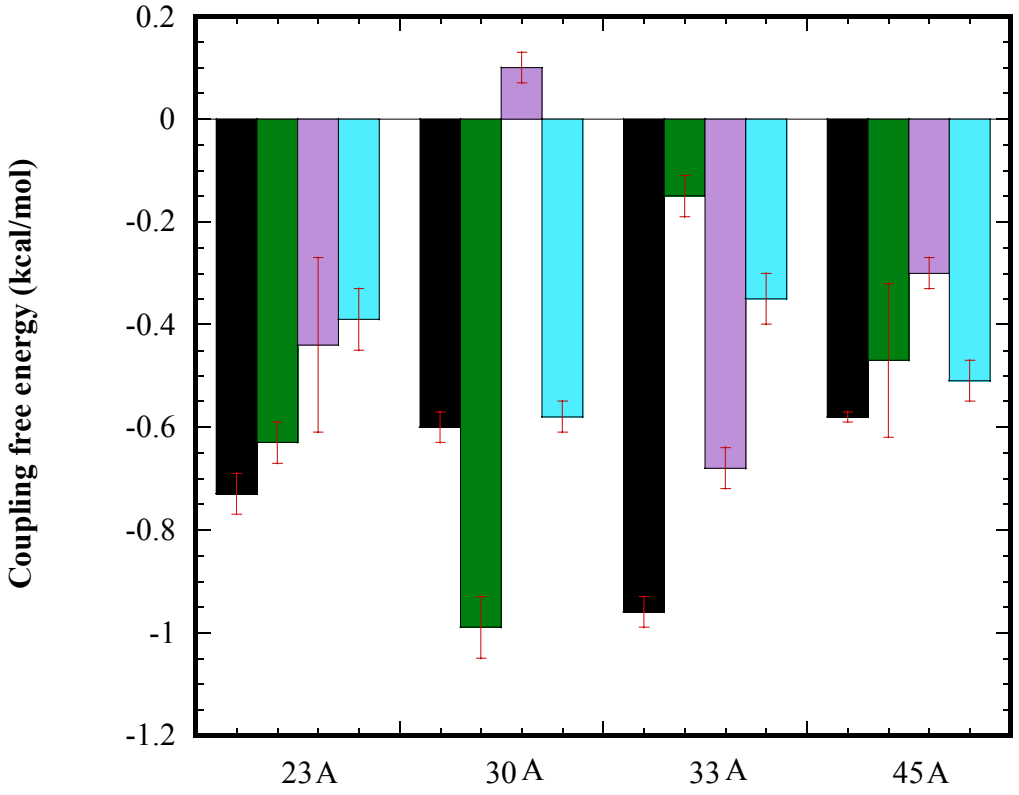

Figure 4-12 Coupling free energy comparisons between wild-type, G184C, D59A and S157A in each isolated heterotropic interaction for MgADP activation. The bar on the left for each heterotropic interaction corresponds to the native interaction (black). The second bar corresponds to the native interaction with G184C mutation (green), the third bar corresponds to the native interaction with D59A mutation (purple), the bar on the right corresponds to the native interaction with S157A mutation (cyan).

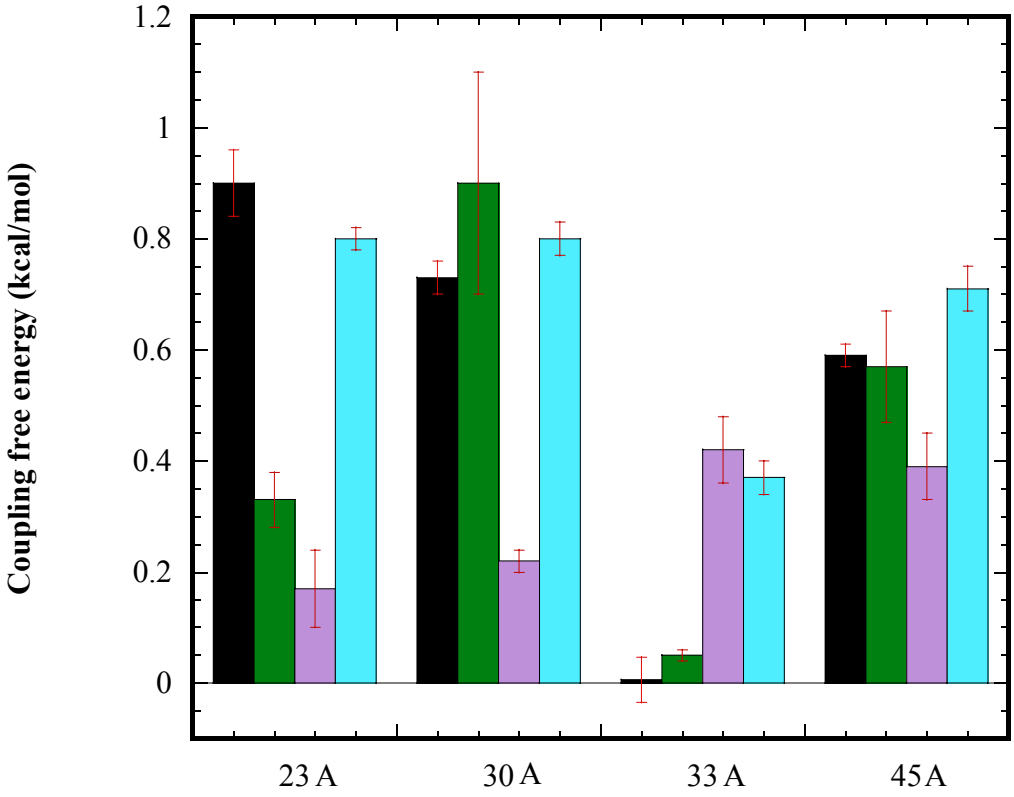

Figure 4-13 Coupling free energy comparisons between wild-type, G184C, D59A and S157A in each isolated heterotropic interaction for PEP inhibition. The bar on the left for each heterotropic interaction corresponds to the native interaction (black). The second bar corresponds to the native interaction with G184C mutation (green), the third bar corresponds to the native interaction with D59A mutation (purple), the bar on the right corresponds to the native interaction with S157A mutation (cyan).

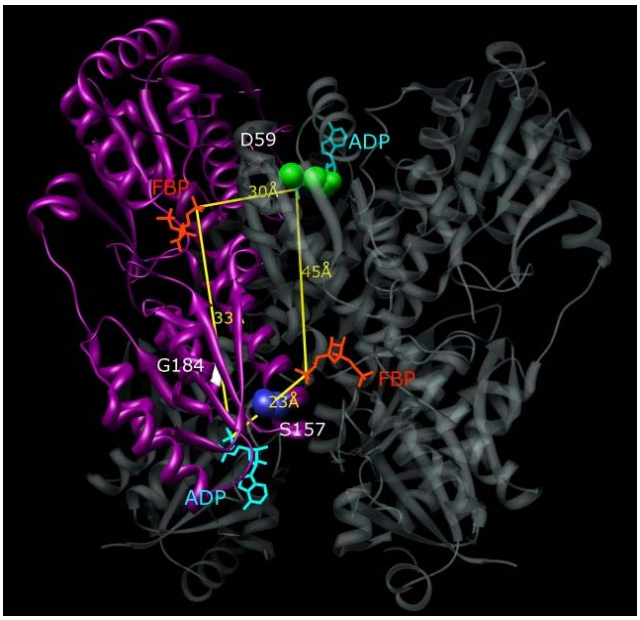

Figure 4-14 The relative position of G184, D59A and S157A in the four unique heterotropic interactions in EcPFK crystal structure. Yellow lines represent the four heterotropic interactions. G184 is shown in white, D59 is in green and S157 is in blue.

and S157A mutation disrupted the 33Å interaction, the 30Å interaction and the 23Å interaction for MgADP activation, respectively. However, the positions of G184 and D59 are far away from the 23Å interaction, which contributes mostly for PEP inhibition. Once again, it indicates PEP inhibition and MgADP activation are using different pathways (Fenton et al., 2003). The relative positions of G184, D59 and S157 in the crystal structure of EcPFK may suggest MgADP activation may use a direct pathway, but PEP inhibition may use an indirect pathway. In addition, D59A mutant protein affects each interaction for MgADP activation but to different extents. The possible reason is that this residue is very close to the allosteric site thus the influence of D59A on the allosteric response may be observed in each heterotropic interaction.

Alternative substitution at position 184

The G184C mutant protein diminished the allosteric response for both MgADP activation and PEP inhibition. To validate the importance of position 184, the G184T mutant protein was characterized and also introduced into the four isolated heterotropic interactions. The G184T mutant EcPFK showed effects similar to the G184C mutant. It has more than a two-fold decrease in MgADP activation and almost a five-fold decrease in PEP inhibition (Figure 4-15). The influence of the G184T mutation on each of the four heterotropic interactions was characterized and compared with the effect of the G184C mutation. Basically, the pattern from the two mutant EcPFKs are very similar (Figure 4-16, Figure 4-17). The sum of each heterotropic interaction equals to the total

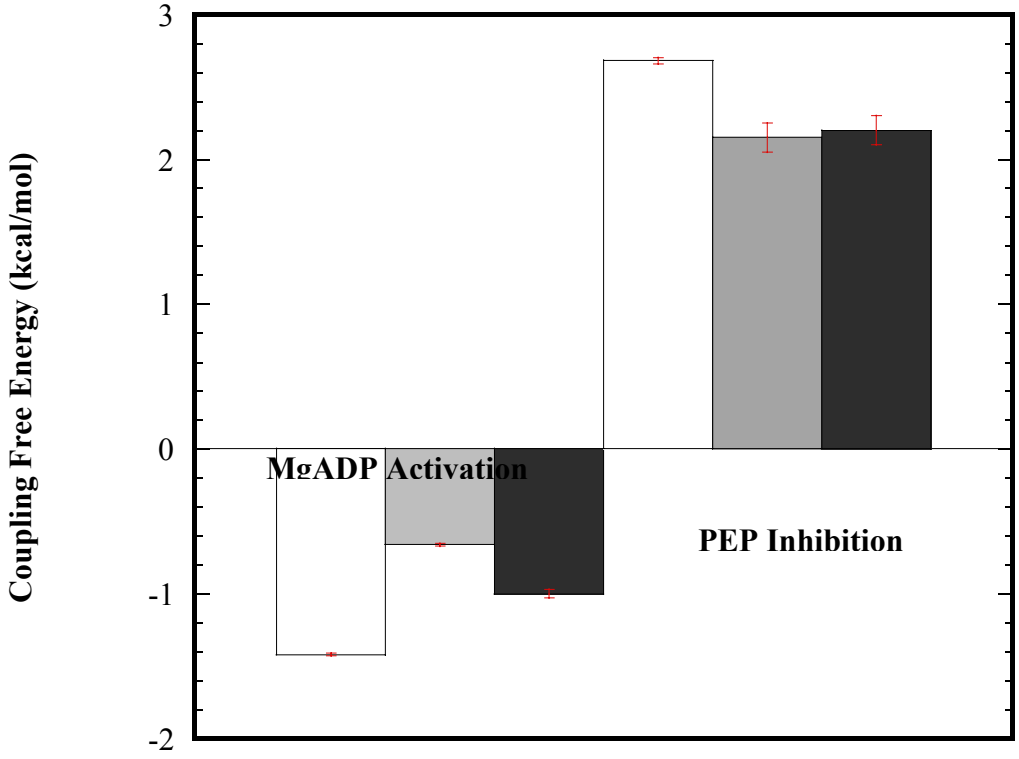

Figure 4-15 Comparisons between wild-type, G184C and G184T in coupling free energy for activation and inhibition. The bar on the left represents the coupling free energy determined for wild-type EcPFK, the bar in the middle represents the coupling free energy determined for G184C mutant protein (light gray) and the bar on the right represent the coupling free energy determined for G184T mutant protein (dark gray).

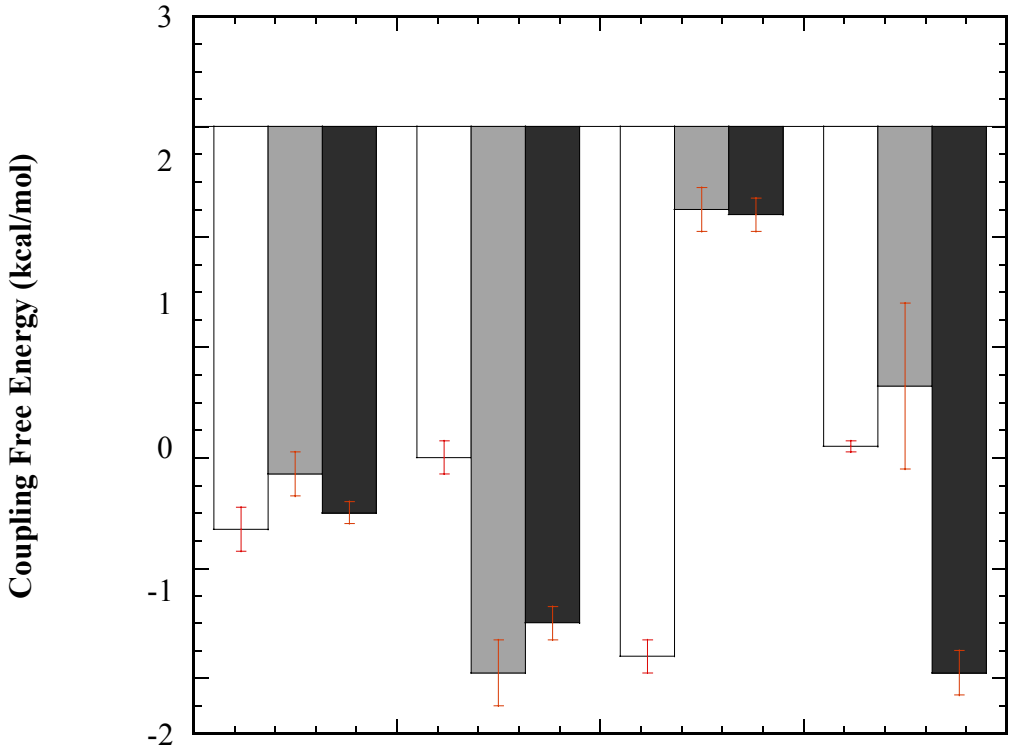

Figure 4-16 Comparisons in coupling free energy for MgADP activation in each of the four heterotropic interactions with either G184C or G184T mutation .The bar on the left at each heterotropic interaction represents the coupling free energy for the native interaction (white), the bar in middle represents the coupling free energy for the native interaction with G184C mutation (light gray) and the bar on the right represents the coupling free energy for the native interaction with G184T mutation (dark gray).

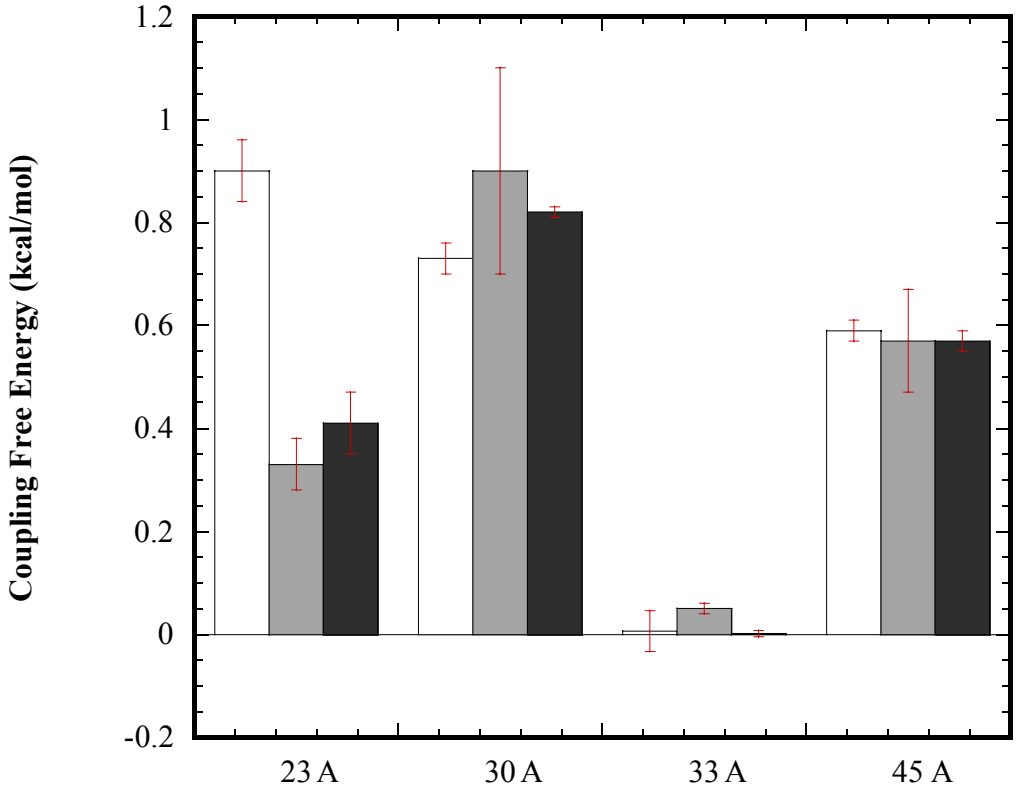

Figure 4-17 Comparisons in coupling free energy for PEP inhibition in each of the four heterotropic interactions with either G184C or G184T mutation. The bar on the left at each heterotropic interaction represents the coupling free energy for the native interaction (white), the bar in middle represents the coupling free energy for the native interaction with G184C mutation (light gray) and the bar on the right represents the coupling free energy for the native interaction with G184T mutation (dark gray).

heterotropic interactions in the mutant EcPFK tetramer without homotropic interactions. G184 was also substituted with valine as well. The G184V mutant protein also has effects similar to the G184C mutant protein. It indicates that the position of 184 is very important for the allosteric signal transmission. However, the side chain of different amino acids may produce different effects on allosteric regulation.

Control hybrids

Each 1:3 hybrid tetramer (1|1) that contains an individual heterotropic interaction, has only one native active site and one native allosteric site. However, homotropic cooperativities between the four native active sites are shown in EcPFK tetramer. Therefore, the sum of each isolated heterotropic interaction cannot be compared with the overall heterotropic interaction in wild-type EcPFK. To eliminate the homotropic cooperativity in the wild-type EcPFK, the 1|4 control hybrid tetramer was constructed, which has only one native active site and four native allosteric sites and has either G184C, D59A or S157A mutation in all the four subunits. For the G184C, D59A and S157A mutant protein, the sum of coupling free energy from each heterotropic interaction equals to the coupling free energy from the 1|4 control hybrid for both PEP inhibition and MgADP activation (Figure 4-18). Importantly, each mutation is in all the four subunits in 1|4 control hybrid protein, but this mutation is in the one native subunit in 1|1 hybrid protein. This result suggests that the presence or absence of a specific mutation in the other three subunits is inconsequential. Therefore, the allosteric signal is transmitted in one subunit. Moreover, the different coupling free energy between each mutant EcPFK, which has both homotropic and heterotropic interactions, and 1|4 control

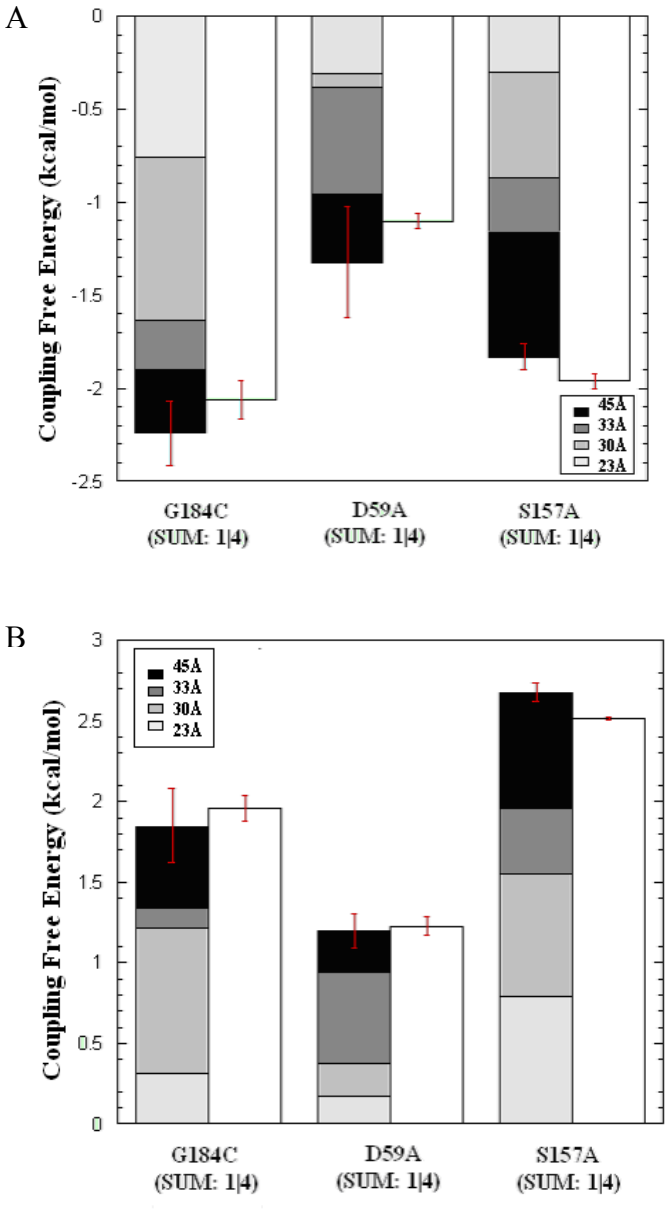

Figure 4-18 The sum of the coupling free energies determined for each heterotropic interaction with G184C mutation, D59A mutation and S157A, respectively, compared to the total heterotropic coupling free energy exhibited by the 1|4 control for MgADP (A) activation and PEP (B) inhibition.

hybrid EcPFK, which has only heterotropic interactions, indicates that homotropic interactions influence the heterotropic interactions.

Conclusions

In summary, three residues, G184, D59, and S157 that are likely to be involved in allosteric information transmission have been identified. Taking advantage of the *in vivo* procedure for making hybrids, the G184C, D59A and S157A mutations were introduced into the 1:3 hybrids that present each heterotropic interaction of EcPFK individually. All mutated residues differently disrupted each heterotropic interaction and showed different patterns for both PEP inhibition and MgADP activation. This result indicates that the allosteric pathway is different for PEP inhibition and MgADP activation in EcPFK. Moreover, different substitutions at G184 position showed similar effects on both PEP inhibition and MgADP activation suggesting that although different side chains may influence coupling free energy, position 184 is very important for allosteric signal transfer. In addition, the sum of each heterotropic interaction is equal to the total heterotropic interaction in each mutant EcPFK tetramer without the homotropic interactions. This is consistent with our previous results in wild-type EcPFK and wild-type BsPFK (Fenton, et al., 2004; Ortigosa, et al., 2004). More importantly, the G184C mutation is in all the four subunits in the 1|4 control hybrid protein, but this mutation is only in the one otherwise native subunit in 1|1 hybrid protein. This result suggests the presence or absence of G184C in the other three subunits is inconsequential. Therefore, the allosteric signal is transmitted in a single subunit. Moreover, the different coupling

free energy between each mutant EcPFK and 1|4 control hybrid EcPFK indicates that homotropic interactions have influence on the heterotropic interactions.

CHAPTER V

STUDY ON THE DYNAMIC PROPERTIES OF ALLOSTERIC COMMUNICATION IN *E. COLI* PHOSPHOFRUCTOKINASE

Introduction

As shown in chapter IV, the heterotropic allosteric signal in EcPFK is transmitted via intra-subunit interactions. The next question to be addressed is how the dynamic properties exhibited in one subunit are influenced by different ligand binding events. Since the four heterotropic interactions each made a unique contribution to the total allosteric effect, and the 23Å heterotropic interaction makes the largest contribution to PEP inhibition, we focus on the dynamic properties of this heterotropic interaction. Fluorescence was used to study the dynamic changes of the 23Å interaction upon ligand binding. Taking advantage of the hybrid formation strategy and the tryptophan-shift mutagenesis method, a tryptophan residue can be placed at different individual locations throughout the otherwise native subunit containing the 23Å heterotropic interaction. Our ultimate goal is to map the dynamic perturbations within an EcPFK subunit to gain insight and understanding of the allosteric pathway.

The fluorescence properties of a tryptophan in a protein are usually sensitive to the conformational change with ligand binding and can be monitored in the absence of turnover. In addition, the advantage of utilizing a single fluorescence probe is that a significant fraction of the fluorescence signal can be affected by the environmental dynamics located within the vicinity of the fluorophore. Thus, to characterize the nature

of the perturbation in the vicinity of a specific tryptophan in the 23Å interaction, we need to monitor the response to the different ligand binding forms appearing in equation 1-6. Steady-state fluorescence anisotropy measurements give us the first indication of changes in motion upon ligand binding in EcPFK. The changes in motion can result from either the global movement of EcPFK or local rotation or flexibility around the tryptophan. Since it is unlikely that the binding a small ligand to EcPFK will affect the global rotation, the changes in anisotropy potentially reflect the local motion of the tryptophan. However, changes in anisotropy can result from changes in the decay rate of the fluorophore, which is the reciprocal of the fluorescence lifetime of the probe. In order to resolve the source of these anisotropy changes, the lifetime for each tryptophan was also measured.

An *in vivo* method for hybrid formation was used to dissect the 23Å heterotropic interaction of EcPFK (Chapter III). Two parent proteins are used to form a 1:3 hybrid that presents the 23Å heterotropic interaction (Table 2-2). Parent A protein is wild-type EcPFK; parent B protein has the active site mutation, R243E, the allosteric site mutation, H215E, and the charge-tag mutations K90E/K91E. The resulting 1:3 hybrid protein has one native subunit that gives rise to a single heterotropic interaction and three mutated subunits that bind ligands very weakly.

To monitor the dynamic properties in the 23Å heterotropic interaction, the native tryptophan at position 311 in EcPFK was used as the first probe. As shown previously, W311 is sensitive to local motion upon ligand binding in the EcPFK tetramer (Johnson and Reinhart 1992,1994 and 1997). There are four native tryptophans in EcPFK tetramer,

one per subunit. The tryptophans in the three mutated subunits were substituted with tyrosine leaving the single tryptophan at position 311 as the fluorescence probe for the native subunit containing the 23Å interaction. To make this 1:3 hybrid, the parent A protein is still wild-type EcPFK; the parent B protein is the 23Å interaction parent B protein with W311Y mutation (23Å parent B-Trp minus). The 1:3 hybrid has one native subunit that contains a single tryptophan and three mutated subunits, which have no tryptophan residues. To monitor the dynamic properties at different positions with the native subunit containing the 23Å interaction, the tryptophan-shift mutagenesis strategy was employed to relocate the tryptophan to different positions in the native subunit. The tryptophan-shift mutagenesis strategy was first used in BsPFK (Riley-Lovingshimer and Reinhart, 2001, 2002 and 2005). BsPFK has a single tryptophan at position 179. However, the fluorescence of this tryptophan is not very responsive to ligand binding events. The native tryptophan was removed from position 179 and an alternative tryptophan substitution was placed in another position in the protein. A tangible fluorescence response was obtained from the tryptophan-shift mutant described. Using the same approach, a protein that has more than one tryptophan can be transformed to a protein with only one tryptophan in order to measure the fluorescence response from a specific tryptophan position. For example, carbamoyl phosphate synthetase (CPS) from *E. coli* has six native tryptophans. To characterize the conformational changes, a tryptophan-free mutant of CPS was made by substituting the six native tryptophans with tyrosines. Each tryptophan was then reinserted to monitor the fluorescence response to different ligand binding events from each specific tryptophan position (Johnson et al.,

2007). Similarity in the side chain structures by substituting a tryptophan with a tyrosine or phenylalanine may have a relatively small alteration to protein structural integrity. Thus, the substitution may not significantly affect the functional properties of proteins. Using this method for EcPFK, the native tryptophan residue at position 311 was substituted with tyrosine. A phenylalanine or tyrosine, located in different regions of the protein, was substituted with a tryptophan. The tryptophan-shift mutant protein is co-expressed with the 23Å parent B-Trp minus protein. As a result, the tryptophan fluorophore was effectively relocated to a different site within the 23Å interaction. Tryptophan at each position is used as fluorescence probe to monitor the dynamics in the 23Å heterotropic interaction upon ligand binding.

Materials and Methods

Materials

All chemical reagents used for protein purification, enzyme kinetic assay and fluorescence experiments were described in chapter II. Mono Q 10/10, an anion exchange column, from Phamacia was used for separation of 1:3 hybrid with different tryptophan-shift mutations in the 23Å heterotropic interaction as in Chapter II. Tryptophan-shift mutants were made using Altered Sites II Mutagenesis System. The following oligonucleotides were ordered from Integrated DNA Technologies (IDT) to be used for mutagenesis.

F76W, 5'- GGA TGT TCT CGT CGC GCC ATT CCG GGA AAC GC -3'

Y106W, 5'- CGC ATT GCA CCC ATC CAG GAA CCG TCA CCG CCG -3'

F140W, 5'- CTC AGC GCA GTC CAG AAA CCG ATA GTG TAG -3'

F188W, 5'- CTT CCG GAA CCA CAA CCC ATT CAC AGC CAC CGG C -3'

F196W, 5'- GGT CTT CAC GGC TCC ATT CAA CTT CCG G -3'

F233W, 5'- CCG GTT TCT TTC TCG ATC CAA TGC GCC AGT TCG -3'

W311Y, 5'- CGC GCA GTC CAG ATA GTC GCC TTT GAA CGG ACG -3'

Formation of the 1:3 hybrid with one specific tryptophan involved in the 23Å heterotropic interaction

The 1:3 hybrid was created using a modified protocol from Chapter III. Two parent proteins were used to generate the 1:3 hybrid of the 23Å heterotropic interaction with the native tryptophan only in the native subunit. Parent A protein is wild-type EcPFK; parent B protein is the 23Å parent B with W311Y mutation (23Å parent B-Trp minus). After co-expression, the 1:3 hybrid protein has only one native tryptophan at position 311 in the subunit that displays the 23Å heterotropic interaction (Figure 5-1). The tryptophans in the other three subunits were mutated to tyrosine. Subsequently, site-directed mutagenesis was performed on pGDR148 to introduce site-specific tryptophan substitutions in EcPFK. A tryptophan was introduced at a different position in the 23Å interaction. To make the corresponding 1:3 hybrid protein, the parent A protein of the hybrid is a tryptophan-shift mutant in which W311 was changed to tyrosine and either a tyrosine or phenylalanine at another position in the protein was mutated to tryptophan. As a result, tryptophan was placed at different positions and the native tryptophan at

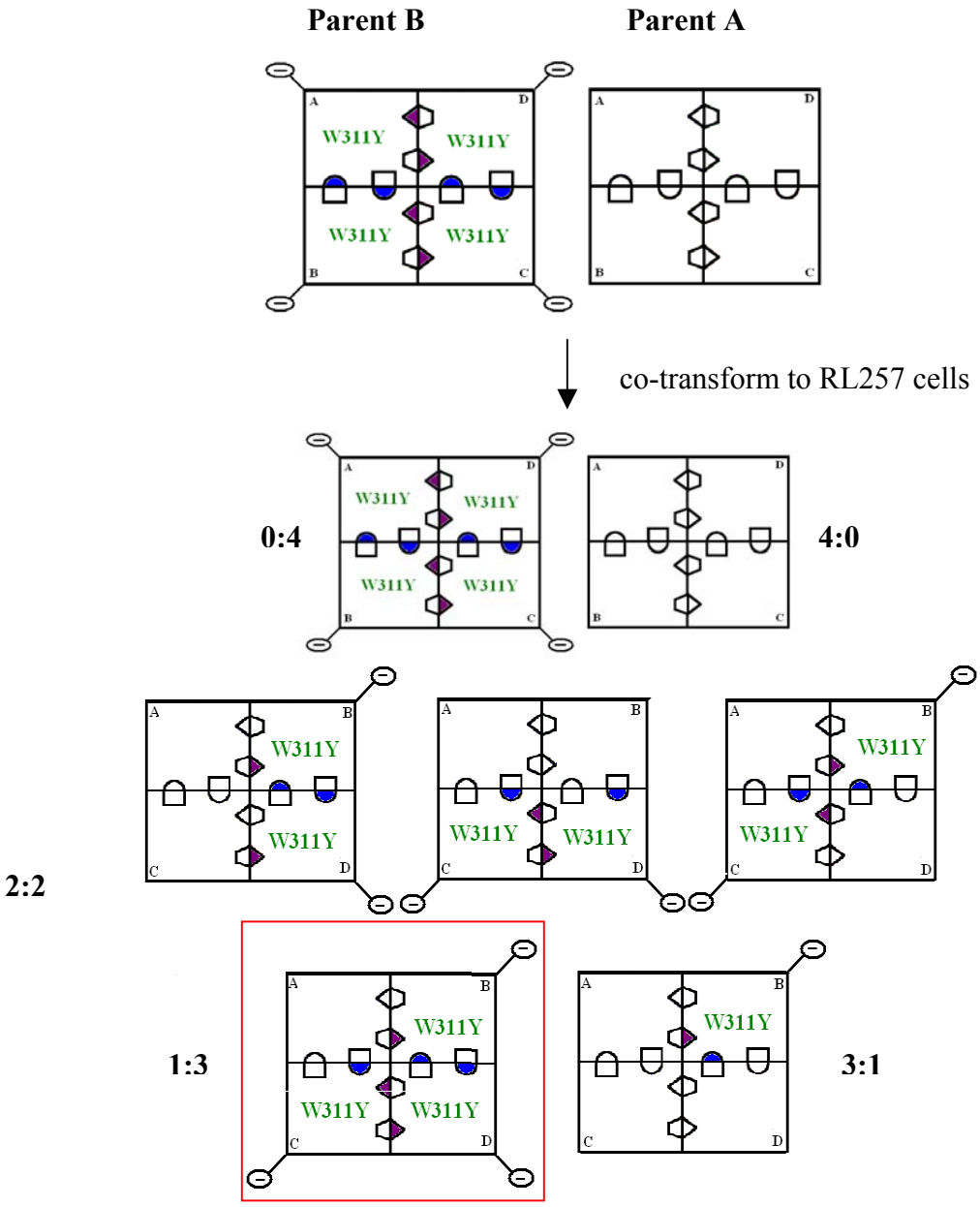

Figure 5-1 Strategy used to create hybrid tetramers of EcPFK containing only one native tryptophan in the 1:3 hybrid protein presenting the 23Å heterotropic interaction. The 1:3 hybrid has W311 in the native subunit and W311Y in the other three mutated subunits.

.

position 311 was removed at the same time. The parent B protein is the 23Å parent B-Trp minus. Each mutation was confirmed by sequencing over the region of interest. After co-expression the two parent proteins in RL257 cells, the 1:3 hybrid was separated by anion-exchange column as described in Chapter II. This 1:3 hybrid that presents the 23Å heterotropic interaction does not have the native tryptophan, but has a tryptophan at a specific position.

Generation of enzyme ligand forms

To study the dynamic properties in the 23Å interaction in EcPFK, the fluorescence response of a tryptophan upon ligand binding was monitored. Thus, EcPFK with different ligands bound at the saturating concentration was generated. Each ligation state of EcPFK, PFK-Fru-6-P, PFK-PEP, PFK-MgADP, was generated via the addition of 2 mM Fru-6-P, 10 mM PEP, 2 mM MgADP, respectively. 10 mM Fru-6-P and 25 mM PEP were added to generate the ternary complex PEP-PFK-Fru-6-P. 2mM F6P, and 2 mM MgADP were added to form the ternary complex MgADP-PFK-Fru-6-P. Based on the ligand dissociation constants determined for each hybrid, less than 5% of the PFK would exist in other forms under these conditions. The ligation state designated MgADP-PFK generated by this manner will also have MgADP bound to the active site. However, since MgADP in the active site has been shown not affect the intensity or anisotropy of the tryptophan fluorescence in EcPFK, its presence in these species has been ignored (Johnson and Reinhart, 1994).

Data analysis

The Perrin equation (1-19, 1-20) was used to analyze the rotational correlation time (θ) for each ligation state. This analysis contains two assumptions: first, we assume EcPFK protein is a sphere; second, the global rotational correlation time is the same in all the measurements. Based on that, the changes in θ represent the changes in the local motion. The decrease of rotational correlation time suggests faster motion around a specific tryptophan position, while an increase in the correlation time indicates slower rotation.

Results and Discussions

Hybrid formation of the 23Å heterotropic interaction with tryptophan at different positions

Six tryptophan-shift mutant proteins were made using Altered Sites II Site-Directed *in vitro* Mutagenesis System. The native tryptophan at position 311 was replaced by tyrosine. Either conserved tyrosine or phenylalanine in other regions of the protein was mutated to tryptophan. The relative positions of the six residues and W311 are shown in the EcPFK crystal structure (Figure 5-2). The distances to the ligand binding sites in the 23Å heterotropic interaction for each position are shown in Table 5-1. Positions 188 and 311 are relatively close to the allosteric site, within 20Å. Positions 140, 233 and 196 are approximately 25Å from the allosteric site. Position 106 and 76 are further away from both active site and allosteric site with more than 35Å distance

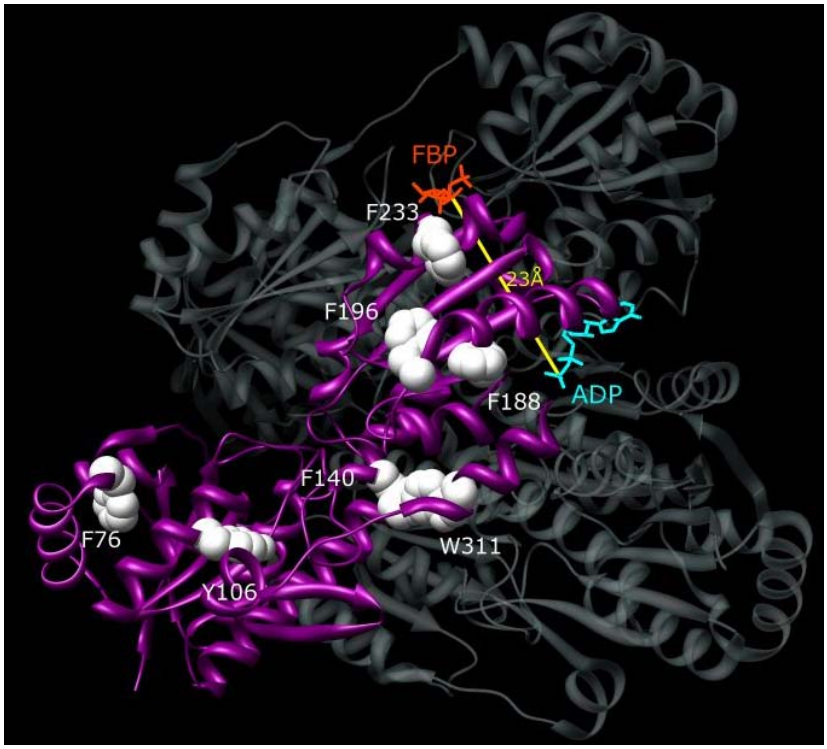

Figure 5-2 The positions of each tryptophan substitution in EcPFK crystal structure. FBP is shown in red, ADP is in cyan. The yellow line represents the 23Å heterotropic interaction. Tryptophan-shift mutant candidates are shown in white space fill.

Table 5-1 The distance between each substituted tryptophan position and the active site or the allosteric site in the 23Å heterotropic interaction.

Trp Position	FBP	ADP
188	24Å	16Å
311	32Å	19Å
106	43Å	36Å
76	49Å	49Å
233	21Å	23Å
140	34Å	22Å
196	23Å	21Å

relative to the active site, positions 188,196 and 233 are within 25Å, while positions 140 and 311 are 35Å away. To use the native tryptophan at position 311 as a fluorescence probe in the 23Å heterotropic interaction, wild-type EcPFK and the 23Å parent B-Trp minus protein were co-expressed. To relocate tryptophan in the 23Å heterotropic interaction, the tryptophan-shift mutant protein was used instead of wild-type EcPFK for the co-expression. All the five hybrid species were formed *in vivo* with each tryptophan at different position involved in the 23Å interaction. The 1:3 hybrid was separated and identified as shown in Chapter II and used to measure steady-state anisotropy and fluorescence lifetime.

Steady-state fluorescence

Steady-state fluorescence was used to measure the response of tryptophan at each position individually to the binding of different ligands relevant to the 23Å interaction. The steady-state fluorescence intensity and anisotropy data are listed in Table 5-2. In addition, the changes in steady-state anisotropy data in each ligation state are plotted in Figure 5-3 and further summarized in the crystal structure shown in Figure 5-4. Compared to the free enzyme form, white indicates no change in anisotropy (we consider a value < 0.04 to be negligible); green and red represent either a decrease or an increase in anisotropy, respectively. Meanwhile, each of the 1:3 hybrid proteins with a different tryptophan-shift mutation in the 23Å interaction were characterized using steady-state kinetics and compared with the native 23Å interaction. The kinetics data are shown in Table 5-3. There were no big differences observed for either the binding constant or the coupling free energy except for the F188W/W311Y mutation.

Table 5-2 Steady-state intensity and anisotropy data for the 23Å interaction with each tryptophan-shift mutation.

23Å	23Å (W311) 1: 3 Hybrid		23Å (W188) 1: 3 Hybrid	
	Intensity	Anisotropy	Intensity	Anisotropy
No ligand		0.178±0.001		0.197±0.001
2 mM Fru-6-P	-18 %	0.171±0.0009	-7%	0.199±0.001
10mM PEP	-6% -12%	0.180±0.001	+126%	0.206±0.001
10mM Fru-6-P+ 25mM PEP	-23%	0.175±0.001	+86%	0.207±0.001
2mM MgADP	-13%-15%	0.190±0.002	-56%	0.206±0.0005
2mM MgADP + 2mM Fru-6-P	-13%-14%	0.192±0.0008	-64%	0.210±0.002
23Å	23Å (W76) 1: 3 Hybrid		23Å (W106) 1: 3 Hybrid	
	Intensity	Anisotropy	Intensity	Anisotropy
No ligand		0.209±0.0009		0.200±0.001
2 mM Fru-6-P	-2 %	0.204±0.0005	-7%	0.198±0.002
10mM PEP	-11%	0.209±0.0008	-7%	0.200±0.0006
10mM Fru-6-P+ 25mM PEP	-12%	0.209±0.0004	-27%	0.207±0.0003
2mM MgADP	-74%	0.205±0.001	-62%	0.192±0.001
2mM MgADP + 2mM Fru-6-P	-73%	0.202±0.001	-64%	0.200±0.001
23Å	23Å (W233) 1: 3 Hybrid		23Å (W140) 1: 3 Hybrid	
	Intensity	Anisotropy	Intensity	Anisotropy
No ligand		0.148±0.0004		0.216±0.0002
2 mM Fru-6-P	+1%	0.139±0.0008	+3%	0.216±0.001
10mM PEP	-6%	0.156±0.001	-4%	0.217±0.0009
10mM Fru-6-P+ 25mM PEP	-17%	0.158±0.0008	-18%	0.222±0.001
2mM MgADP	+2%	0.172±0.001	-9%	0.219±0.001
2mM MgADP + 2mM Fru-6-P	-7%	0.175±0.0006	-4%	0.219±0.0008
23Å	23Å (W196) 1: 3 Hybrid			
	Intensity	Anisotropy		
No ligand		0.143±0.001		
2 mM Fru-6-P	-3%	0.142±0.001		
10mM PEP	-9%	0.143±0.001		
10mM Fru-6-P+ 25mM PEP	-16%	0.143±0.0009		
2mM MgADP	-8%	0.141±0.0008		
2mM MgADP + 2mM Fru-6-P	-10%	0.141±0.001		

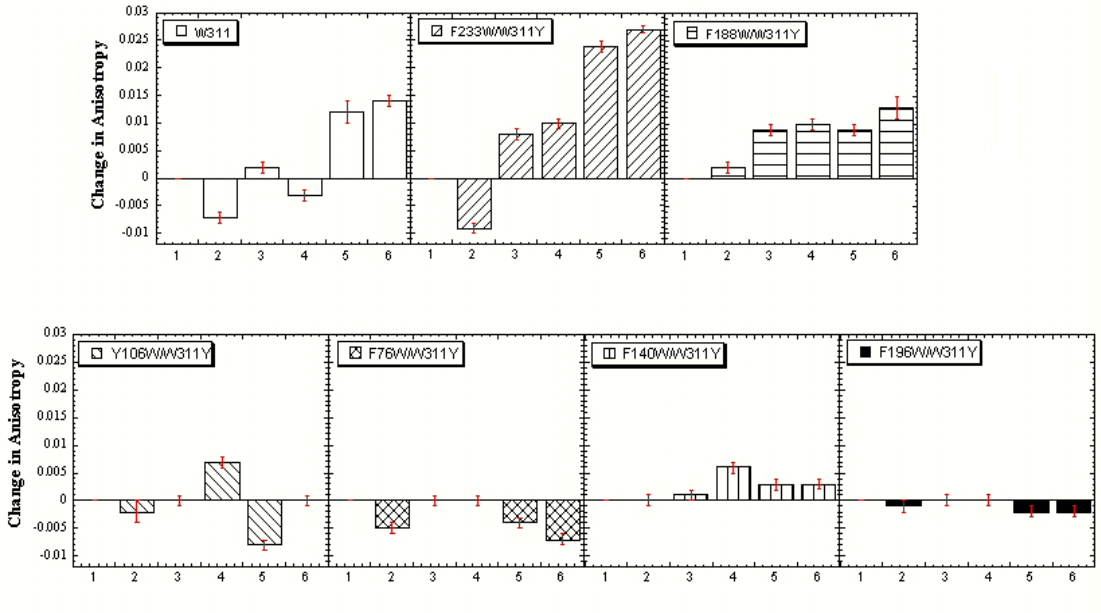

Figure 5-3 The comparisons in anisotropy changes at each tryptophan position in the 23Å interaction with different ligand bound forms of the enzyme. On the x-axis: (1).no ligand, (2). + 2mM Fru-6-P, (3). + 10 mM PEP, (4). + 10mM Fru-6-P+25 mM PEP, (5). + 2mM MgADP, (6). + 2 mM MgADP+ 2 mMFru-6-P.

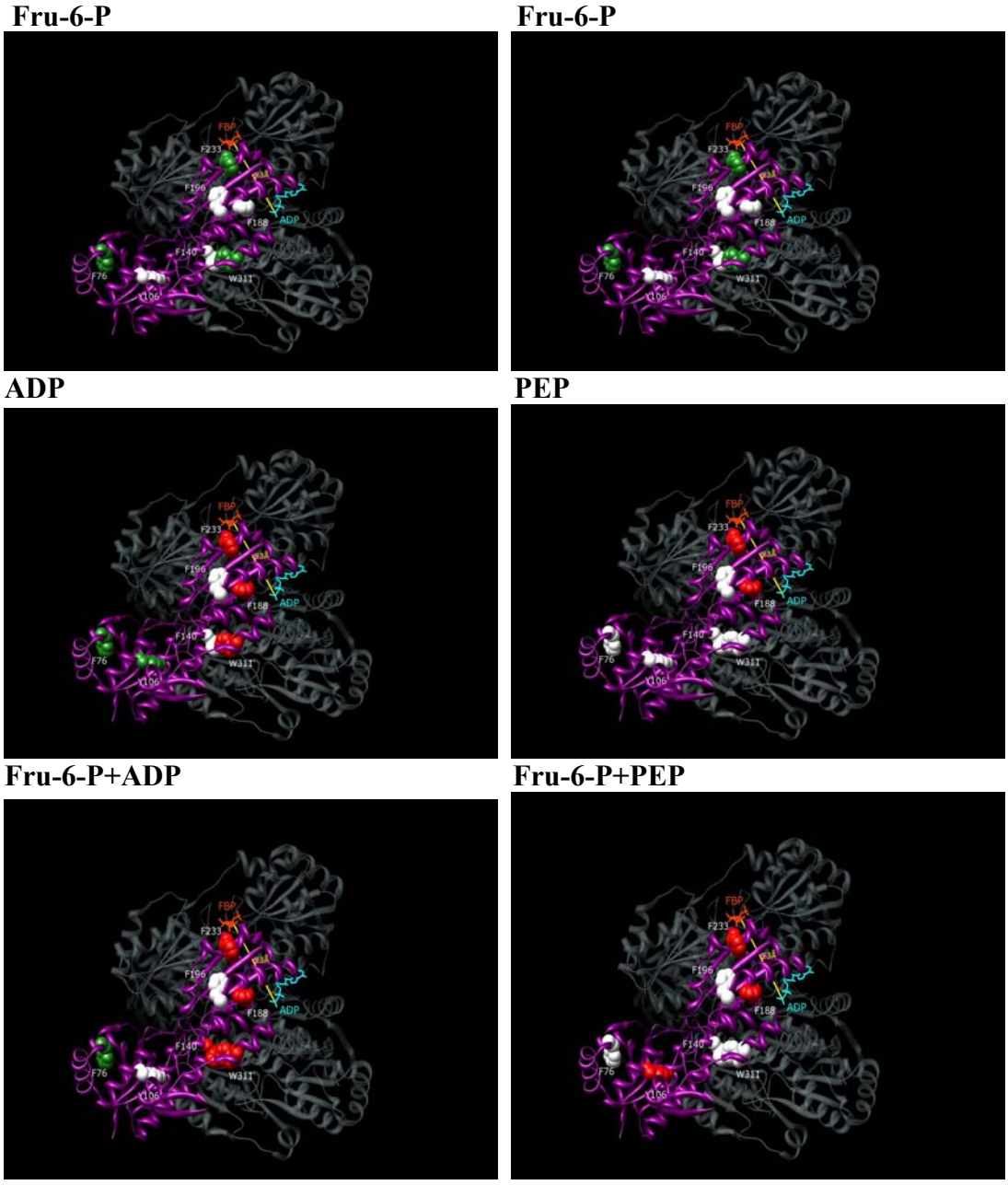

Figure 5-4 The anisotropy changes in the 23Å interaction at each substituted tryptophan position in EcPFK crystal structure. Relative to the free enzyme, white: no change; green: anisotropy decrease; red: anisotropy increase. Anisotropy decreases or increases above 0.04 is considered as a change.

Table 5-3 Kinetics and thermodynamics data for the 1:3 hybrid containing the 23Å interaction with different tryptophan-shift mutations.

Hybrid protein	K°_{ia} mM	K°_{ix} mM	K°_{iy} mM	ΔGax	ΔGay
23Å	0.69±0.07	0.05±0.008	0.14±0.01	-0.71±0.08	0.90±0.06
23Å(F76W/W311Y)	0.21±0.007	0.048±0.01	0.37±0.04	-0.68±0.04	1.03±0.03
23Å(Y106W/W311Y)	0.23±0.002	0.32±0.03	0.48±0.04	-1.02±0.02	0.87±0.02
23Å(F188W/W311Y)	9.24±0.45	0.1±0.02	0.56±0.07	-0.66±0.03	1.23±0.03
23Å(F233W/W311Y)	0.32±0.01	0.67±0.08	0.1±0.01	-1.05±0.04	0.93±0.04
23Å(F140W/W311Y)	0.21±0.003	0.18±0.03	0.51±0.04	-1.30±0.06	0.99±0.03
23A(F196W/W311Y)	0.8±0.03	0.19±0.02	0.4±0.08	-1.11±0.04	1.17±0.09

Positions 311 and 233 in the 23Å interaction showed relatively large changes in anisotropy compared to the free enzyme form in most of the ligation states. Positions 140 and 196 had almost no response in the presence of any ligand. However, positions 140 and 196 are located in different regions in the protein. Position 188, which is close to the allosteric site, had increased anisotropy with every ligand bound. Interestingly, although 76 and 106 are far away from the ligand binding sites, anisotropy changes were observed at both positions. The decreases in anisotropy may indicate there is some local motion around the region of that specific tryptophan. The increase in anisotropy suggests a more rigid region around that specific tryptophan. However, the anisotropy change may also be due to a lifetime change for that specific tryptophan resulting from ligand binding. In the following experiment, the lifetime of each tryptophan was measured.

Time-resolved fluorescence

Time-resolved fluorescence experiments can be used to measure the tryptophan lifetime. Here, the lifetime of each tryptophan in the 23Å heterotropic interaction was measured individually using an ISS K2 multi-frequency phase fluorometer. The frequency dependence of the phase and the modulation of tryptophan at the native position 311 in the 23Å heterotropic interaction in the different ligation states is presented in Figure 5-5 A and B, for MgADP activation and PEP inhibition, respectively. In addition, the frequency dependence of the phase and the modulation of each tryptophan at different positions in the 23Å heterotropic interaction in the free enzyme form is show in Figure 5-6. The data were fit to various models and evaluated on the basis of their relative χ^2 values. In all cases, the phase and the modulation data

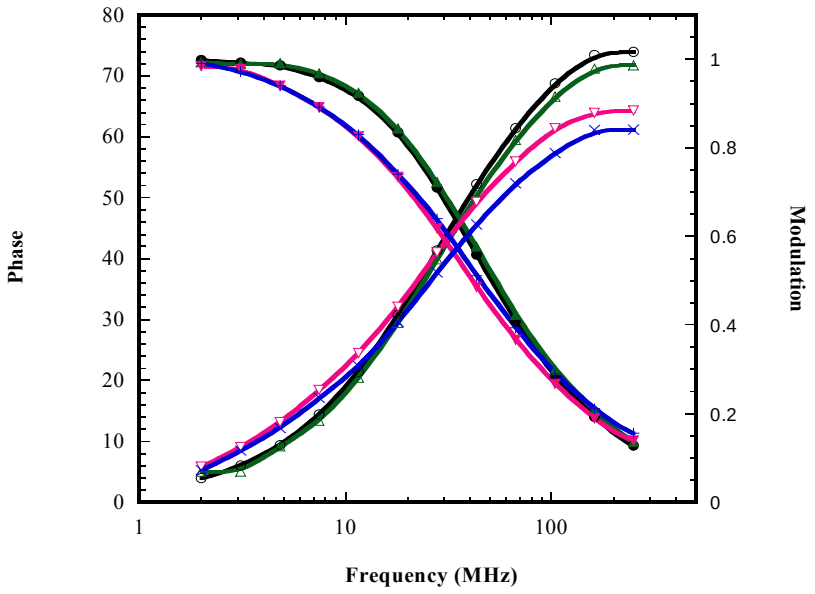

Figure 5-5 Frequency-domain lifetime determinations of the 23Å interaction with tryptophan at native position 311 in each different ligation states. Variation in phase and modulation with frequency are shown for each of the enzyme forms appearing in the disproportionation equilibria describing MgADP activation of Fru-6-P binding (A) and PEP inhibition of Fru-6-P binding (B). The phase and modulation are represented as follows no ligand (○,●), Fru-6-P (△,▲), PEP (□,■), Fru-6-P+PEP (◇,◆), MgADP (▽,▼), Fru-6-P+MgADP (×, +). The lines drawn represent the best fit of the data to a two components model: featuring a Lorentzian continuous distribution and discrete exponential decay.

.

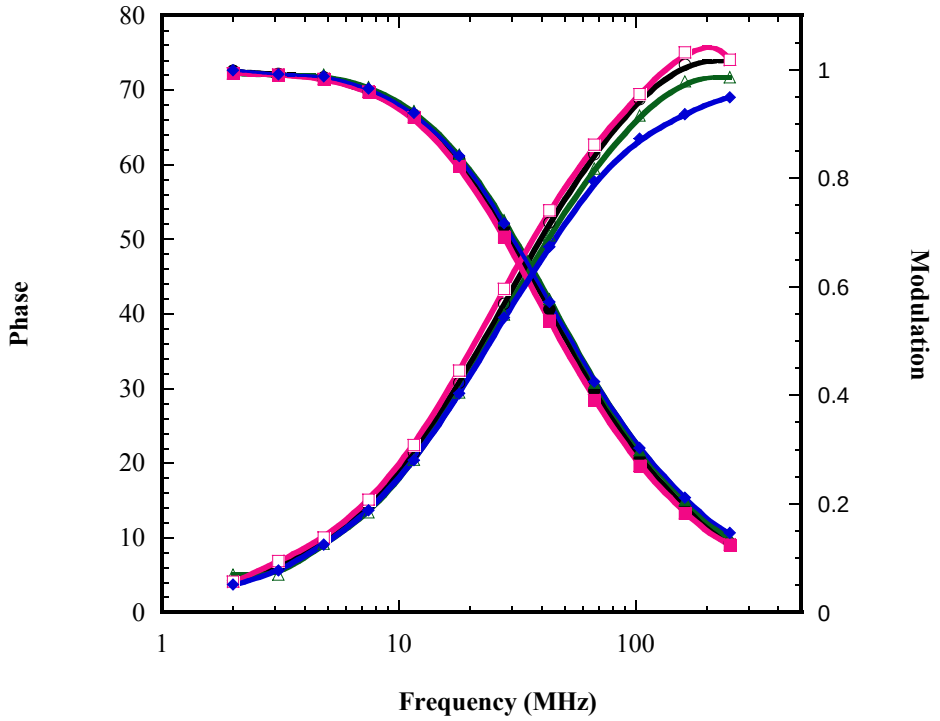

Figure 5-5 continued.

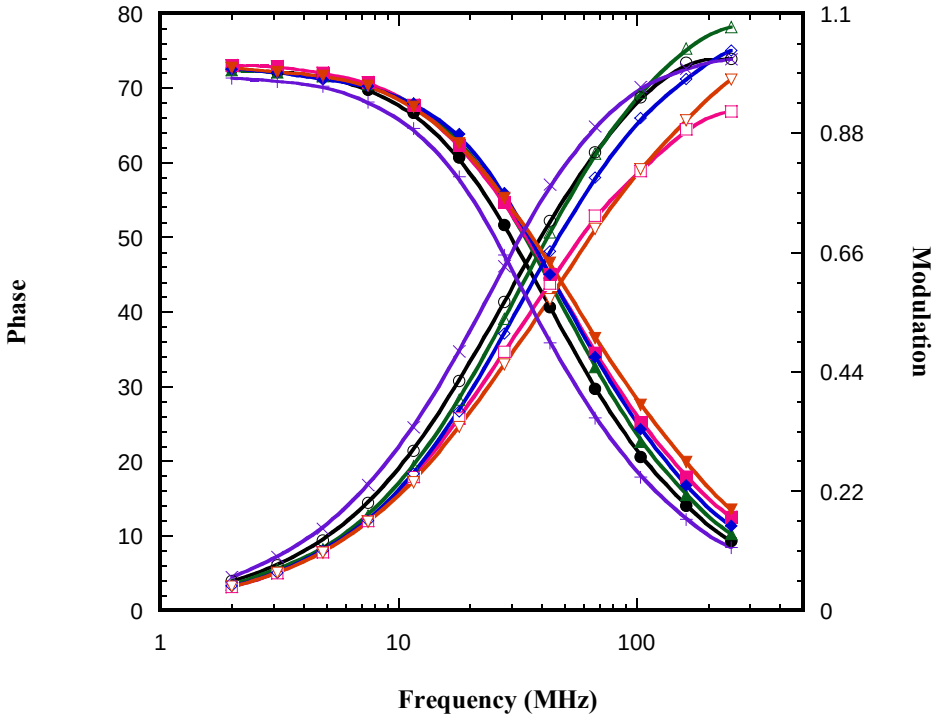

Figure 5-6 Frequency-domain lifetime determinations of the 23Å interaction with tryptophan at different positions in the absence of ligand. Variation in phase and modulation with frequency are shown for each tryptophan-shift mutant. The phase and modulation are represented as follows: W311 (○,●), W311Y/ F76W (△,▲), W311Y/Y106W (□,■), W311Y/F140W (◇,◆), W311Y/F188W (▽,▼), W311Y/F233W (×, +). The lines drawn represent the best fit of the data to a two components model: featuring a Lorentzian continuous distribution and one discrete exponential decay.

were fit best to a model providing for a Lorentzian and discrete exponential decays. The first component is represented by Lorentzian distribution, described by the center of the distribution, τ_1, the width of the distribution, w_1, and the fractional contribution this component makes to the total fluorescence, f_1. The second component is a discrete exponential decay with fluorescence lifetime, τ_2. The corresponding lifetimes obtained from this analysis are shown in Table 5-4. In all the ligation states, the majority of the fluorescence intensity arises from the longer component and ranges from 4.0 to 6.5 ns. In addition, the lifetime of the long component exhibits significant variation depending on the ligation states of the enzyme. The short lifetime component did not vary significantly in all samples. After repeating fluorescence lifetime data of all the mutant proteins, the averaged long component lifetime data are presented in Table 5-5 for each enzyme form. In addition, the lifetime variations mimic the commensurate changes in intrinsic fluorescence intensity that results from the binding of these ligands. As an example, F188W/W311Y, an increase in lifetime from 4.4 to 5.7 ns was observed with PEP bound; correspondingly, there is a 126% increase in fluorescence intensity. To get information of the rotational property of each tryptophan, the Perrin equation was used to relate the lifetime change and steady-state anisotropy change together. The rotational correlation time is obtained from the Perrin equation, which reflects the dynamic properties of protein in the vicinity of the tryptophan. Previous research indicates the global rotation does not change (Johnson and Reinhart, 1994 and 1997). A decrease in the rotational correlation time indicates a relative faster motion; increase in rotational

Table 5-4 Fluorescence lifetime responses to saturating concentration of ligands.

		No ligand	Fru-6-P	PEP	Fru-6-P +PEP	ADP	Fru-6-P +ADP
W311	τ_1	5.35	5.09	5.28	5.68	5.87	4.99
	w_1	0.989	1.088	0.978	1.015	5.716	6.295
	f_1	0.987	0.981	0.949	0.988	0.98	0.977
	τ_2	0	0.09	0.45	0	0.04	0
	X^2	1.9	4.7	1.6	6.2	3.8	4.0
W76	τ_1	4.76	4.78	4.79	4.62	4.73	4.36
	w_1	0.579	0.501	0.377	0.677	2.56	2.65
	f_1	0.995	0.987	0.993	0.976	0.825	0.852
	τ_2	0.12	0.31	0.08	0.28	0.31	0.28
	X^2	0.5	0.47	0.72	0.61	1.8	2.2
W106	τ_1	4.48	4.17	4.33	3.95	4.49	4.14
	w_1	1.468	1.743	1.702	1.754	4.097	4.44
	f_1	0.939	0.935	0.948	0.92	0.967	0.953
	τ_2	0.48	0.36	0.40	0.37	0	0.08
	X^2	4.8	8.0	5.9	8.5	5.4	6.7
W140	τ_1	4.57	4.56	4.51	4.36	4.50	4.51
	w_1	0.706	0.722	0.733	0.91	3.729	3.569
	f_1	0.973	0.97	0.979	0.955	0.999	1
	τ_2	0.57	0.39	0.52	0.45	0	0.98
	X^2	0.6	0.4	0.5	2.0	3.0	3.2
W188	τ_1	4.37	4.20	5.67	4.43	6.10	5.26
	w_1	1.849	1.962	1.558	2.074	10.558	10.8
	f_1	0.894	0.907	0.927	0.955	0.926	0.951
	τ_2	1.11	0.78	1.56	0.48	0.96	0.76
	X^2	2.4	2.2	1.2	3.6	11.7	13.3
W233	τ_1	6.45	6.44	6.27	6.09	6.50	5.83
	w_1	0.873	1.184	0.724	1.29	2.768	3.334
	f_1	0.979	0.956	0.981	0.948	0.968	0.962
	τ_2	0.29	0.39	0.07	0.38	0.23	0.25
	X^2	2.0	2.0	3.0	1.0	2.0	1.9

Table 5-5 Lifetime data and the rotational correlation time data calculated using Perrin equation.

23A (W311)	τ (ns)	r	θ (ns)	Δ θ (ns)
No ligand	5.34±0.049	0.178±0.001	11.6±0.14	
Fru6-P	5.09±0.071	0.171±0.0009	9.8 ±0.22	-1.8±0.26
PEP	5.28±0.09	0.180±0.001	11.9±0.21	0.3±0.26
Fru-6-P+PEP	5.67±0.05	0.175±0.001	11.7±0.13	0.1±0.2
ADP	5.87±0.09	0.190±0.002	15.9±0.31	4.3±0.34
Fru-6-P+ADP	4.99±0.09	0.192±0.0008	14.1±0.27	2.5±0.3
23A (W233)	τ	r	θ ns	Δ θ
No ligand	6.47±0.04	0.148±0.0004	8.6±0.06	
Fru-6-P	6.33±0.03	0.139±0.0008	7.3±0.07	-1.3±0.09
PEP	6.06±0.07	0.156±0.001	9.1±0.14	0.5±0.15
Fru-6-P+PEP	5.91±0.03	0.158±0.0008	9.2±0.07	0.6±0.09
ADP	6.03±0.04	0.172±0.001	11.8±0.12	3.2±0.13
Fru-6-P+ADP	5.61±0.03	0.175±0.0006	11.6±0.09	3.0±0.11
23A (W140)	τ	r	θ ns	Δ θ
No ligand	4.57±0.02	0.216±0.0002	22.4±0.11	
Fru-6-P	4.56±0.02	0.216±0.001	22.4±0.17	0±0.2
PEP	4.51±0.02	0.217±0.0009	22.7±0.17	0.3±0.2
Fru-6-P+PEP	4.36±0.04	0.222±0.001	25.4±0.30	3.0±0.3
ADP	4.50±0.05	0.219±0.001	24.0±0.33	1.6±0.35
Fru-6-P+ADP	4.51±0.05	0.219±0.0008	24.1±0.36	1.7±0.38
23A (W106)	τ	r	θ ns	Δ θ
No ligand	4.58±0.09	0.200±0.001	15.3±0.20	
Fru-6-P	4.27±0.07	0.198±0.002	13.6±0.21	-1.7±0.29
PEP	4.39±0.09	0.200±0.0006	14.6±0.31	-0.7±0.37
Fru6-P-+PEP	3.72±0.08	0.207±0.0003	14.5±0.32	-0.8±0.37
ADP	4.58±0.04	0.192±0.001	12.9±0.15	-2.4±0.25
Fru-6-P+ADP	3.81±0.04	0.200±0.001	12.7±0.19	-2.6±0.28
23A (W76)	τ	r	θ ns	Δ θ
No ligand	4.76±0.02	0.206±0.0009	18.2±0.15	
Fru-6-P	4.78±0.02	0.204±0.0005	17.4±0.1	-0.8±0.18
PEP	4.79±0.02	0.209±0.0008	19.6±0.16	1.4±0.22
Fru-6-P+PEP	4.62±0.02	0.209±0.0004	18.9±0.11	0.7±0.19
ADP	4.73±0.06	0.205±0.001	17.6±0.31	-0.6±0.34
Fru-6-P+ADP	4.36±0.06	0.202±0.001	15.2±0.24	-3.0±0.28
23A (W188)	τ	r	θ ns	Δ θ
No ligand	4.37±0.05	0.197±0.001	13.7±0.19	
Fru-6-P	4.20±0.05	0.199±0.001	13.7±0.19	0±0.27
PEP	5.67±0.04	0.206±0.001	21.6±0.21	7.9±0.28
Fru-6-P+PEP	4.43±0.06	0.207±0.001	17.3±0.25	3.6±0.31
ADP	6.10±0.60	0.206±0.0005	23.3±2.28	9.6±2.29
Fru-6-P+ADP	5.26±0.60	0.210±0.002	22.1±2.50	8.4±2.5

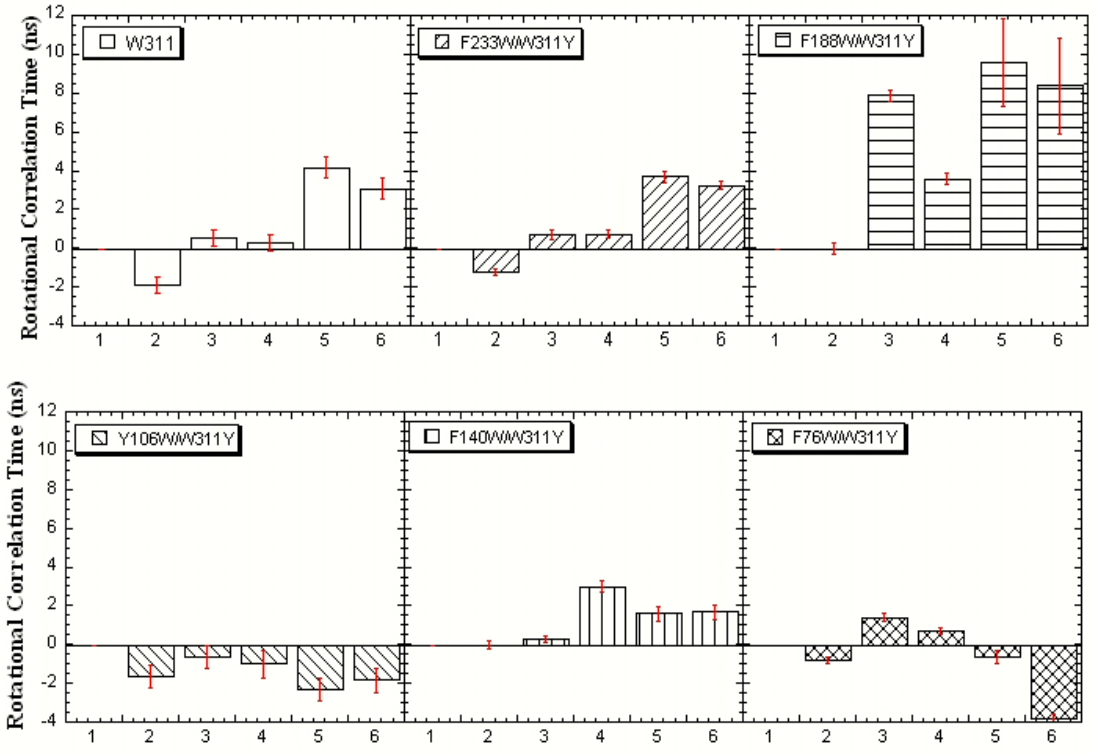

Figure 5-7 The comparisons in the rotational correlation time at each tryptophan mutants position in the 23Å interaction with different ligand binding. In the x-axis: (1).no ligand, (2). + 2mM Fru-6-P, (3). + 10 mM PEP, (4). + 10mM Fru-6-P+25 mM PEP, (5). + 2mM MgADP, (6). + 2 mM MgADP+ 2 mMFru-6-P.

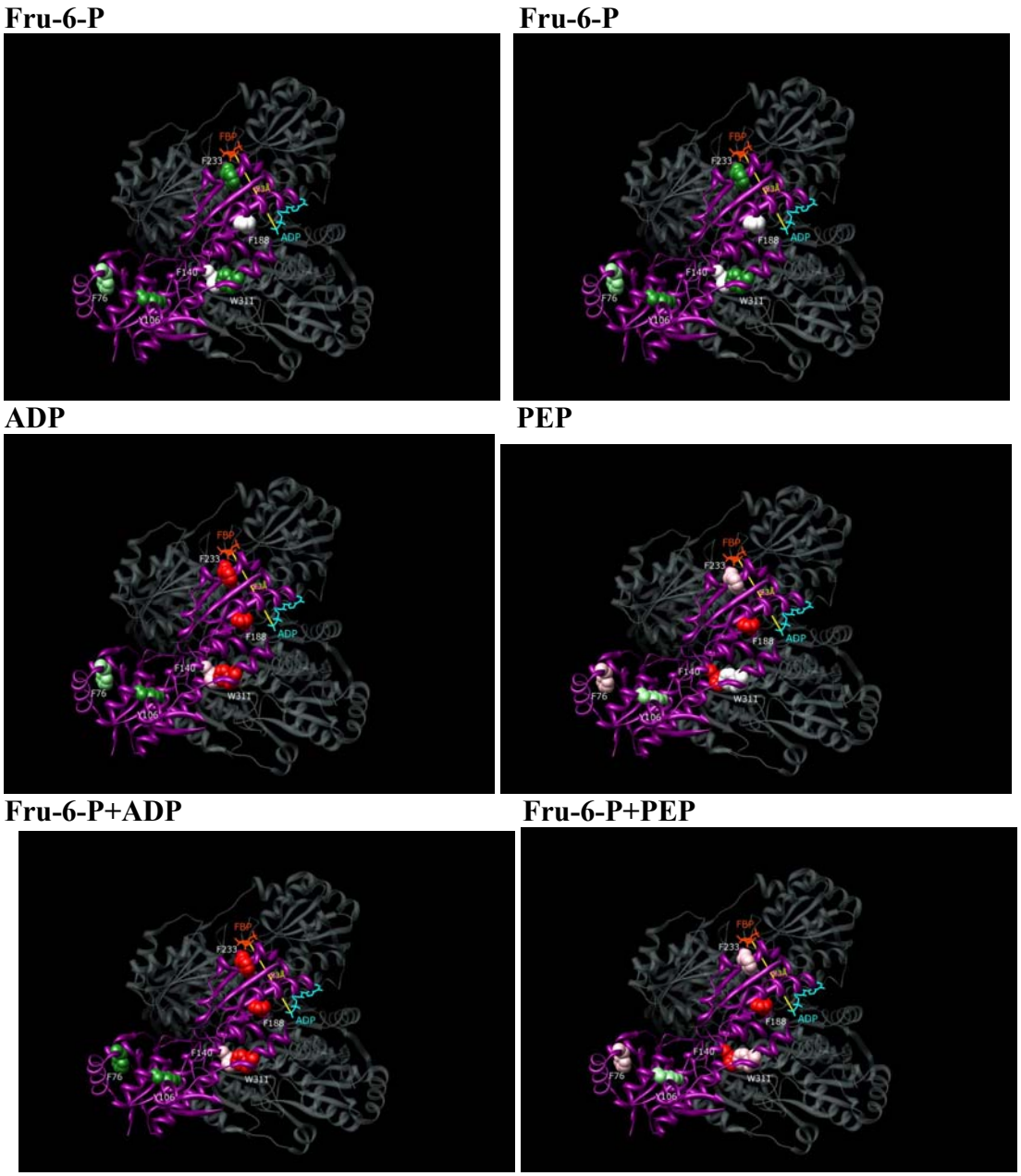

Figure 5-8 The changes in the rotational correlation time at each substituted tryptophan position in the 23Å interaction in EcPFK crystal structure. White: no change; green and light green: the rotational correlation time decreases above or below 1 ns, respectively; red and pink: the rotational correlation time increase above or below 2 ns, respectively.

correlation suggests a much slower motion. The plots of the changes in the rotational correlation time versus different ligation states are shown in Figure 5-7. In addition, the changes of the rotational correlation time for each tryptophan-shift mutant was shown in different colors in the crystal structure of EcPFK for each ligation state in Figure 5-8. Compared with free enzyme form, white indicates no change in lifetime; green and light green represent the rotational correlation time decrease either above or below 1 ns, respectively; red and pink indicate the rotational correlation time increase either above or below 2 ns, respectively.

Position 106 being relatively far away from the ligand binding sites in the 23Å interaction, the rotational correlation times are decreased in all the ligation states, which suggests a faster local motion around position 106 upon ligand binding. Position 76 is also far away from the ligand binding sites. The rotation correlation times are decreased in the presence of Fru-6-P, MgADP and Fru-6-P+MgADP, respectively. With either PEP or Fru-6-P+PEP bound, the rotational correlation times are increased. Although positions 106 and 76 are both far away from the ligand binding sites, they are perturbed differently. Positions 311 and 233 are near to the allosteric and active site, respectively. There are local motions around these two positions with Fru-6-P bound. Position 188 is located in a more rigid region since rotational correlation times are increased in all ligation states. From the other view, in the Fru-6-P ligation state, every tryptophan-shift mutant position has some motion except positions 188 and 140. Positions 188 and 140 have almost no change in any of the ligation states. This indicates the region close to positions 140 and 188 is probably more rigid. Interestingly, although ADP and PEP have

distinct effects on EcPFK, with either ADP bound or PEP bound individually, the structure gets more rigid for every position except position 106.

Conclusions

A tryptophan-shift mutagenesis strategy was used to place the intrinsic fluorescence probe in different positions in EcPFK protein. Coupled with the hybrid formation method, we successfully relocated each tryptophan in a different position in the 23Å heterotropic interaction. The fluorescence response of a specific tryptophan in the different places was monitored upon ligand binding in the 23Å heterotropic interaction.

Steady-state fluorescence experiments gave us the first indication based on changes in anisotropy for each different ligation state. The changes in anisotropy from each tryptophan position are different upon ligand binding. The fluorescence lifetime for each tryptophan was measured to evaluate whether the anisotropy change is related to a change in the fluorescence lifetime for each tryptophan position except position 196, which is a silent position from the anisotropy data. Based on the lifetime data and steady-state anisotropy data, the Perrin equation was used to calculate the rotational correlation time, which can indicate the perturbation around the tryptophan. The changes in the rotational correlation time data are consistent with the changes in steady-state anisotropy data for each tryptophan position, except position 106 in one ligation state. The regions around position 106, 43Å away from the active site and 36Å away from the allosteric site in the 23Å interaction, are involved in the perturbation of tryptophan side-

chain dynamics upon ligand binding. Position 76 is also far away from the ligand binding sites. The rotation correlation times are decreased or increased depending on the different ligation states. Thus, different positions at remote regions relative to the ligand binding sites are perturbed differently upon ligand binding. The regions around positions 140 and 188 , 24Å and 34Å away from the active site, respectively, are relatively rigid in all ligation states compared with the unbound enzyme form. Positions 311 and 233 are near to the allosteric and the active site, respectively. There are changes in local motions around these two positions with Fru-6-P bound. From the other view, in Fru-6-P ligation state, every tryptophan-shift mutant position has some changes in motion except positions 188 and 140. Interestingly, although ADP and PEP have distinct functions for EcPFK, with either ADP bound or PEP bound individually, the structure gets more rigid for every position except position 106. The responses of the ternary complex with either Fru-6-P+PEP or Fru-6-P+MgADP exhibit patterns similar to the binary complexes but to different extents. To take the analysis on step further, differential polarized phase/modulation fluorometry can be used to discriminate between and quantify global rotation verse local rotation.

CHAPTER VI

CONCLUSIONS

Previous research has extensively investigated the allosteric regulation of *E. coli* PFK. In our lab, we were able to isolate each of the four heterotropic interactions using the hybrid strategy and to quantify the contribution from each heterotropic interaction to the total heterotropic effect. In the current study, we focus on understanding the pathway or residues that are important for the allosteric communication.

In Chapter III, we improved the yield of the methodology for producing the 1:3 hybrids that contains a specific heterotropic interaction by developing an *in vivo* hybrid formation method. Previously in our lab, hybrid tetramers of PFK were successfully created *in vitro*. Among the five different hybrid species possible, the 1:3 hybrid, which has one native active site and one native allosteric site, presents a specific heterotropic interaction. However, the *in vitro* method is plagued with low yield and can be time consuming. In addition, KSCN, a mild chaotropic reagent, is used in the process to dissociate PFK tetramers. Thus, the hybrid formation is not a natural process. In the current study, we co-expressed the two parent proteins of the hybrid *in vivo* so that the chemical treatment is unnecessary. It is a natural process and cuts the hybrid production time in half. The efficiency of making hybrid proteins is also improved using the *in vivo* method as can be seen by the increased yield for the 1:3 hybrid. To improve the 1:3 hybrid yield for the 23Å heterotropic interaction even more, different charge-tag and allosteric site mutations were used without changing the kinetic characteristics of the protein K2E/3E were changed to K90E/91E and H215E was used instead of K213E.

In Chapter IV, we addressed the questions of which residues in EcPFK are important for allosteric signal transmission and whether the disruption in the total allosteric response can be differentially manifested in each heterotropic interaction. Two basic methods were used to pursue the first question. The first was based on sequence alignment between EcPFK and LbPFK. LbPFK is a weakly regulated allosteric protein. It shows no MgADP activation and very weak PEP inhibition. The idea is to make specific individual substitutions in EcPFK to the non-identical residues in LbPFK and evaluate the changes in the allosteric response. The second method used to address this question is to propose that residues that lie directly between the active site and the allosteric site play a role in the allosteric communication. The crystal structure of EcPFK was used to identify possible residues important for the signal transmission. Specific residues that lie between the active site and the allosteric site were mutated to alanine and the influence on coupling between Fru-6-P and effectors was assessed.

Of the six mutant proteins examined, G184C, D59A and S157A showed a reduction in coupling free energy for both PEP inhibition and MgADP activation. The question then becomes, how is the observed reduction in the allosteric response manifested in each of the four heterotropic interactions. G184C, D59A and S157A were introduced into the each of the four 1:3 hybrids that present each single heterotropic interaction, respectively. Each mutation has its own diminished pattern for both activation and inhibition in coupling free energy terms. We determined that G184C diminishes PEP inhibition by perturbing the 23Å coupling, whereas the MgADP activation is diminished through a disruption in the 33Å interaction. The position of

G184 in the crystal structure lies directly in between the active site and the allosteric site in the 33Å interaction. D59A influences PEP inhibition from the 23Å interaction and MgADP activation from the 30Å interaction. The position of D59 lies in the 30Å interaction. S157A only affects MgADP activation through both the 23Å and 33Å interactions. The influence on PEP inhibition does not result from a disruption of any of the four heterotropic interactions. The position of S157 is in the 23Å interaction. The relative positions of the three residues in EcPFK are related to their influence on MgADP activation. It seems that the MgADP activation traverses the protein through a likely direct pathway. However, more experiments are needed to verify this conclusion. Moreover, the results suggest that the structural basis for PEP inhibition differs from MgADP activation. Most significantly, because the sum of each heterotropic interaction with a specific mutation in one subunit equals the total heterotropic interaction with a specific mutation in all the four subunits, the heterotropic allosteric signal is likely transmitted within a single subunit.

In Chapter V, based on the conclusion that the heterotropic allosteric information is transmitted within a single subunit, the dynamic response of the 23Å heterotropic interaction in EcPFK with respect to each ligand binding event was investigated. Taking advantage of the hybrid strategy and tryptophan-shift mutagenesis, we measured the anisotropy change in the 23Å interaction in each ligation state with tryptophan at different positions individually.

The fluorescence responses from each tryptophan position are different upon ligand binding from steady-state anisotropy measurement that gives us the first

impression of motion around each tryptophan. To further study the dynamic properties of EcPFK, the fluorescence lifetime was measured in each case in order to evaluate whether the anisotropy change is related to a change in the fluorescence lifetime. Based on the lifetime data and steady-state anisotropy data, the Perrin equation is used to calculate the rotational correlation time, which can indicate the perturbation around the tryptophan side chain.

The changes in rotational correlation time data were consistent with the changes in steady-state anisotropy data for each tryptophan position, except position 106 in one ligation state. Despite position 106 being relatively far away from the active and the allosteric sites in the 23Å interaction, the rotational correlation time decreased in all the ligation states, which suggests that a relatively faster local motion occurs upon ligand binding. Position 76 is also far away from the ligand binding sites. The rotation correlation time decreased in the presence of Fru-6-P, MgADP and Fru-6-P+MgADP, respectively. However, with either PEP or Fru-6-P+PEP bound, the rotational correlation time increased. Although position 106 and 76 are all far away from the ligand binding sites, they are perturbed differently. Position 311 and 233 are near to the allosteric site and the active site, respectively. There are local motion changes around these two positions with Fru-6-P bound. Position 188 is located at a more rigid region since the rotational correlation time is increased in all ligation states. From the other view, in Fru-6-P ligation state, every tryptophan-shift mutant position has some changes in motion except position 188 and 140. Interestingly, although ADP and PEP have distinct functions in regulating EcPFK, with either ADP bound or PEP bound individually, the

structure gets more rigid for every position except position 106. To take the analysis on step further, differential polarized phase/modulation fluorometry can be used to discriminate between and quantify global rotation verse local rotation.

In summary, we have successfully improved the yield of the 1:3 hybrid that is required for studying the allosteric regulation in EcPFK. In addition, we have identified three residues in EcPFK that are important in transmitting allosteric information both for PEP inhibition and MgADP activation. Each residue affects each heterotropic interaction differently. More importantly, the heterotropic allosteric signal transmission is realized in one subunit. Although the allosteric pathway of EcPFK is difficult to define, we may follow the route to go further. Meanwhile, the same idea can be applied to BsPFK to study its allosteric communication. Moreover, the 23Å allosteric interaction involves the perturbation of tryptophan side-chain dynamics both near and quite far away from the respective ligand binding sites. Thus, using fluorescence spectroscopy to study protein dynamics coupled with placing the tryptophan fluorescence probe at different positions in the protein may be used as an alternative tool to map the dynamic properties of other proteins as well.

REFERENCES

Ackers, G. K., M. L. Doyle, D. Myers, and M. A. Daugherty. 1992. Molecular code of cooperativity in hemoglobin. *Science*. 255: 54-63.

Ackers, G. K., P. M. Dalessio, G. H. Lew, M. A. Daugherty, and J. M. Holt. 2002. Single residue modification of only one dimer within the hemoglobin tetramer reveals autonomous dimer function. *Proc. Natl. Acad. Sci. USA*. 99: 9777-9782.

Ackers, G. K., and J. M. Holt. 2006. Asymmetric cooperativity in a symmetric tetramer: human hemoglobin. *J. Biol. Chem.*281: 11441-11443.

Babul, J. 1978. Phosphofructokinase from *Escherichia coli*. Purification and characterization of the nonallosteric isozyme. *J. Biol. Chem.* 253: 4350-4355.

Blangy, D., H. Buc, and J. Monod. 1968. Kinetics of the allosteric interactions of phosphofructokinase from *Escherichia coli. J. Mol. Biol.* 31: 13-35.

Braxton, B. L., V. L. Tlapak-Simmons, and G. D. Reinhart. 1994. Temperature induced inversion of allosteric phenomena. *J. Biol. Chem.* 269: 47-50.

Cantor, C., and P. Schimmel. 1980. Techniques for the study of biological structure and function. *In* Biophysical Chemistry. P. Schimmel, editor. Freeman and Co. San Francisco. 433-465.

Clifton, D., and D. G. Fraenkel. 1982. Mutant studies of yeast phosphofructokinase *Biochemistry*. 21(8): 1935-1942.

Cohen, S. N., A. C. Y. Chang, and L. Hsu. 1972. Nonchromosomal antibiotic resistance in bacteria: Genetic transformation of *Escherichia coli* by Rfactor DNA. *Proc. Natl. Acad. Sci. USA*. 69: 2110-2115.

Demas, J. 1983. Excited State Lifetime Measurements. Academic Press, New York.

Deville-Bonne, D., G. Le Bras, W. Teschner, and J. R. Garel. 1989. Ordered disruption of subunit interfaces during stepwise reversible dissociation of *Escherichia coli* phosphofructokinase with KSCN. *Biochemistry*. 28: 1917- 1922.

Deville-Bonne, D., R. Laine, and J. R. Garel. 1991. Substrate antagonism in the kinetic mechanism of *E. coli* phosphofructokinase-1. *FEBS Letters*. 290: 173-176.

Evans, P. R., and P. J. Hudson. 1979. Structure and control of phosphofructokinase from *Bacillus stearothermophilus*. *Nature*. 279: 500-504.

Evans, P. R., G. W. Farrants, and P. J. Hudson. 1981. Phosphofructokinase: structure and control. *Phil. Trans. R. Soc. Lond. B.* 293: 53-62.

Evans, P. R., G. W. Farrants, and M. C. Lawrence. 1986. Crystallographic structure of allosterically inhibited phosphofructokinase at 7Å resolution. *J Mol. Biol*. 191: 713-720.

Fenton, A. W., and G. D. Reinhart. 2002. Isolation of a single activating allosteric interaction in phosphofructokinase from *Escherichia coli*. *Biochemistry*. 41: 13410-13416.

Fenton, A. W., and G. D. Reinhart. 2003. Mechanism of substrate inhibition in *Escherichia coli* phosphofructokinase. *Biochemistry*. 42: 12676-12681.

Fenton, A. W., N. M. Paricharttanakul, and G. D. Reinhart. 2003. Identification of substrate contact residues important for the allosteric regulation of phosphofructokinase from *Escherichia coli. Biochemistry*. 42: 6453-6459.

Fenton, A. W., N. M. Paricharttanakul, and G. D. Reinhart. 2004. Disentangling the web of allosteric communication in a homotetramer: heterotropic activation in phosphofructokinase from *Escherichia coli*. *Biochemistry*. 43: 14104-14110.

Freire, E. 1999. The propagation of binding interactions to remote sites in proteins. Analysis of the binding of the monoclonal antibody D1.3 to lysozyme. *Proc. Natl. Acad. Sci. USA*. 96: 10118-10122.

Gold, L., and G. Stormo.1987. Translational initiation. *In Escherichia coli* and *Salmonella typhimurium* Cellular and Molecular Biology. Vol 2. F. C. Neidhardt, editor. American Society for Microbiology. Washington, DC 1302-1307.

Hardy, J., J. Lam, J. Nguyen, T.O'Brien, and J. Wells. 2004. Discovery of an allosteric site in the caspases. *Proc. Natl. Acad. Sci. USA*. 101: 12461-12466

Hill, A. V. 1910. The possible effects of the aggregation of the molecules of hemoglobin on its dissociation curves. *J. Physiol.* 40: iv-vii.

Hilser, V. J., T. Oas, D. Dowdy, and E. Freire. 1998. The structural distribution of cooperative interactions in proteins: Analysis of the native state ensemble. *Proc. Natl. Acad. Sci. USA*. 95: 9903-9908.

Holt, J. M., and G. K. Ackers. 1995. The pathway of allosteric control as revealed by hemoglobin intermediate states. *FASEB J.* 9: 210-218.

Hutchinson, C. A., S. Phillips, M.H. Edgell, S. Gillam, P. Jahnke, and M. Smith. 1978. Mutagenesis at a specific position in a DNA sequence. *J. Biol. Chem*. 253: 6551-6560.

Jaworek, D., W. Gruber, and H. U. Bergmeyer. 1974. Adenosine-5'-diphosphate and adenosine-5'-monophosphate. *In* Methods of Enzymatic Analysis. Vol 4. H. U. Bergmeyer, editor. Academic Press, Inc., New York. 2127-2131.

Johnson, J. L., and G. D. Reinhart. 1992. MgATP and fructose-6-phosphate interactions with phosphofructokinase from *Escherichia coli. Biochemistry.* 31: 11510-11518.

Johnson, J. L., and G. D. Reinhart. 1994. Influence of MgADP on phosphofructokinase from *Escherichia coli*. Elucidation of coupling interactions with both substrates. *Biochemistry*. 33: 2635-2643.

Johnson, J. L., and G. D. Reinhart. 1997. Failure of a two-state model to describe the influence of phospho(enol)pyruvate on phosphofructokinase from *Escherichia coli*. *Biochemistry*. 36: 12814-12822.

Johnson, J.L., J. K. West, A. D. Nelson, and G. D. Reinhart. 2007. Resolving the fluorescence response of *Escherichia coli* carbamoyl phosphate synthetase: mapping intra- and intersubunit conformational changes. *Biochemistry*. 46: 387-397.

Kemp, R. G., and D. Gunasekera. 2002. Evolution of the allosteric ligand sites of mammalian phophofructo-1-kinase. *Biochemistry*. 41: 9426-9430.

Kimmel, J. L., and G. D. Reinhart. 2000. Reevaluation of the accepted allosteric mechanism of phosphofructokinase from *Bacillus stearothermophilus*. *Proc. Natl. Acad. Sci. USA*. 97: 3844-3849.

Kimmel, J. L. 2001. Investigation into the molecular basis for the allosteric regulation of phosphofructokinase from *Bacillus stearothermophilus*. Ph.D. Dissertation, Texas A&M University.

Kimmel, J. L., and G. D. Reinhart. 2001. Isolation of an individual allosteric interaction in tetrameric phosphofructokinase from *Bacillus stearothermophilus*. *Biochemistry*. 40: 11623-11629.

Kolartz, D., and H. Buc. 1977. Two *Escherichia coli* fructose-6-phosphate kinases: preparative purification, oligomeric structure, and immunological studies. *Biochem. Biophys. Acta.* 484: 35-48.

Kolartz, D., and H. Buc. 1982. Phosphofructokinase from *Escherichia coli*. *Methods Enzymol*. 90: 60-70.

Koshland, D. E., G. Nemethy, and D. Filmer. 1966. Comparison of experimental binding data and theoretical models in proteins containing subunits. *Biochemistry*. 5: 365-385.

Kramer, B., W. Kramer, and H. J. Fritz. 1984. Different base/base mismatches are corrected with different efficiencies by the methyl-directed DNA mismatch-repair system of *E. coli*. *Cell*. 38: 879-887.

Laemmli, U. K. 1970. Cleavage of structural proteins during the assembly of the head of bacteriophage T4. *Nature*. 227: 680-685.

Laine, R., D. Deville-Bonne, I. Auzat, and J. R. Garel. 1992. Interactions between the carboxyl groups of Asp 127 and Asp 129 in the active site of *Escherichia coli* phosphofructokinase. *Eur. J. Biochem*. 207: 1109-1114.

Lakowicz, J. R., and I. Gryczynski. 1991. Frequency domain fluorescence spectroscopy. *In* Topic of Fluorescence Spectroscopy, Vol 1. J. R. Lakowicz, editor. Plenum Press, New York. 293-335.

Lakowicz, J. R., 1999. *In* Principle of Fluorescence Spectroscopy. 2nd ed. Plenum Press, New York.

Lau, F. T., and A. R. Fersht. 1987. Conversion of allosteric inhibition to activation in phosphofructokinase by protein engineering. *Nature.* 326: 811-812.

Lau, F. T., A. R. Fersht, H. W. Hellinga, and P. R. Evans. 1987. Site-directed mutagenesis in the effector site of *Escherichia coli* phosphofructokinase. *Biochemistry*. 26: 4143-4148.

Lau, F. T., and A. R. Fersht. 1989. Dissection of the effector-binding site and complementation studies of *Escherichia coli* phosphofructokinase using site-directed mutagenesis. *Biochemistry.* 28: 6841-6847.

Le Bras, G., D. Deville-Bonne, and J. R. Garel. 1991. Purification and properties of the phosphofructokinase from *Lactobacillus bulgaricus*. A non-allosteric analog of the enzyme from *Escherichia coli*. *Eur. J. Biochem*. 198: 683-687.

Le Bras, G., I. Auzat, and J. R. Garel. 1995. Tetramer-dimer equilibrium of phosphofructokinase and formation of hybrid tetramers. *Biochemistry*. 34: 13203-13210.

Li, Y., D. Rivera, W. Ru, D. Gunasekera, and R. G. Kemp. 1999. Identification of allosteric sites in rabbit phosphofructokinase. *Biochemistry*. 38: 16407-16412.

Lindsley, J., and J. Rutter. 2006. Whence cometh the allosterome? *Proc. Natl. Acad. Sci. USA*. 103: 10533-10535.

Lockless, S. W., and R. Ranganathan. 1999. Evolutionarily conserved pathways of energetic connectivity in protein families. *Science*. 286: 295-299.

Lovingshimer, M. R., D. Siegele, and G. D. Reinhart. 2006. Construction of an inducible, pfkA and pfkB deficient strain of Escherichia coli for the expression and purification of phosphofructokinase from bacterial sources. *Protein Expr Purif*. 46(2): 475-482.

Luque, I., and E. Freire. 2000. Structural stability of binding sites: consequences for binding affinity and allosteric effects. *Prot. Struct. Func. Gene.* 4: 63-71.

Monod, J., J. Wyman, and J. P. Changeux. 1965. On the nature of allosteric transitions: a plausible model. *J. Mol. Biol.* 12: 88-118.

Munro, I., Pecht, I., and Stryer, L. 1979. Subnanosecond motions of tryptophan residues in proteins. *Proc. Natl. Acad. Sci. USA*. 76: 56-60.

Ortigosa, A. D., J. L. Kimmel, and G. D. Reinhart. 2004. Disentangling the web of allosteric communication in a homotetramer: heterotropic inhibition of phosphofructokinase from *Bacillus stearothermophilus*. *Biochemistry*. 43: 577-586.

Pace, C. N., F. Vajdos, L. Fee, G. Grimsley, and T. Gray. 1995. How to measure and predict the molar absorption coefficient of a protein. *Prot. Science*.4: 2411-2423.

Parichar ttanakul, N. M., S. Ye, A. L. Menefee, F. Javid-Majd, J. C. Sacchettini, and G.D. Reinhart. 2005. Investigation into the structure-function relationship of phosphofructokinase from *Lactobacillus bulgaricus*. *Biochemistry*. 44(46): 15280-15286.

Perrin, F. 1926. Polarisation de la lumière de fluorescence. *J. Phys. Radium*. 7: 390-398.

Pham, A. S., F. Tlapak-Simmons, and G. D. Reinhart. 2001. Persistent binding of MgADP to the E187A mutant of *Escherichia coli* phosphofructokinase in the absence of allosteric effects. *Biochemistry*. 40: 4140-4149.

Poorman, R. A., A. Randolph, R. G. Kemp, and R. L. Heinrikson. 1984. Evolution of phosphofructokinase: gene duplication and reaction of new effector sites. *Nature*. 309: 467-469.

Reinhart, G. D., and H. A. Lardy. 1980. Rat liver phosphofructokinase: kinetic and physiological ramifications of the aggregation behavior. *Biochemistry.* 19: 1491-1495.

Reinhart, G. D. 1983. The determination of thermodynamic allosteric parameters of an enzyme undergoing steady-state turnover. *Arch. Biochem. Biophys*. 224: 389-401.

Reinhart, G. D. 1985. Influence of pH on the regulatory kinetics of rat liver phosphofructokinase: a thermodynamic linked-function analysis. *Biochemistry*. 24: 7166-7172.

Reinhart, G. D. 1988. Linked-function origins or cooperativity in a symmetrical dimer. *Biophys. Chem*. 30: 159-172.

Reinhart, G. D., S. B. Hartleip, and M. M. Symcox. 1989. Role of coupling entropy in establishing the nature and magnitude of allosteric response. *Proc. Natl. Acad. Sci.USA*. 86: 4032-4036.

Reinhart, G. D. 2004. Quantitative analysis and interpretation of allosteric behavior. *Methods Enzymol*. 380: 187-203.

Riley-Lovingshimer, M. R., and G. D. Reinhart. 2001. Equilibrium binding studies of a tryptophan-shifted mutant of phosphofructokinase from *Bacillus stearothermophilus*. *Biochemistry*. 40: 3002-3008.

Riley-Lovingshimer, M. R., and G. D. Reinhart. 2002. Reversible ligand-induced dissociation of a tryptophan-shifted mutant of phosphofructokinase from *Bacillus stearothermophilus*. *Biochemistry*. 41: 12967-12974.

Riley-Lovingshimer, M. R., and G. D. Reinhart. 2005. Examination of MgATP binding in a tryptophan-shift mutant of phosphofructokinase from *Bacillus sterothermophilus*. *Arch Biochem Biophys*. 436: 178-186.

Sanger, F., S. Nicklen, and A. R. Coulson. 1977. DNA sequencing with chainterminating inhibitors. *Proc. Natl. Acad. Sci. USA*. 74: 5463-5467.

Schirmer, T., and P. R. Evans. 1990. Structural basis of the allosteric behavior of phosphofructokinase. *Nature*. 343: 140-145.

Shirakihara, Y., and P. R. Evans. 1988. Crystal structure of the complex of phosphofructokinase from *Escherichia coli* with its reaction products. *J. Mol. Biol.* 204: 973-994.

Smith, D. K., R. I. Krohn, G. T. Hermanson, A. K. Mallia, F. H. Gartner, M. D. Provenzano, N. M. Goeke, B. J. Olson, and D. C. Klenk. 1985. Measurement of protein using bicinchoninic acid. *Anal. Biochem*. 150: 76-85.

Spencer, R.G., and G. Weber. 1969. Measure of subnanosecond fluorescence lifetimes with a cross-correlation phase fluorometer. *Ann. N.Y. Acad. Sci.* 158: 361-376.

Spencer, R. D., and G. Weber. 1970 Influence of Brownian rotations and energy transfer upon the measurements of fluorescence lifetime. *J. Chem. Phys*. 52: 1654-1663.

Symcox, M. M., and G. D. Reinhart. 1992. A steady-state kinetic method for the verification of the rapid-equilibrium assumption in allosteric enzymes. *Anal. Biochem*. 206: 394-399.

Tlapak-Simmons, V. L., and G. D. Reinhart. 1994. Comparison of the inhibition of phospho(enol)pyruvate and phosphoglycolate of phosphofructokinase from *Bacillus stearothermophilus*. *Arch. Biochem. Biophys*. 308: 226-230.

Tlapak-Simmons, V. L., and G. D. Reinhart. 1998. Obfuscation of allosteric structure-function relationships by enthalpy-entropy compensation. *Biophys. J.* 75: 1010-1015.

Uyeda, K. 1979. Phosphofructokinase. *Adv. Enzymol. Relat. Areas Mol. Biol*.48: 193-244.

Valdez, B. C., B. A. French, E. S. Younathan, and S. H. Chang. 1989. Site-directed mutagenesis in *Bacillus stearothermophilus* fructose-6-phosphate 1-kinase. *J Biol. Chem*. 264: 131-135.

Wang, X., and R. G. Kemp. 1999. Identification of residues of *Escherichia coli* phosphofructokinase that contribute to nucleotide binding and specificity. *Biochemistry*. 38: 4313-4318.

Weber, G. 1971. Theory of fluorescence depolarization by anisotropic Brownian rotations. Discontinuous distribution approach. *J. Chem. Phys.* 55: 2399-2407.

Weber, G. 1972. Ligand binding and internal equilibrium in proteins. *Biochemistry*. 11: 864-878.

Weber, G. 1975. Energetics of ligand binding to proteins. *Adv. Prot. Chem*. 29: 1-83.

Weber, G. 1977. Theory of differential phase fluorometer: detection of anisotropic molecular rotation. *J. Chem. Phys.* 66: 4081-4091.

Weber, G. 1978. Limited rotational motion: recognition by differential phase fluorometer. *Acta. Phys. Pol.* A54: 859-865.

Weber, G. 1981. Resolution of fluorescence lifetime in a heterogeneous system by phase and modulation measurement. *J. Chem. Phys.* 85: 849-853.

Wilson, C. J., H. Zhan, L. Swint-Kruse, and K. S. Matthews. 2007. The lactose repressor system: paradigms for regulation, allosteric behavior and protein folding. *Cell Mol Life Sci.* 64(1): 3-16.

Wyman, J. 1964. Linked functions and reciprocal effects in hemoglobin: a second look. *Adv. Protein Chem*. 19: 223-286.

Wyman, J. 1967. Allosteric linkage. *J. Am. Chem. Soc*. 89: 2202-2218.

Zell, R., and H. J. Fritz. 1987. DNA mismatch-repair in *Escherichia coli* counteracting the hydrolytic deamination of 5-methyl-cytosine residues. *EMBO Journal*. 6: 1809-1815.

Zhan, H. L., L. Swint-Kruse, and K.S. Matthews. 2006. Extrinsic interactions dominate helical propensity in coupled binding and folding of the lactose repressor protein hinge helix. *Biochemistry*. 45(18): 5896-906.

APPENDIX

Introduction

In Chapter V, the dynamic perturbations in the 23Å heterotropic interaction upon ligand binding were monitored by measuring the tryptophan fluorescence changes at different positions. Using the idea, the other three heterotropic interactions, 30Å, 33Å, and 45Å were studied as well. Here, only the perturbations at the native tryptophan position 311 were shown by measuring steady-state anisotropy. The results suggest that the response of different ligands binding for the four heterotropic interactions are distinct.

Methods and Materials

Materials All chemical reagents used for protein purification, enzyme kinetic assay and fluorescence experiments were the same as chapter II. The following oligonucleotides were ordered from Integrated DNA Technologies (IDT) and used for mutagenesis.

W311N, 5'- CGC GCA GTC CAG ATT GTC GCC TTT GAA CGG ACG -3'

W311T, 5'- CGC GCA GTC CAG CGT GTC GCC TTT GAA CGG ACG -3'

W311M, 5'- CGC GCA GTC CAG CAT GTC GCC TTT GAA CGG ACG -3'

W311I, 5'- CGC GCA GTC CAG GAT GTC GCC TTT GAA CGG ACG -3'

W311L, 5'- CGC GCA GTC CAG CAA GTC GCC TTT GAA CGG ACG -3'

Results

Hybrids formation for each heterotropic interaction with tryptophan at position 311

The 1:3 hybrid with tryptophan at position 311 in the other three heterotropic interaction were formed individually. The 1:3 hybrid represents the 33Å interactions were formed successfully with W311Y mutation. However, the 1:3 hybrid of the 30Å interaction could not be formed and the 1:3 hybrid of 45Å interaction was not stable with the W311Y mutation. Several other mutations were made at 311 position, W311L, W311N, W311T and W311M. Eventually, with the W311M mutation, the 30Å interaction and the 45Å interaction were able to form all the hybrid species with a stable 1:3 hybrid. As a result, the 23Å and the 33Å interactions had W311Y mutation; the 30Å and the 45Å interactions had W311M mutation.

Steady-state anisotropy

For each heterotropic interaction, the anisotropy varied differently at W311 position responding to different ligation states. This implies that the environment around W311 for each heterotropic interaction is affected distinctly with different ligand binding.

Taking advantage of the hybrid strategy, we measured the anisotropy changes in each of the four heterotropic interactions in different ligation states corresponding the native tryptophan 311 position. The data showed that anisotropy changes at W311 are distinct in each heterotropic interaction. Compared with free enzyme, when Fru-6-P bound, the anisotropy decreased in all the four heterotropic interaction. With PEP bound,

the 30Å and the 33Å heterotropic interactions showed decreased anisotropy, however the 23Å and the 45Å heterotropic interaction had no change. The anisotropy of the ternary complex Fru-6-P--PFK--PEP was decreased in all the four heterotropic interactions. With MgADP bound, three of the four heterotropic interaction increased the anisotropy except the 45 Å interaction. With both MgADP and Fru-6-P bound, the anisotropy increased in the 23 Å and the 33 Å interaction, but decreased in the 30 Å and the 45 Å interaction. The anisotropy decreases may indicate more dynamic around the tryptophan at position 311. All of the above data indicated that the changes of steady-state anisotropy in the 23 Å and the 33 Å interactions have similar pattern in the Fru-6-P, PEP and Fru-6-P-PEP ligation state. The 23 Å and the 45 Å interactions have a similar pattern in the Fru-6-P, MgADP and Fru-6-P MgADP ligation state.

The data showed that anisotropy changes at W311 were distinct in each heterotropic interaction. The data indicated that the changes in steady-state anisotropy in the 23Å and the 33Å interactions had a similar pattern with Fru-6-P, PEP and both Fru-6-P and PEP bound. The 23Å and the 45Å interactions had a similar pattern with Fru-6-P, MgADP and both Fru-6-P and MgADP bound. Most importantly, the anisotropy decreases may be indication of the motion around W311. However, we need more evidence from lifetime measurements to support this conclusion.

Table A-1 Steady-state intensity and anisotropy for the each of the four heterotropic interaction at W311 position.

	23Å (W311Y) 1: 3 Hybrid		33Å (W311Y) 1: 3 Hybrid	
	Intensity	Anisotropy	Intensity	Anisotropy
No ligand		0.181±0.001		0.190±0.001
2 mM F6P	-18 %	0.171±0.0009	-17-21%	0.177±0.0007
10mM PEP	-6% -12%	0.180±0.001	+3+9%	0.180±0.0002
10mM F6P+ 25mM PEP	-23%	0.175±0.001	-15%	0.180±0.001
2mM MgADP	-13%-15%	0.190±0.002	-3%	0.202±0.001
2mM MgADP + 2mM F6P	-13%-14%	0.192±0.001	-22%	0.198±0.002
	30Å (W311M) 1: 3 Hybrid		45Å (W311M) 1: 3 Hybrid	
	Intensity	Anisotropy	Intensity	Anisotropy
No ligand		0.168±0.0007		0.159±0.0001
2 mM F6P	-14%	0.153±0.001	-11%	0.149±0.0002
10mM PEP	-2%	0.164±0.001	-1%	0.159±0.001
10mM F6P+ 25mM PEP	-26%-28%	0.154±0.001	-22-24%	0.149±0.0004
2mM MgADP	+2%	0.173±0.0006	NC	0.155±0.001
2mM MgADP + 2mM F6P	-23%	0.161±0.0009	-35%	0.153±0.0006

VITA

Cuijuan Tie

Department of Biochemistry and Biophysics
Texas A&M University
College Station, TX, 77843-2128

Education:

Nanjing University, China	Biology	B.S. 1997
Institute of Microbiology, China Academy of Science	Biochemistry	M.S. 2002
Texas A&M University	Biochemistry	Ph.D. 2008

Publications:

Tie, C., and G.D. Reinhart. Selective perturbation of individual allosteric interaction in *E. coli* phosphofructokinase. (manuscript in preparation)

Tie, C., and G.D. Reinhart. Fluorescence dynamic studies on *E. coli* phosphofructokinase. (manuscript in preparation)

Presentation:

In vivo formation of hybrid tetramers of *E. coli* phosphofructokinase. Biophysical Society, Long Beach, California. February 14-18, 2004

Selective perturbation of individual allosteric interaction in *E. coli* phosphofructokinase. Molecular Biophysics Annual Retreat, Texas A&M University, Camp Allen, Texas. November 5-6, 2005

Selective perturbation of individual allosteric interactions in *E.coli* phosphofructokinase Biophysical Society, Salt Lake City, Utah. February 18-22, 2006

Allosteric communication in a homotetramer: the inside story. Biophysical Society, Long Beach, California. February 2-6, 2008

Professional Society:

Biophysical Society